EFFECT OF HOOP REINFORCEMENT SPACING ON THE CYCLIC RESPONSE OF LARGE REINFORCED CONCRETE SPECIAL MOMENT FRAME BEAMS

Marios Panagiotou
Tea Visnjic
Grigorios Antonellis
Panagiotis Galanis
Jack P. Moehle

Department of Civil and Environmental Engineering
University of California, Berkeley

PEER Report 2013/17
Pacific Earthquake Engineering Research Center
Headquarters at the University of California

June 2013

ABSTRACT

Recent developments in the construction of high-rise buildings in the highly seismic regions of the United States have resulted in construction of reinforced concrete special moment frame beams that are larger compared to those used previously. Governing building code requirements (ACI 318-08) for these beams were introduced in ACI 318-83 and are based on prevailing practices and technical knowledge from that period. When the existing provisions are applied to the larger beams that are now prevalent, hoop spacing can be as large as 305 mm (12 in.) in the beam plastic-hinge zone. An experimental study was conducted to explore the effectiveness of the ACI 318-08 provisions and to identify needed changes for ACI 318-11. Two large special moment frame beams were constructed and tested. The beams were 1219 mm (48 in.) deep by 762 mm (30 in.) wide, and constructed of normal-weight aggregate concrete having target compressive strength of 34 MPa (5000 psi). Longitudinal reinforcement consisted of five No. 36 (11) ASTM A706 Grade 60 bars at top and bottom faces. Transverse reinforcement consisted of No. 16 (5) hoops, where each hoop set was made up of a stirrup closed by a crosstie with an additional vertically oriented crosstie. Center-to-center spacing of hoop sets was either 279 mm (11 in.) or 152 mm (6 in.). The beams were subjected statically to cyclic displacement reversals to simulate effects of earthquake-induced deformations.

ACKNOWLEDGMENTS

We are grateful for financial support and in-kind contributions from Pankow Foundation, Webcor Builders, ACI Foundation's Concrete Research Council, and the CRSI Foundation, which provided the capability for constructing the test specimens and conducting the laboratory study. The work was conducted under the auspices of the Pacific Earthquake Engineering Research Center, using the laboratory test facilities of the Department of Civil and Environmental Engineering of the University of California, Berkeley.

The study arose from a concern by Robert Englekirk (Englekirk Structural Engineers) conveyed in a letter and a technical presentation to representatives of the American Concrete Institute (ACI). The Institute responded by promoting and partially sponsoring the development of the test program reported here, as well as an ACI 318 Code Change proposal that resulted in modifications of the Building Code Requirements for Structural Concrete [ACI 318-11 2011].

The study was guided by Robert Tener, Executive Director of Pankow Foundation, and by an expert Industry Advisory Committee comprising: Robert Englekirk (Englekirk Structural Engineers); Ron Klemencic (Magnusson Klemencic Associates); Joseph Maffei (Rutherford + Chekene); Mehran Pourzanjani (Saiful Bouquet Structural Engineers); Mark Sarkisian (Skidmore, Owings & Merrill LLP); and James Wight (University of Michigan). Ron Klemencic served as “Industry Champion” for the project in accordance with established practices for projects funded by the Pankow Foundation. These individuals had a very positive influence in directing the project work toward results that will affect industry and are readily usable.

Subcommittee H (Seismic) of the ACI’s Committee 318 (Building Code) reviewed results of the test program and worked with the authors to craft the building code language recommended in this report and later adopted as part of ACI 318-11. The close collaboration among funding agencies, expert practitioners, building code committee, and project participants streamlined the development and adoption of the building code provisions.

The authors thank Mr. Ross Yamamoto and Mr. James Sonu, undergraduate students in the Department of Civil and Environmental Engineering, University of California, Berkeley, for their work on data reduction as well as on developing the figures presented in Appendix A.

The opinions, findings, conclusions, and recommendations expressed in this publication are those of the authors and do not necessarily reflect the views of the study sponsors or the Pacific Earthquake Engineering Research Center.

CONTENTS

LIST OF TABLES AND FIGURES

1 Final Report

1.1 INTRODUCTION

Construction of tall buildings is increasing in earthquake-prone regions of the United States (U.S.) and around the world. Reinforced concrete special moment resisting frames (referred to as "special moment frames" in ACI 318 [2011] and sometimes abbreviated to SMRFs) are commonly selected as the seismic force-resisting system in such buildings. In taller buildings, SMRF beams with height as deep as 1219 mm (48 in.) are not uncommon. In the U.S., reinforced concrete SMRFs are generally designed and detailed in accordance with ACI 318 [ACI 2008]. The ACI 318 provisions are structured around the strong column-weak beam philosophy, whereby the majority of inelastic flexural deformations are designed to occur in the columns at the bottom of the first story and in the beams along the height of the building. Therefore, it is important that SMRF beams be capable of stable inelastic flexural response at deformation levels consistent with the building code design provisions.

The numerical seismic response of tall reinforced concrete SMRFs designed according to ACI 318 provisions has been studied by Haselton et al. [2008] and Visnjic et al. [2012]. Visnjic et al. [2012] reported 2% and 3% mean interstory drift ratios in generic 20-story tall SMRFs located in Los Angeles, California, at design basis earthquake (DBE) and maximum considered earthquake (MCE) levels of shaking, respectively. Although the exact relationship between interstory drift ratio and beam chord rotation depends on the geometry of the framing system and varies continuously during earthquake shaking, typically the beam rotation is found to be approximately equal to the interstory drift ratio. For example, for the frames reported in Visnjic et al. [2012], beam rotations are about 1.3 times the interstory drift ratios, resulting in mean beam rotations of 0.026 and 0.039 at the DBE and the MCE hazard levels, respectively. According to that study, more than 30% of the beams along the height of the frame may reach this rotation amplitude.

Few experimental studies of reinforced concrete beams or beam-column subassemblies have been carried out with beam depth h greater than 610 mm (24 in.). For example, in Popov et al. [1972] h = 737 mm (29 in.); Blakeley et al. [1975,] h = 889 mm (35 in.); Birss [1978] h = 610 mm (24 in.); Beckingsale [1980] h = 610 mm (24 in.); Restrepo et al. [1990] h = 700 mm (27.5 in.); Warcholik and Priestley [1997] h = 737 mm (29 in.); and Chang et al.[2008] h = 914 mm (36 in.). These studies have shown that the degree of damage at different amplitudes of deformation depends primarily on the amount of longitudinal reinforcement; the shear span ratio (defined as the moment at the beam end divided by the product of the shear force and the beam height); and the quantity, spacing, configuration, and material properties of the transverse reinforcement. Predominant modes of failure of flexure-dominated beams under cyclic loading include moderate inelastic response of the transverse reinforcement and diagonal cracking resulting in stiffness degradation, bond degradation of the longitudinal reinforcement, and buckling of the longitudinal reinforcement.

Among the three beam tests reported in Popov et al. [1972], only one (beam 43) would satisfy ACI 318-08's shear strength requirements. This beam had longitudinal tension reinforcement ratio $\rho = A_s/bd$ = 1.58% (A_s = area of tension reinforcement, b = beam width, and d = distance from extreme compression fiber to centroid of longitudinal reinforcement), longitudinal compression reinforcement ratio $\rho^{'}$= 1.58%, and ratio of hoop spacing to longitudinal bar diameter s_h / d_b = 2.66. It sustained seven cycles of increasing displacement amplitude and 4.5% peak drift ratio (defined as the lateral displacement of the beam divided by the beam length) before significant stiffness degradation due to inelastic strains of the stirrups and major diagonal cracking occurred. Beams tested by Blakeley et al. [1975], as part of beam-column subassemblies, with ρ = 1.1% and 1.03%, $\rho^{'}$ = 0.7%, s_h / d_b = 5.3, and yield strength of steel f_y = 300 MPa (44 ksi), sustained cycles of increasing displacement amplitude to more than 5% peak drift ratio before significant stiffness degradation occurred due to bar buckling and diagonal cracking. The transverse reinforcement of these beams consisted of two No. 16 (5) hoops with 127 mm (5 in.) long hooks. Beams 5 and 6 tested by Restrepo et al. [1990], with ρ = 0.93% and s_h / d_b = 4.2, sustained five and six cycles, respectively, of increasing displacement amplitude and a peak drift ratio of 3.6% before major stiffness degradation occurred due to bond failure of the longitudinal reinforcement and crushing of the corresponding cover concrete in one of the beams; major diagonal cracking and shear deformations occurred in the other. No major buckling of the longitudinal reinforcement occurred in any of the beams described above. Two out of the four beams tested by Chang et al. [2008] had a rectangular section shape, used ductile threaded rods for longitudinal reinforcement with ρ = 0.6%, had transverse reinforcement layout with s_h / d_b = 1.5, and used normal- and high-strength concrete. Both beams sustained more than 5.5% peak drift ratio before major stiffness degradation occurred. No major buckling of the longitudinal reinforcement was observed up to this level of response.

According to ACI 318-08, design shear strength is the shear corresponding to development of probable flexural strength, M_{pr}, acting at beam ends concurrent with design gravity loads. Within a length $2h$ from the end of a SMRF beam end, hoops must be designed to resist the entire shear (the concrete contribution is ignored). A hoop may consist of a single piece of reinforcement, or it may consist of a stirrup closed at the top by a crosstie. To improve lateral support for the longitudinal reinforcement, ACI 318 also requires that at least the corner and alternate bars must have lateral support provided by the corner of a tie or crossties, with no unsupported bar more than 152 mm (6 in.) clear from a supported bar. Furthermore, Section 21.5.3.2 requires that hoop spacing, s_h, within $2h$ of the beam ends shall not exceed the least of $d / 4$, $8d_b$, $24d_{bh}$, and 305 mm (12 in.), where d_{bh} is the hoop-bar diameter. The amount and configuration of the hoops determines not only the shear strength of a beam but also its resistance against buckling of the longitudinal reinforcement, which has been shown by Monti and Nuti [1992] and Rodriguez et al. [1999] to depend strongly on s_h / d_b.

The study reported herein investigates the experimental static cyclic response of two 1219-mm- (48-in.-) deep × 762-mm- (30-in.-) wide reinforced concrete beams designed according to ACI 318-08. These are believed to be the largest SMRF beams to have been tested under simulated seismic loading in a laboratory. The beams had longitudinal tension reinforcement consisting of five No. 36 (11) ASTM A706 bars corresponding to $\rho = 0.58\%$. The beams had No. 16 (5) hoops having longitudinal spacing of 279 mm (11 in.) in one beam and 152 mm (6 in.) in the other beam, corresponding to s_h / d_b equal to 7.8 and 4.3, respectively. The specified concrete compressive strength in both beams was 34 MPa (5000 psi).

1.2 TEST SPECIMENS

Two test beams were designed and constructed to test the ACI 318-08 Building Code provisions and proposed code changes. The beams cantilevered from a common reaction block that was anchored to the laboratory floor; see Figure 1 (refer to Figure 12 and Figure 29 for test fixture photos). The beams were tested by imposing displacement cycles (upward and downward) to simulate the effects of deformation reversals that occur during a major earthquake. Positive displacement and force values correspond to downward displacement imposed 3810 mm (150 in.) from the interface of the beam with the anchorage block.

Beam 1 [Figure 2(a)] was designed to satisfy all provisions for special moment frame beams according to ACI 318-08. The beam hoops [No. 16 (5) at spacing s_h = 279 mm (11 in.)] were each made up of three pieces: a stirrup with seismic hooks, a crosstie at the top to close the hoop, and an additional vertical crosstie to restrain longitudinal bars along the top and bottom faces. The crossties were alternated end-for-end along the length of the beam. The volumetric confinement reinforcement ratio was $\rho'' = 0.31\%$, where ρ'' = volume of vertical legs of hoops divided by volume of the concrete core. This corresponds to a nominal confinement pressure $\rho'' f_{yt} = 0.038 f_c'$, where f_{yt} = 413 MPa (60 ksi) is the specified yield stress of the steel used for the transverse reinforcement and f_c' = 34 MPa (5 ksi) is the specified compressive strength of concrete. In Beam 2 [Figure 2(b)], the hoop spacing s_h was reduced to 152 mm (6 in.), corresponding to a volumetric reinforcement ratio $\rho'' = 0.57\%$ and nominal confinement pressure $0.068 f_c'$. Longitudinal reinforcement in both beams was identical.

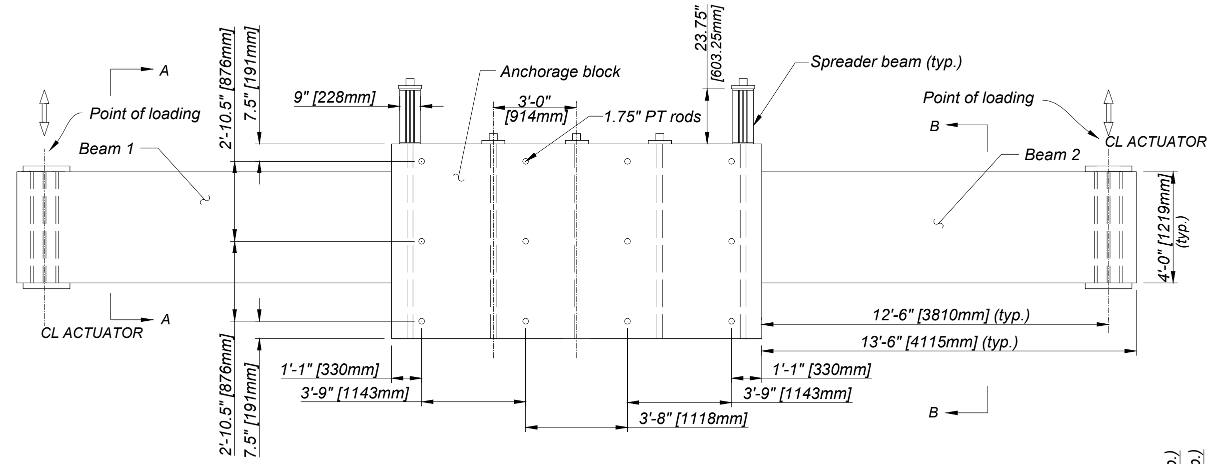

a) BEAMS 1 AND 2 ELEVATION

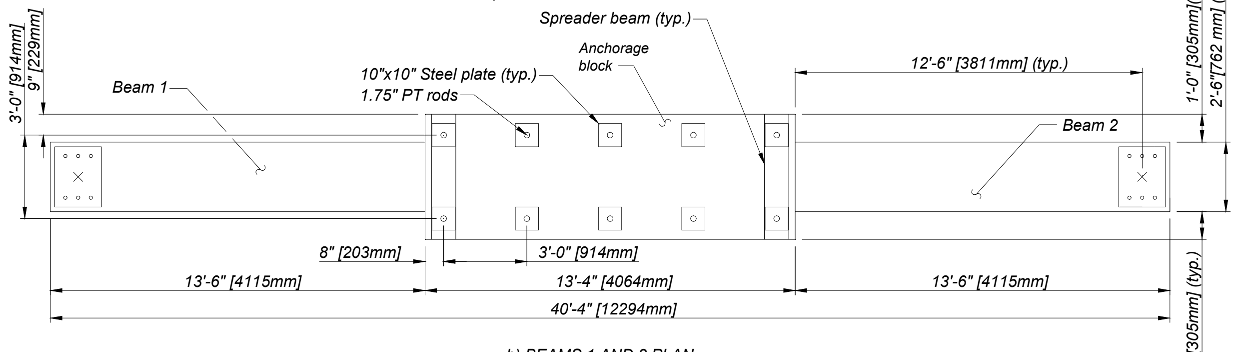

b) BEAMS 1 AND 2 PLAN

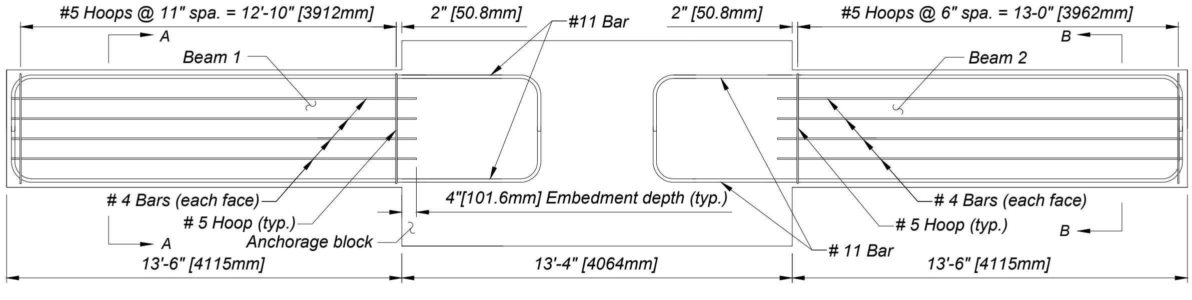

c) BEAM REINFORCEMENT

Figure 1 (a) Side view of the two beams; (b) plan view of the two beams; and (c) beam reinforcement details (25.4 mm = 1 in.).

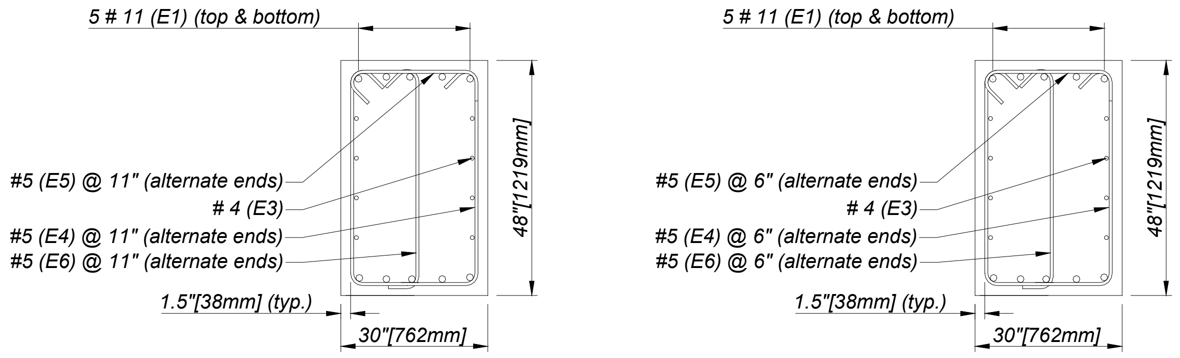

a) SECTION A-A
BEAM 1 CROSS SECTION

b) SECTION B-B
BEAM 2 CROSS SECTION

Figure 2 **Cross sections of Beams 1 and 2 including reinforcing steel details. (25.4 mm = 1 in.).**

1.3 DESCRIPTION OF MATERIALS USED IN CONSTRUCTION

1.3.1 Concrete

Normal-weight concrete was used, with pea gravel (not crushed) as the maximum size aggregate, with target compressive strength of 34 MPa (5 ksi). A total of 19.6 cubic meters (25.6 cubic yards) of concrete was required for construction of the two beam specimens and the reaction block. Three batches of concrete were used; 18 standard 152 mm (6 in.) × 305 mm (12 in.) cylinders were cast for material testing. The first batch was cast mainly on the bottom of the reaction block and a portion of the bottom part of both beams. The second batch was cast over the middle portion of the beams and the reaction block, and the third batch topped off the remaining part of the block and the beams. Table 1 summarizes the compressive strength results obtained at 28, 60, and 86 days after casting for each of the three concrete batches. The last two tests were conducted on the days the experiments took place for Beams 1 and 2, respectively.

The 28-day strength test included 9 cylinders, three for each batch. Compressive strengths for the three batches ranged from 36.0 to 38.4 MPa (5.23 to 5.58 ksi), with average of 36.8 MPa (5.34 ksi).

Testing of the first beam took place 60 days after casting the beams and cylinders, at which time two cylinders were tested for each concrete batch. Their corresponding stress-strain relations are plotted in Figure 3. The labeling convention for each curve is "mNo. - No.", where "mNo." signifies batch number, and "-No." signifies specimen number. For example, "m2-1" stands for specimen 1 of batch number 2. Average compressive strength calculated for the six cylinders was f_c' = 40.0 MPa (5.8 ksi), and the average strain at maximum compressive strength was calculated to be ε_o = 0.3%.

Testing of the second beam took place 86 days after casting and the remaining three cylinders were tested on this day (one for each concrete batch). The stress-strain curves for these three specimens are plotted in Figure 3. The calculated average compressive strength was f_c' = 42.3 MPa (6.1ksi). Again, the average strain at maximum compressive strength was ε_o = 0.3%.

Table 1 28-day, 60-day, and 86-day concrete compressive strengths.

Concrete Age	Batch	Compressive strength of concrete f_c', MPa (ksi)				
		Specimen 1	Specimen 2	Specimen 3	Average	Average
28 days	1	37.3 (5.41)	35.5 (5.15)	35.7 (5.17)	36.1 (5.24)	36.8 (5.34)
	2	36.3 (5.27)	36.2 (5.25)	35.6 (5.17)	36.0 (5.23)	
	3	38.6 (5.60)	39.0 (5.66)	37.7 (5.48)	38.4 (5.58)	
60 days	1	39.2 (5.69)	39.1 (5.68)	-	39.2 (5.69)	40.1 (5.82)
	2	38.3 (5.55)	39.0 (5.66)	-	38.6 (5.61)	
	3	41.9 (6.09)	43.1 (6.26)	-	42.5 (6.17)	
86 days	1	40.7 (5.91)	-	-	40.7 (5.91)	42.3 (6.13)
	2	40.4 (5.87)	-	-	40.4 (5.87)	
	3	45.8 (6.65)	-	-	45.8 (6.65)	

Note: Beam 1 was tested at concrete age of 60 days. Beam 2 was tested at concrete age of 86 days.

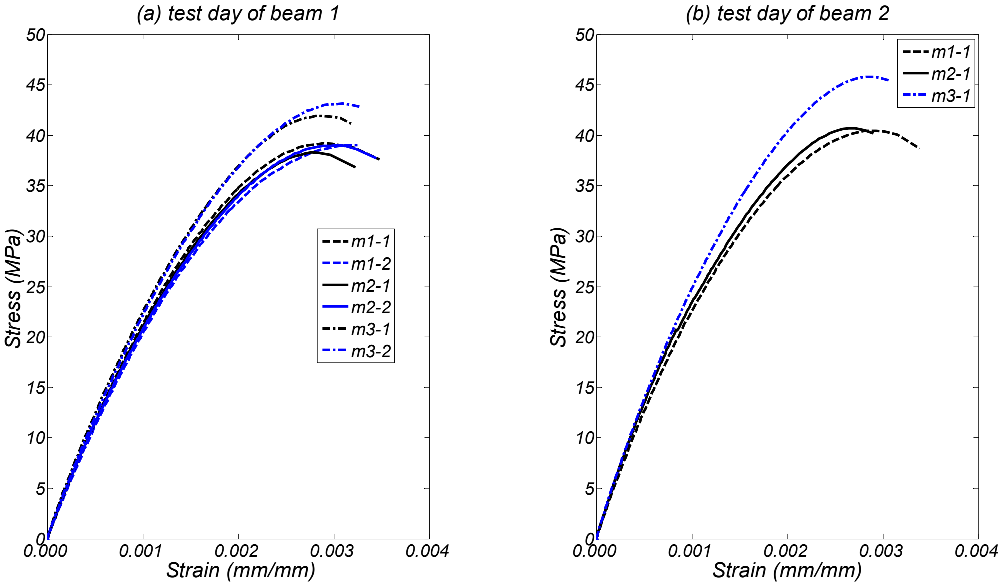

Figure 3 **Compressive stress-strain relationship of cylinders: (a) test day of Beam 1 (60 days); and (b) test day of Beam 2 (86 days). (1 ksi = 6.895 MPa, 1 in. = 25.4 mm).**

1.3.2 Steel

The longitudinal reinforcement consisted of five No. 36 (11) bars at the top and bottom of the beam. The transverse reinforcement consisted of No. 16 (5) reinforcing bars. Type ASTM A706

Grade 60 steel was used for both the longitudinal and transverse reinforcement. Three steel deformed bars were tested for each of the two reinforcement sizes. Figure 4 plots the measured stress-strain relations. As can be seen in Figure 4(a), the No. 16 (5) reinforcement did not display a yield plateau. The average yield stress was f_y = 455 MPa (66 ksi). The three coupons reached an average maximum stress of f_u = 710 MPa (103 ksi).

For the No. 11 longitudinal bars, the average yield stress was f_y = 503 MPa (73 ksi). A well-defined yield plateau developed for all three specimens, with the average strain at the onset of strain hardening equal to ε_{sh} = 1.2% [Figure 4(b)]. Maximum measured stress in steel had an average of f_u = 723 MPa (105 ksi).

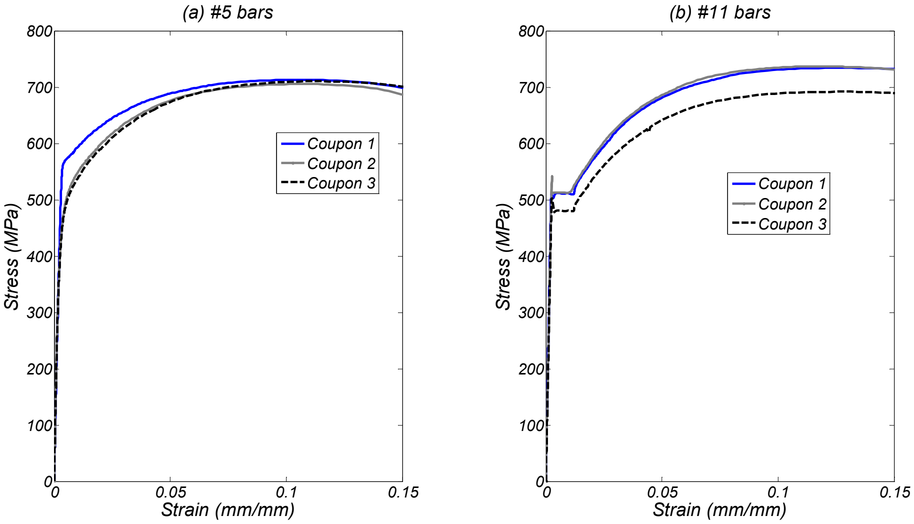

Figure 4 **Tension stress-strain relationship of steel coupon tests: (a) No. 16 (5) bars used for the stirrups; and (b) No. 36 (11) bars used for the longitudinal reinforcement. (25.4 mm = 1 in., 1 ksi = 6.895 MPa).**

1.4 INSTRUMENTATION

The instrumentation of the test specimens included displacement transducers [linear variable differential transformers (LVDTs)] connected between steel rods attached to the concrete, which extended through the cover and approximately 40 mm (1.5 in.) into the concrete core at the top, side, and bottom faces of the specimen. Strain gauges were attached to the reinforcing steel at selected locations. In addition, displacement transducers were placed between the bottom face of the beam and the strong floor at the point where the load was applied. Figure 5 shows a plan view of the displacement transducers at the top and bottom faces of the beam, as well as an elevation view of the transducers attached along the side face of the beams. Two rows of displacement transducers were placed along the top face (TL, TR series) and bottom face (BL, BR series) of each beam. Figure 6 depicts the location of the gauges, and the longitudinal bars and stirrups that were instrumented with strain gauges.

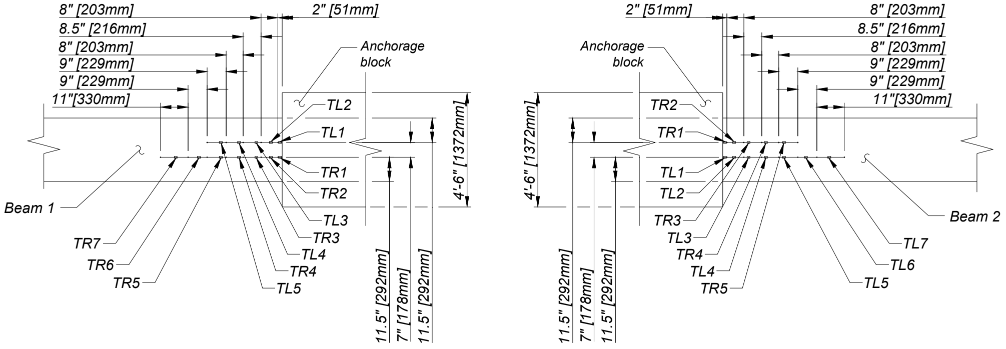

a) LOCATION OF TOP DISPLACEMENT TRANSDUCERS

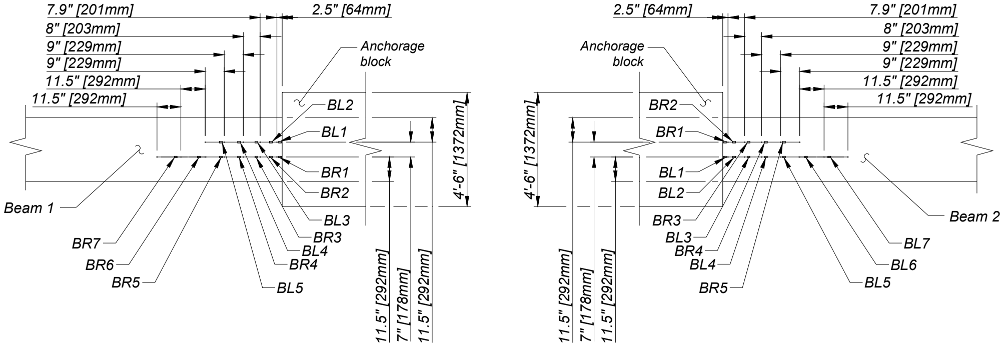

b) LOCATION OF BOTTOM DISPLACEMENT TRANSDUCERS

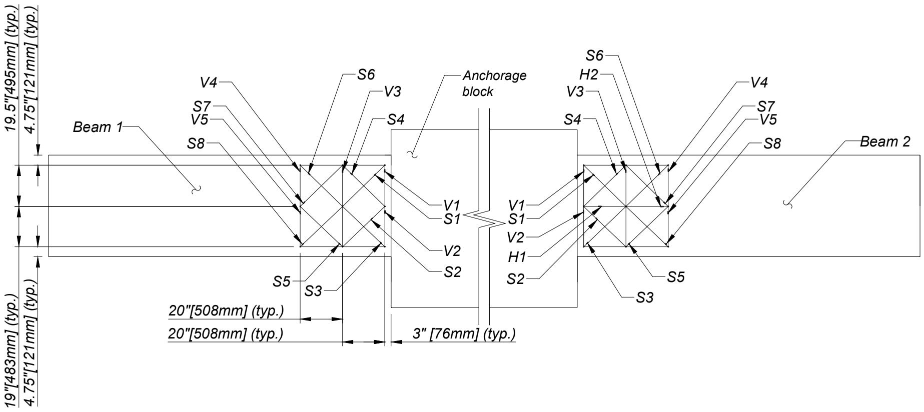

c) LOCATION OF SIDE DISPLACEMENT TRANSDUCERS

Figure 5 Layout of displacement transducers: (a) plan view of top face of the beams; (b) plan view of bottom face of the beams; and (c) elevation view of side face of the beams (25.4 mm = 1 in.).

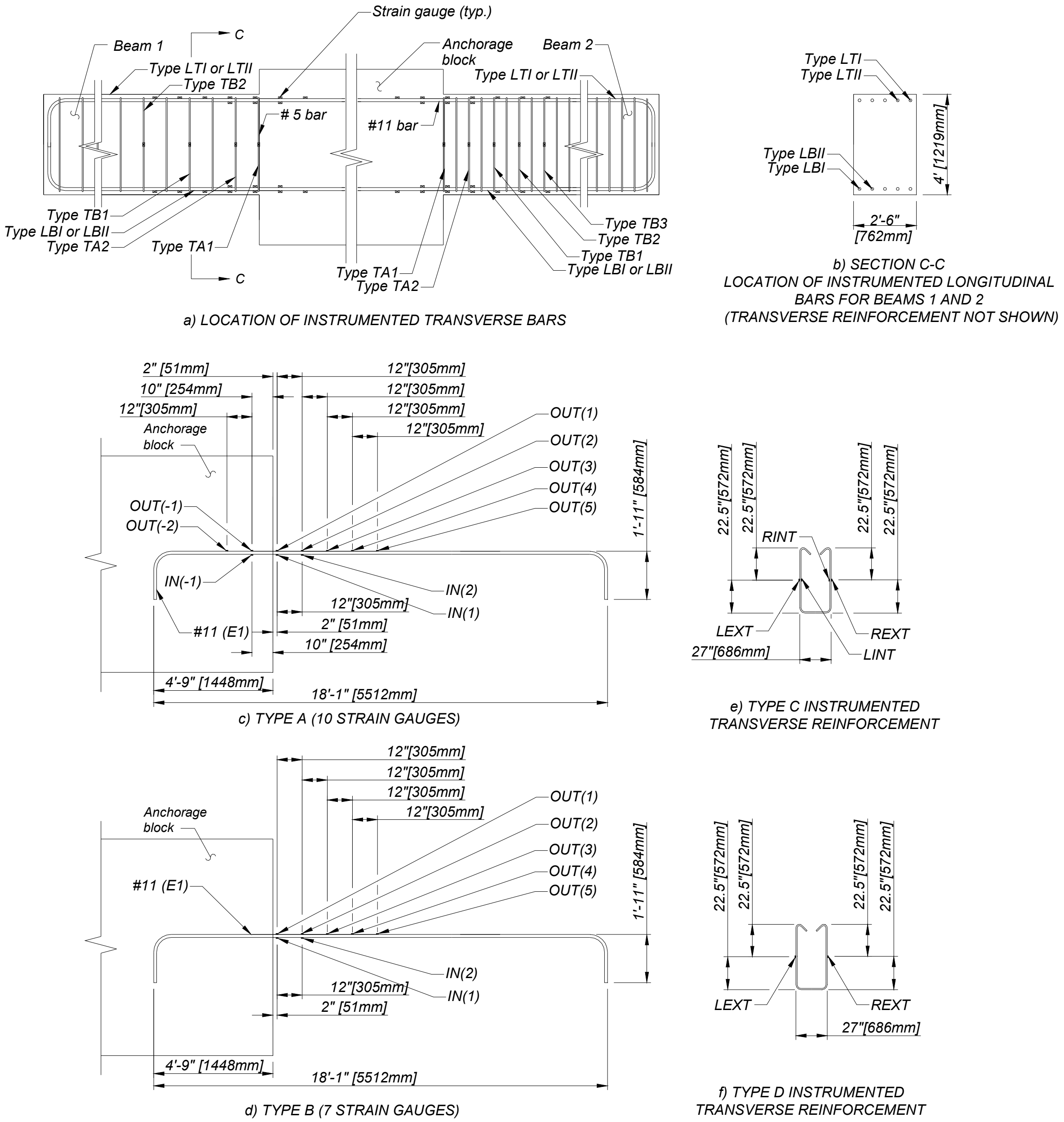

a) LOCATION OF INSTRUMENTED TRANSVERSE BARS

b) SECTION C-C
LOCATION OF INSTRUMENTED LONGITUDINAL
BARS FOR BEAMS 1 AND 2
(TRANSVERSE REINFORCEMENT NOT SHOWN)

c) TYPE A (10 STRAIN GAUGES)

e) TYPE C INSTRUMENTED
TRANSVERSE REINFORCEMENT

d) TYPE B (7 STRAIN GAUGES)

f) TYPE D INSTRUMENTED
TRANSVERSE REINFORCEMENT

Figure 6 **Layout of strain gauges attached on the longitudinal and transverse reinforcement of Beams 1 and 2: (a) location of instrumented hoops; (b) instrumented longitudinal bars; location of gauges attached on longitudinal bars: (c) type A, and (d) type B. Location of strain gauges on stirrups: (e) type C stirrup, and (f) type D stirrup (25.4 mm = 1 in.).**

1.5 TEST PROTOCOL

The displacement test protocol of Beams 1 and 2 is described below. Table 2 lists the displacement amplitude Δ (measured with a displacement transducer connected between the bottom face of the beam and the strong floor), the number of cycles at each displacement amplitude, the equivalent drift ratio Θ (defined as Δ / L, where L = distance from face of anchorage block to point where load was applied and Δ was measured), and the displacement ductility $\mu_\Delta = \Delta / \Delta_y$, where Δ_y is the yield displacement. The yield displacement was calculated as $\Delta_y = \varphi_y L^2 / 3 + \Delta_{sp}$, where φ_y = calculated yield curvature = 2.55×10^{-6} rad/mm, and Δ_{sp} = calculated displacement due to strain penetration at the anchorage block = 5 mm. Yield curvature, which is defined as the curvature corresponding to first yielding of the longitudinal reinforcement, was calculated with moment curvature analysis assuming linear variation of strain through the beam depth. For the values described above Δ_y = 18 mm (0.7 in.). As shown in Table 2, for step 16 of Beam 2 the peak positive and negative displacement were different with the negative indicated in parenthesis.

Table 2 Displacement test protocol (25.4 mm = 1 in.).

	Displacement Δ (mm)		Number of cycles	Drift ratio $\Theta = \Delta / L * 100$		Displacement ductility $\mu_\Delta = \Delta / \Delta_y$	
Step	Beam 1	Beam 2		Beam 1	Beam 2	Beam 1	Beam 2
1	3	3	3	0.07	0.07	0.2	0.2
2	7	6	3	0.18	0.16	0.4	0.3
3	11	11	3	0.28	0.28	0.6	0.6
4	14	15	3	0.38	0.40	0.8	0.9
5	31	33	3	0.81	0.87	1.7	1.9
6	46	46	2	1.2	1.2	2.6	2.6
7	13	13	1	0.33	0.33	0.7	0.7
8	69	69	2	1.8	1.8	3.9	3.9
9	13	13	1	0.33	0.33	0.7	0.7
10	103	109	2	2.7	2.9	5.8	6.2
11	13	13	1	0.33	0.33	0.7	0.7
12	139	147	2	3.6	3.9	7.8	8.3
13	13	13	1	0.33	0.33	0.7	0.7
14	194	203	1	5.1	5.3	10.9	11.4
15	13	13	1	0.33	0.33	0.7	0.7
16	210	222 (-244)	1	5.5	5.8 (-6.4)	11.8	12.5 (-13.7)

1.6 BEAM 1 TEST: RESPONSE OVERVIEW AND OBSERVATIONS

This section presents the main observations from the test of Beam 1 designed according to the ACI 318-08 provisions, with No. 16 (5) hoops at 279 mm (11 in.) spacing. Figure 7(a) shows the measured relations between resisting beam moment and beam drift ratio Θ for all the cycles. Figure 7(b) shows the response up to the peak drift ratio up to 2.7%, where strength degradation due to buckling of the longitudinal reinforcement was observed. The reported moment is the sum of moments due to actuator force and beam self-weight, assuming a self-weight of the beam equal to 90.1 kN (20.3 kips). The initial deflection due to self-weight of the beam is negligible and is not accounted for in the reported drift values.

Figure 7 shows the calculated probable flexural strength, M_{pr} = 2870 kN-m (2110 kip-ft), calculated in accordance with Chapter 21 of ACI 318-08. As required by ACI 318, M_{pr} is calculated for nominal (specified) concrete compressive strength of 34 MPa (5000 psi) and elasto-plastic steel stress-strain relation with yield stress taken equal to 1.25 times specified yield stress [that is, 1.25 x 414 MPa = 517 MPa (75 ksi)]. Skin reinforcement is not included in the strength calculation because the skin reinforcement is not fully developed into the anchor block [Figure 1(c)]. Consideration of the skin reinforcement, if assumed fully developed into the anchor block, would result in a 9% increase in M_{pr}. The peak measured moment was equal to 2850 kN–m (2100 kip-ft), which is very close to the calculated M_{pr}.

The test specimen developed cracks primarily perpendicular to the longitudinal axis (attributable to moment) and cracks inclined to the longitudinal axis (attributable to shear), see Figure 8. The peak shear force of 739 kN (164 kips) corresponds to a nominal shear stress of 0.83 MPa (121 psi), or $0.13\sqrt{f_c'}$ MPa ($1.6\sqrt{f_c'}$ psi) using measured compressive strength. According to ACI, for beams of special moment frames, the nominal shear strength within the twice the member thickness from the column face (that is, the intended plastic hinge zone) is calculated assuming no contribution from concrete, that is, with $V_c = 0$. Thus, using the specified material properties, the nominal shear strength for this beam is $V_n = V_s = A_v f_{yt} d/s$ = 1020 kN (229 kips). If the shear strength is defined as $V_n = V_c + V_s$, where $V_c = 0.17\sqrt{f_c'} b_w d,$ MPa ($2\sqrt{f_c'} b_w d,$ psi), then the calculated nominal shear strength is V_n = 1870 kN (421 kips). As shown in Figure 8, visible movement along steeply inclined cracks resulted in horizontal cracks along the longitudinal reinforcement (initially attributable to dowel action, but possibly also influenced by bond stress and initiation of longitudinal bar buckling).

The test specimen sustained the first half cycle to 2.7% drift ratio without evident failure. Upon deformation reversal during the second half cycle, however, all the top longitudinal bars buckled extensively, creating a “crack cave” that remained open for all the remaining cycles (Figure 9). During the second cycle with a peak drift ratio of 2.7%, the maximum resistance of the beam reduced by 30% (Figure 7). For the next two cycles with drift ratio amplitudes 3.6% and 5.1%, the resistance of the beam reduced to 50% of the peak resistance. As explained subsequently in the section on measured local response, buckling also occurred at the bottom of the beam during cycle with 2.7% peak drift ratio. Bulging of the bottom face of the beam is visible in Figure 10.

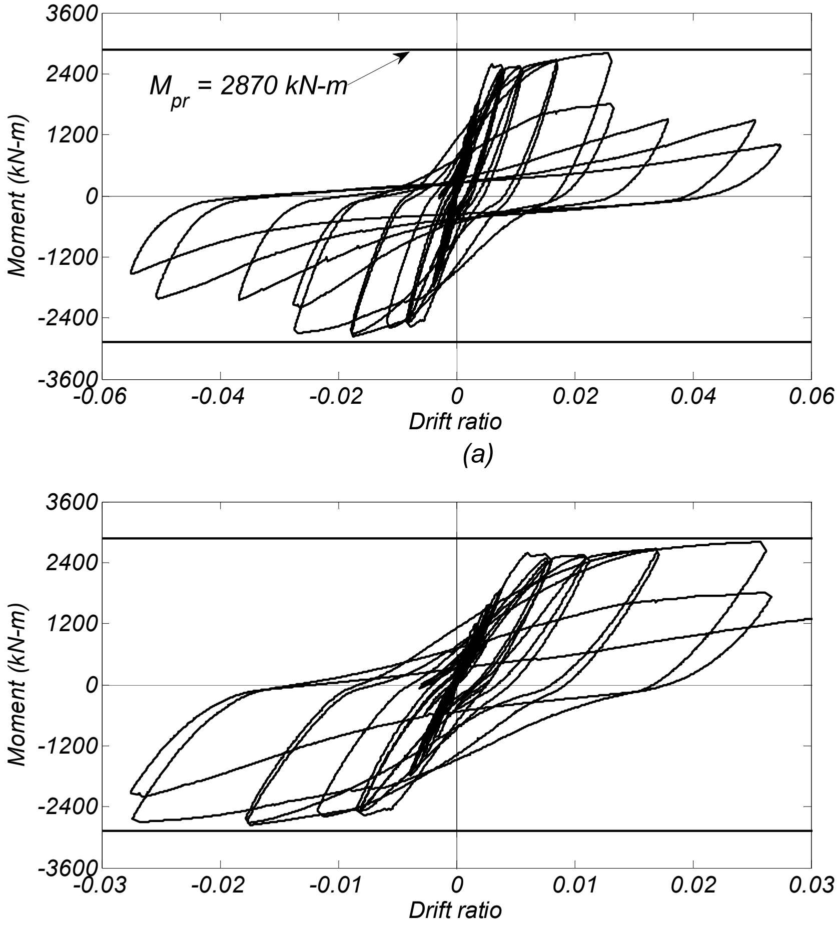

(a)

(b)

Figure 7 **Beam 1: relation between maximum beam moment and drift ratio; (a) all cycles; and (b) cycles up to and including a drift ratio of 2.7% (1 kN-m = 0.737 kip-ft).**

Figure 11 shows the crack pattern at the top of the beam for downward displacement of the beam. Wide cracks developed from the fixed end along a length of the beam equal to approximately half the beam depth. These major cracks were about 250 mm (10 in.) apart, which is close to the hoop spacing [279 mm (11 in.)] of this beam. After longitudinal reinforcement buckling occurred, shearing deformations contributed significantly to the total beam displacement and were especially notable for downward displacement (Figure 12 through Figure 14).

Figure 8 Beam 1: damage state at the beginning of cycle in which buckling occurred (first cycle with peak drift ratio = 2.7%, instantaneous drift ratio = -0.9%).

Figure 9 Beam 1: buckling of the top longitudinal bars (first cycle with peak drift ratio = 2.7%, instantaneous drift ratio = -2.7%).

Figure 10 Beam 1: buckling of the top longitudinal bars (first cycle with peak drift ratio = 2.7%, instantaneous drift ratio = 2.7%).

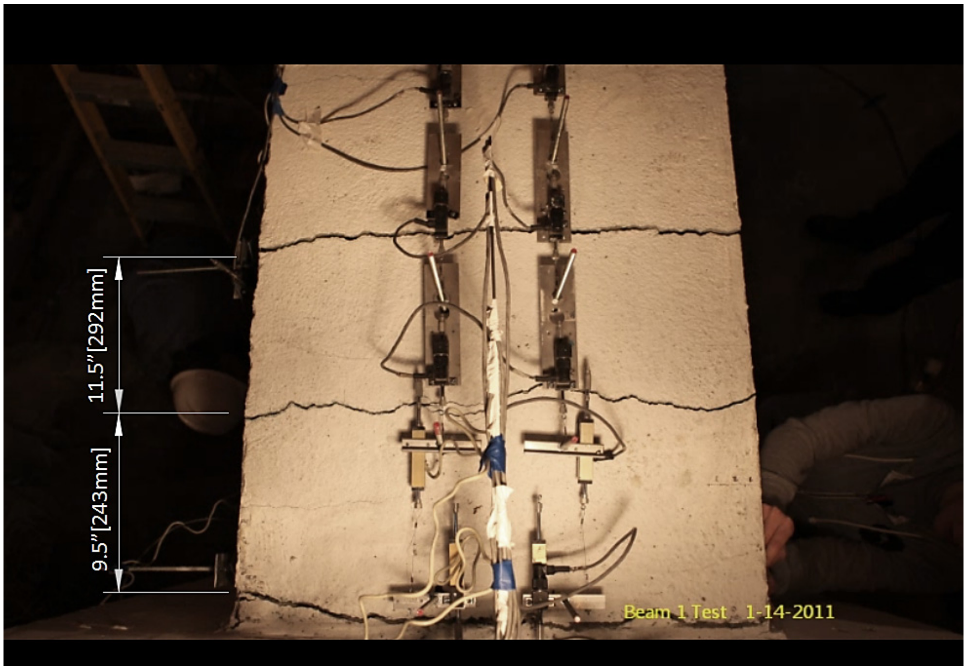

Figure 11 Beam 1:Top view of damage state (first cycle with peak drift ratio = 2.7%, instantaneous drift ratio = 2.7%).

Figure 12 Beam 1: overview after the buckling of the top longitudinal bars (first cycle with peak drift ratio = 2.7%, instantaneous drift ratio = -2.7%).

Figure 13 Beam 1: overview at the maximum positive displacement (cycle with peak drift ratio = 5.5%, instantaneous drift ratio = 5.5%).

Figure 14 Beam 1: overview at the maximum negative displacement (cycle with peak drift ratio= -5.5%, instantaneous drift ratio= -5.5%).

1.7 BEAM 1 TEST: MEASURED LOCAL RESPONSE

Measured local responses include reinforcement strains, slip of reinforcement from the anchorage block due to strain penetration, and local deformations along the top, bottom, and side faces of the beams. Strains were measured by electrical resistance strain gauges attached to reinforcement; LVDTs were connected to steel instrumentation rods that were anchored into the concrete, enabling measurement of deformations between fixed points. Initially, measurements from these LVDTs were used to estimate average longitudinal strains, defined as the elongation measured by an LVDT divided by its gauge length. After buckling of longitudinal reinforcement initiated, however, distortion of the concrete cover resulted in displacement and rotation of the steel instrumentation rods, such that the resulting measurement no longer represented the average strain correctly. Nonetheless, these instruments proved valuable in identifying the onset and extent of buckling. For all reported strain measures, positive strain indicates elongation.

The response of this beam during later stages of testing was characterized by extensive buckling of the longitudinal reinforcement that initiated during the cycles with 1.8% peak drift ratio and became more extensive during the cycles with 2.7% peak drift ratio. The onset of buckling can be identified by examining the data from the LVDTs spanning across steel instrumentation rods attached to the top and bottom faces of the beam. Figure 15 plots the LVDT readings, normalized to their respective gauge lengths, for peak displacement amplitudes during various displacement cycles. For LVDTs attached to the top face (TL series and TR series), data are presented for upward displacement peaks, while for LVDTs attached to the bottom face (BL series and BR series), data are presented for downward displacement peaks. Along the top face, the data show an "elongation bulge" associated with buckling of the top longitudinal reinforcement, which becomes apparent for the 1.8% drift cycles, and is centered around 500 mm (20 in.) from the beam end. Along the bottom face, the data show a similar bulge associated with buckling of the bottom longitudinal reinforcement, which initiated during the cycles with 1.8% peak drift ratio and became more noticeable for the 2.7% drift cycles, and is centered around 381 mm (15 in.) from the beam end.

Figure 16 plots the histories of two LVDTs spanning the center of the buckling region for the top and bottom of the beam. It is noteworthy that the deformation measurements indicate that only tensile strains develop throughout the history. Apparently, cracks that open under flexural tension never fully close under flexural compression. For loading in the direction that would tend to result in flexural compression, the gauges indicate partial crack closure (due to compression) except for the cycle in which significant buckling occurs, for which case the outward buckle results in a tensile reading of the displacement gauge.

Strains were measured with strain gauges attached on the longitudinal and transverse reinforcement. Figure 17 compares strain histories inferred from the displacement transducers and those “measured” by the strain gauges for select gauges. Figure 17(a) and (b) show similar trends in peak tensile strains, although values differed notably during some portions of the history. The average vertical strains of the side face of the beam, measured with LVDTs (Figure 5), are shown in Figure 17(c). The readings suggest transverse strains exceeding 0.2%, corresponding to the yield strain for the transverse reinforcement. Figure 17(d) shows strains up to 0.35% were measured using strain gauges attached to the stirrups, suggesting that stirrup yielding may have occurred. The majority of these strain gauges failed after measuring a strain around 2%, such that strains were not recorded during the largest displacement cycles, including those for which buckling was observed.

Figure 18 depicts the strain histories of a top longitudinal bar at 51 mm (2 in.) from the fixed end of the beam. Note that strain gauges were located at both the top surface and the bottom surface of the bar at this location. For the cycles with a peak drift ratio up to 2.7%, similar peak strains were measured on the top surface (Gauge LTI-OUT1, Figure 6) and the bottom surface (Gauge LTI-IN1, Figure 6) of the bar. After this drift ratio, where significant buckling initiated, the measured strains on top and bottom of the bar differed significantly, apparently because of curvature as the bar buckled. Note that at -5.1% drift ratio, the strain at the top and the bottom of the reinforcing bar was 5.9%, and -2%, respectively.

As shown in Figure 5, displacement transducer TL1 measured displacement of the “fixed end” of the beam relative to the anchorage block. In effect, this instrument measured slip of the longitudinal reinforcement from the block. Figure 19 shows the measured slip versus drift ratio. The contribution of fixed-end rotation at the total drift ratio of the specimen was significant. For example, at 2.7% drift ratio the measured displacement of TL1 was 15.5 mm (0.6 in.). Assuming zero deformation at the bottom of the beam, this corresponds to a rotation angle of 15.5/1219 = 1.27%, or 47% of the total drift ratio.

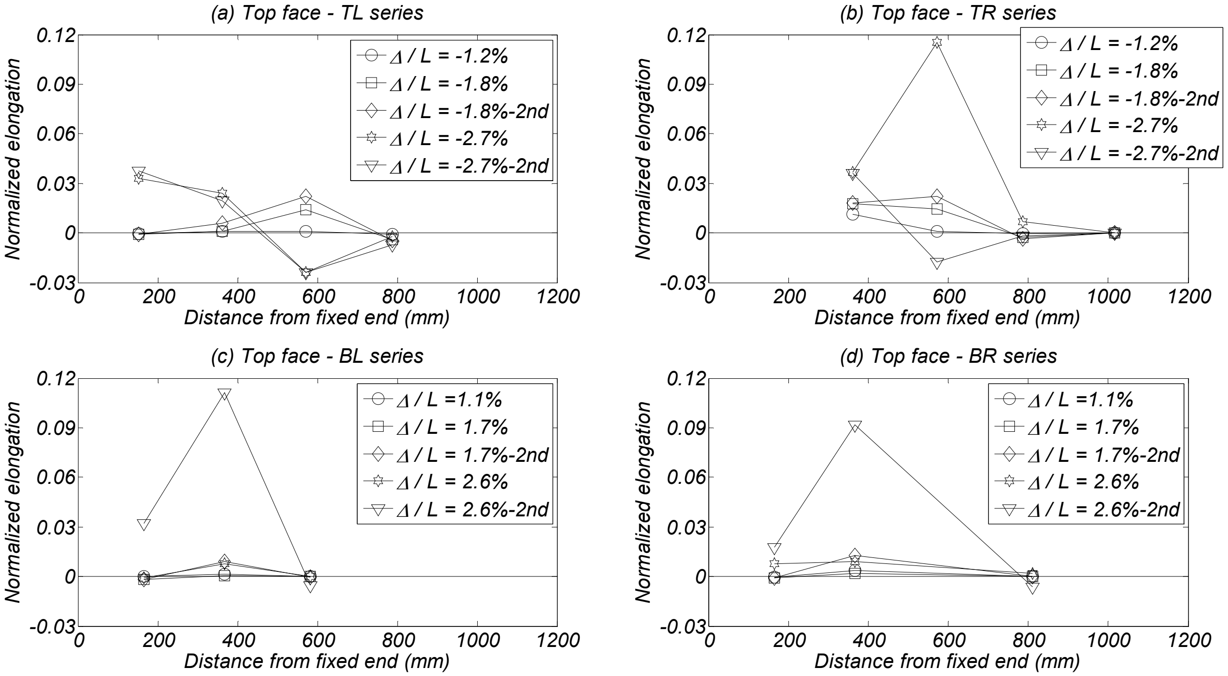

Figure 15 **Beam 1: profiles of elongation measured between steel instrumentation rods normalized to gauge length. Note: negative elongation corresponds to shortening.**

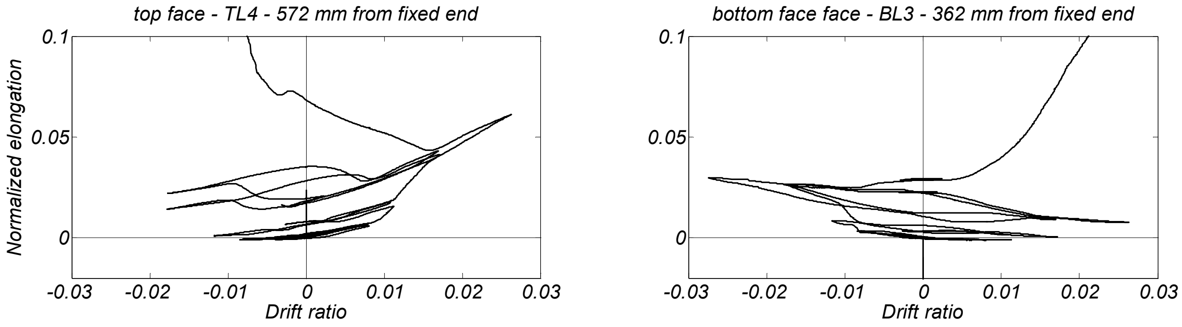

Figure 16 **Beam 1: histories of elongation measured between steel instrumentation rods normalized to gauge length. Response only up to peak drift ratio of 2.7% is shown.**

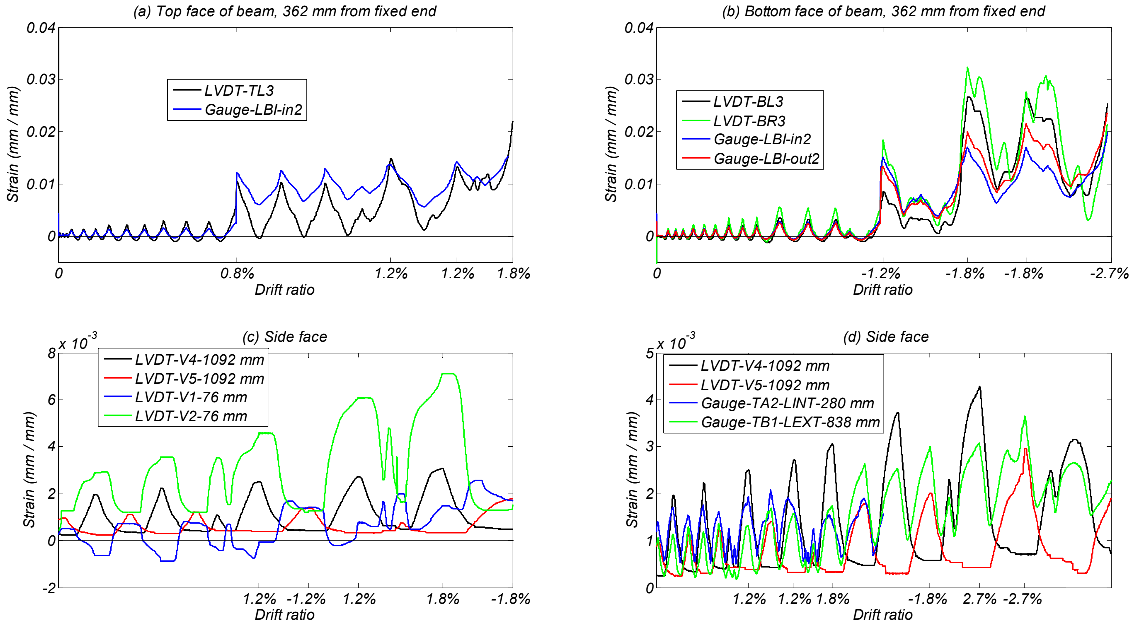

Figure 17 Beam 1: histories of strain measured using LVDTs and strain gauges: (a) top face; (b) bottom face; (c) side face; and (d) side face. Characteristic instants of peak drift ratios are shown in the *x*-axis.

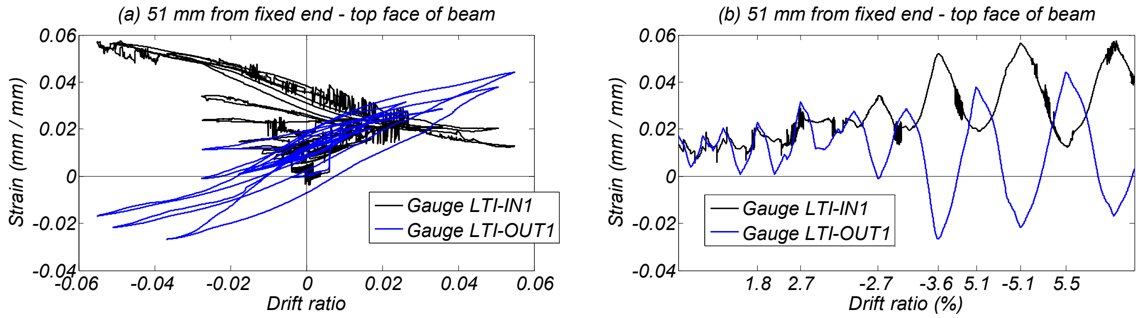

Figure 18 Beam 1: strains measured with gauges on steel reinforcement 51 mm (2 in.) from the face of the beam (top and bottom of the reinforcing bar); (a) presented as strain versus drift ratio; and (b) history of strains.

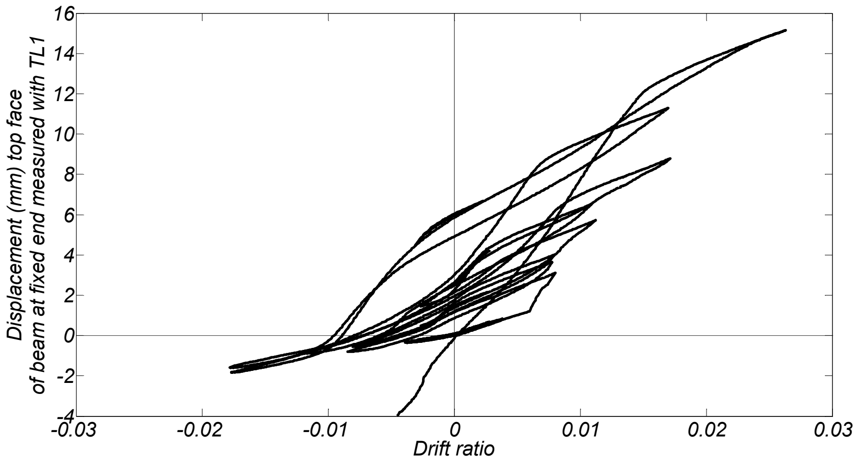

Figure 19 Beam 1: drift ratio due to fixed-end rotation versus total drift ratio.

1.8 BEAM 2 TEST RESPONSE OVERVIEW AND OBSERVATIONS

This section presents the main observations from the test of Beam 2, designed according to ACI 318-08 provisions, but with No. 16 (5) hoop spacing reduced to 152 mm (6 in.). Figure 20(a) and (b) illustrate the beam moment versus drift ratio response up to 6.4%, and 3.9% drift ratio, respectively. Significant longitudinal bar buckling initiated upon reversal from peak drift during the second cycle with 2.9% peak drift ratio. Bar buckling became excessive and obvious in the measured moment-drift response in the cycle with 3.9% peak drift ratio.

For this beam, the calculated value of M_{pr} is that same as that obtained for Beam 1 (because M_{pr} is based on nominal properties), resulting in M_{pr} = 2870 kN-m (2110 kip-ft). The measured maximum moment was M_{max} = 3148 kN-m, which is 10% greater than the M_{pr}. The peak measured shear force of 805 kN (181 kips) corresponds to a nominal shear stress of 0.90 MPa (133 psi), or $0.14\sqrt{f_c'}$ MPa ($1.7\sqrt{f_c'}$ psi) using measured compressive strength. Nominal shear strength calculated using specified material properties in accordance with ACI 318 is $V_n = V_s = A_v f_{yt} d/s$ = 1870 kN (420 kips). Here, the assumption was that $V_c = 0$. If the strength is defined as $V_n = V_c + V_s$, with $V_c = 0.17\sqrt{f_c'} b_w d,$ MPa $(2\sqrt{f_c'} b_w d,$ psi), then calculated nominal shear strength is V_n = 2720 kN (612 kips). The behavior of Beam 2 was similar to Beam 1 in the early cycles, including development of cracks apparently associated with flexure, shear, and dowel action. Figure 21 shows the visible condition of the beam during the second cycle to 2.9% drift ratio.

During the second cycle to a drift ratio of 2.9%, as the beam drift was being reversed from positive drift to negative drift, horizontal cracks associated with initiation of bar buckling and top bar dowel action grew noticeably (see Figure 21 and Figure 22). Figure 23 shows the damage state, as viewed from the top, at the beginning of the negative half of this cycle. Figure 24 shows the same view but at the peak negative drift. Bulging of the top surface of the beam was noted due to buckling of the top reinforcement. Buckling of the top longitudinal reinforcement became more apparent during the following loading cycle to a peak drift ratio of 3.9%. As shown in Figure 25, compression zone crushing of concrete extended deep into the beam at this time. The peak resistance of the beam after longitudinal bar buckling was 10% less than the maximum strength for this direction of loading.

Buckling of the bottom longitudinal bars became obvious during a cycle with a peak drift of 5.3% (Figure 26 and Figure 27).

During the last loading cycle, corresponding to a 5.8% peak positive drift ratio, one of the top corner bars fractured (Figure 28) at a beam drift ratio of 0.7%, resulting in a sudden strength loss in the beam of approximately 38%. The peak resistance for this cycle was 43% lower than for the previous downward cycle and 48% lower than the peak strength for loading in this direction. Figure 29 through Figure 31 show overall views of Beam 2 during large displacement cycles.

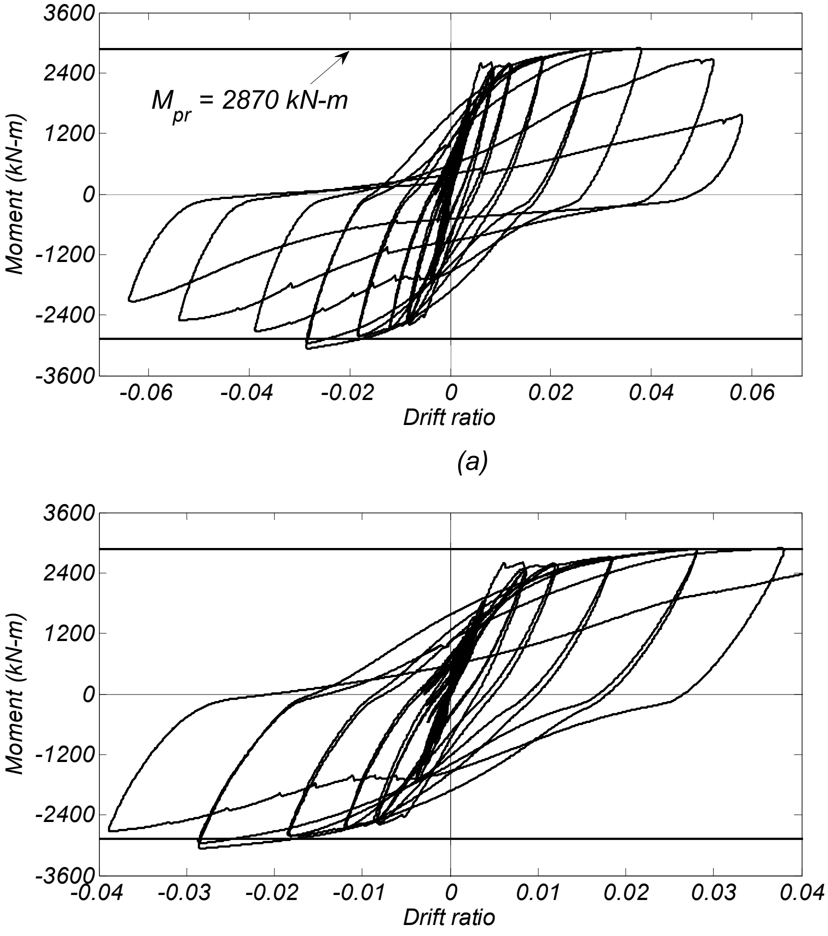

(a)

(b)

Figure 20 **Beam 2: relation between maximum beam moment and beam drift ratio; (a) all cycles; and (b) cycles up to and including a drift ratio of 3.9% (1 kN-m = 0.737 kip-ft).**

Figure 21 Beam 2: damage state during the second cycle with a peak drift ratio of 2.9% (instantaneous drift ratio = -2.0%).

Figure 22 Beam 2: damage state during the second cycle with a peak drift ratio of 2.9% (instantaneous drift ratio = -2.9%).

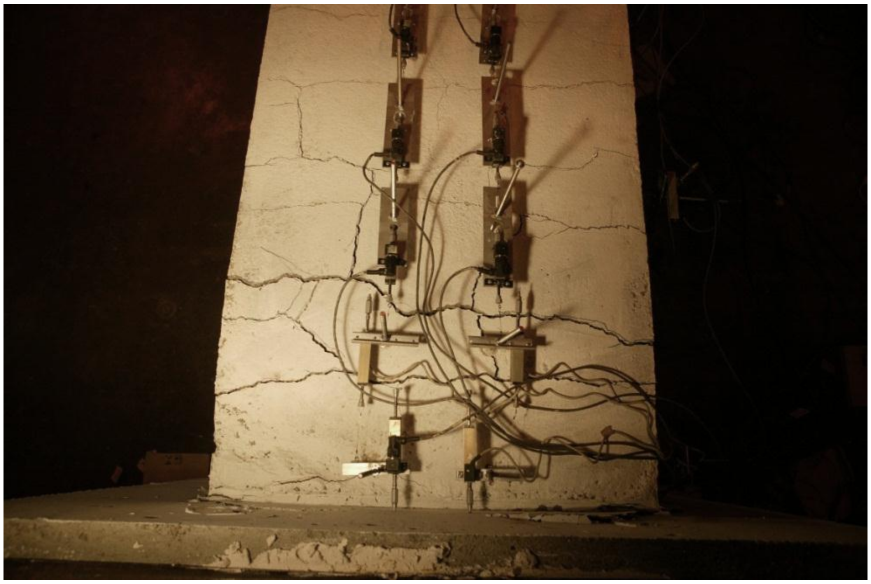

Figure 23 Beam 2: top view of damage state (first cycle with peak drift ratio = 2.9%, instantaneous drift ratio = -0.6%).

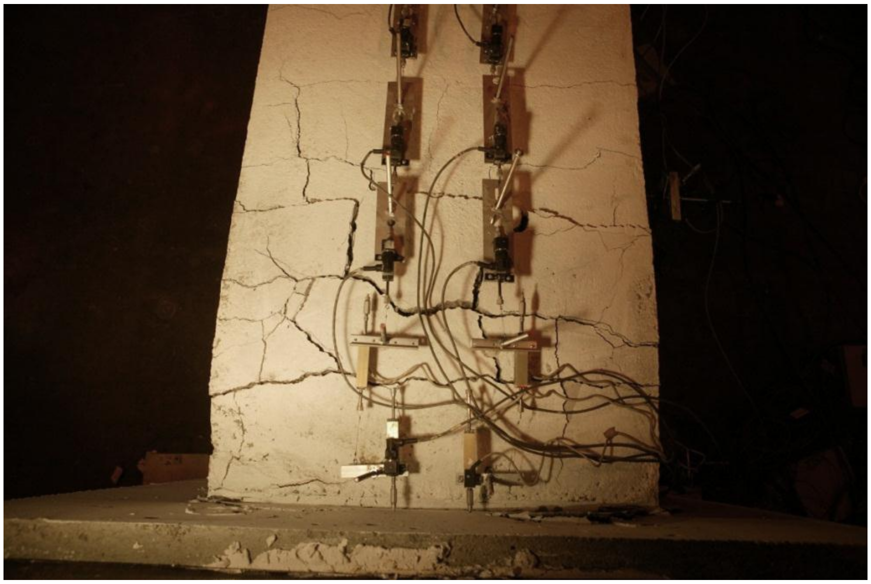

Figure 24 Beam 2: top view of damage state (first cycle with peak drift ratio = 2.9%, instantaneous drift ratio = -2.9%).

Figure 25 Beam 2: buckling of the top longitudinal reinforcement (first cycle with peak drift ratio = 3.9%, instantaneous drift ratio = -3.9%).

Figure 26 Beam 2: damage state at the beginning of the displacement cycle in which bottom longitudinal reinforcement buckled (maximum drift ratio = 5.3 %, instantaneous drift ratio = 0.8%).

Figure 27 Beam 2: buckling of bottom longitudinal reinforcement (instantaneous drift ratio equal to peak cycle drift ratio of 5.3%).

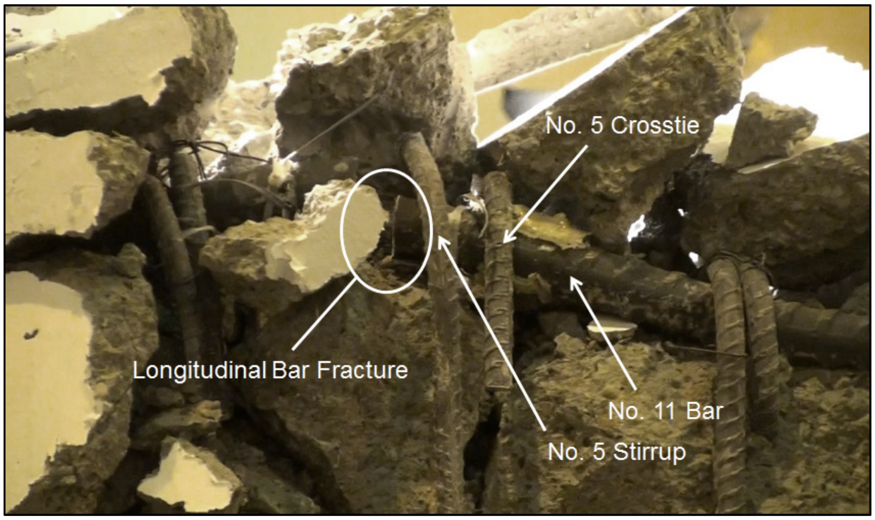

Figure 28 Beam 2: rupture of a top longitudinal bar (instantaneous drift ratio = 0.7 %, peak cycle drift ratio = 5.8 %).

Figure 29 Beam 2: overview at the instant of top reinforcement buckling (first cycle with peak drift ratio = 3.9%, instantaneous drift ratio = -3.9%).

Figure 30 Beam 2: overview at the maximum positive displacement (drift ratio = 5.8%).

Figure 31 Beam 2: overview at the maximum negative displacement (drift ratio = -6.4%).

1.9 BEAM 2 TEST: MEASURED LOCAL RESPONSE

As with Beam 1, the response of this beam during later stages of testing was characterized by extensive buckling of the longitudinal reinforcement. The onset of buckling can be identified by examining the data from the LVDTs spanning across steel instrumentation rods attached to the top and bottom faces of the beam. Figure 32 plots the LVDT readings, normalized to their respective gauge lengths, for peak displacement amplitudes during various displacement cycles. For LVDTs attached to the top face (TL series and TR series), data are presented for upward displacement peaks, while for LVDTs attached to the bottom face (BL series and BR series), data are presented for downward displacement peaks. Along the top face, the data show an "elongation bulge" associated with buckling of the top longitudinal reinforcement, which becomes apparent for the second set of cycles at 2.9% drift ratio, and is centered around 400 mm (15 in.) from the beam end. Along the bottom face, the data show a similar bulge associated with buckling of the bottom longitudinal reinforcement, which becomes apparent for the 2.9% drift cycles, and is centered around 381 mm (15 in.) from the beam end.

Figure 33 plots the histories of LVDTs spanning the buckling region for the top and bottom of the beam. As with Beam 1, the deformation measurements indicate that only tensile strains develop throughout the history. For loading in the direction that would tend to result in flexural compression, the gauges indicate partial crack closure (due to compression) except for the cycle in which significant buckling occurs, for which case the outward buckle results in a tensile reading of the displacement gauge.

Figure 34 plots histories of LVDTs and strain gauges. Figure 34(a) shows the similar strains measured with BL3 LVDT and a strain gauge LBI-OUT(2) at 363 mm (14.3 in.) and 352 mm (13.86 in.) from the fixed end of the beam, respectively. Figure 34(b) shows the significant difference in the strain measured at the top and bottom of a top longitudinal bar due to bending after the second cycle, with a peak drift ratio of 1.8%. The histories of the vertical displacement transducers V1 to V5 (Figure 5) are shown in Figure 34(c). The strain in the vertical direction at 584mm from the fixed end of the beam began to exceed 0.2% for drift ratio larger than 1.8%. Similar levels of strain were observed 76 mm (3 in.) from the fixed end of the beam but only for negative drift ratios. The strains at 76 mm (3 in.) and 584 mm (23 in.) from the fixed end of the beam reached 0.6% at a drift ratio of 2.9%. The average concrete strain in the vertical direction, measured with LVDTs, at 1092 mm (43 in.) from the fixed end of the beam was similar to the strain in the stirrups measured with gauge TB2, as shown in Figure 34(d).

Fixed-end rotation, Θ_{fe}, due to strain penetration and bond slip of the longitudinal reinforcement in the anchorage block, made a notable contribution to the total drift of the beam. Figure 35 plots the drift ratio due to fixed-end rotation versus total drift ratio of the beam. The fixed end rotation was calculated based on the measurement of instruments TL1, TR1, BL1, and BR1 (Figure 5) as:

$$\Theta_{fe} = \frac{(\Delta_{TL1}+\Delta_{TR1})/2-(\Delta_{BL1}+\Delta_{BR1})/2}{1270} \tag{1}$$

where Δ is the displacement measurement of the LVDTs in mm; 1270 mm (50 in.) is the distance between the top and the bottom LVDTs. For positive drift ratios: 29%, 38%, and 45% of the total drift ratio was due to fixed end rotation at peak drift ratio equal to 2.9% (first cycle), 2.9% (second cycle), 3.9%, respectively. The corresponding contributions for negative drift ratios were 36%, 57%, and 49%.

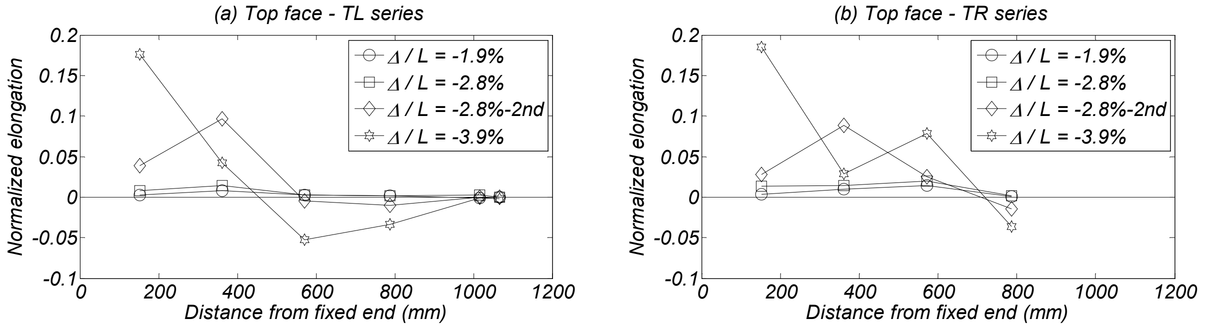
(a) Top face - TL series

(b) Top face - TR series

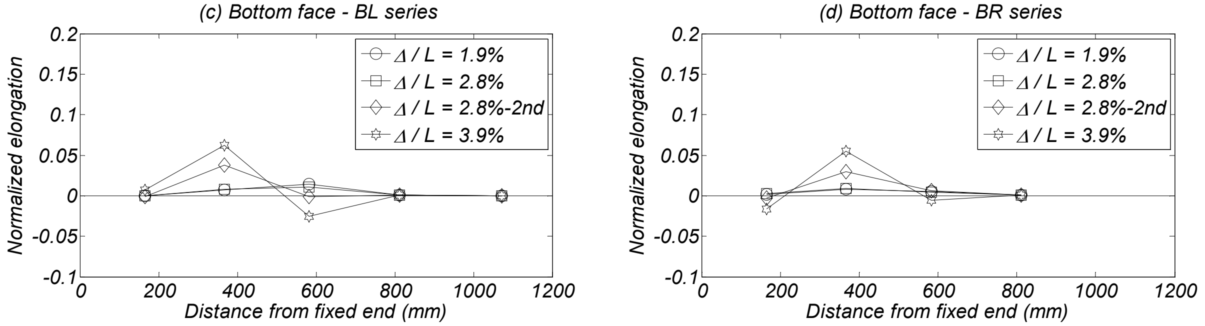
(c) Bottom face - BL series

(d) Bottom face - BR series

Figure 32 **Beam 2: profiles of elongation measured between steel instrumentation rods normalized to gauge length. Note: negative elongation corresponds to shortening.**

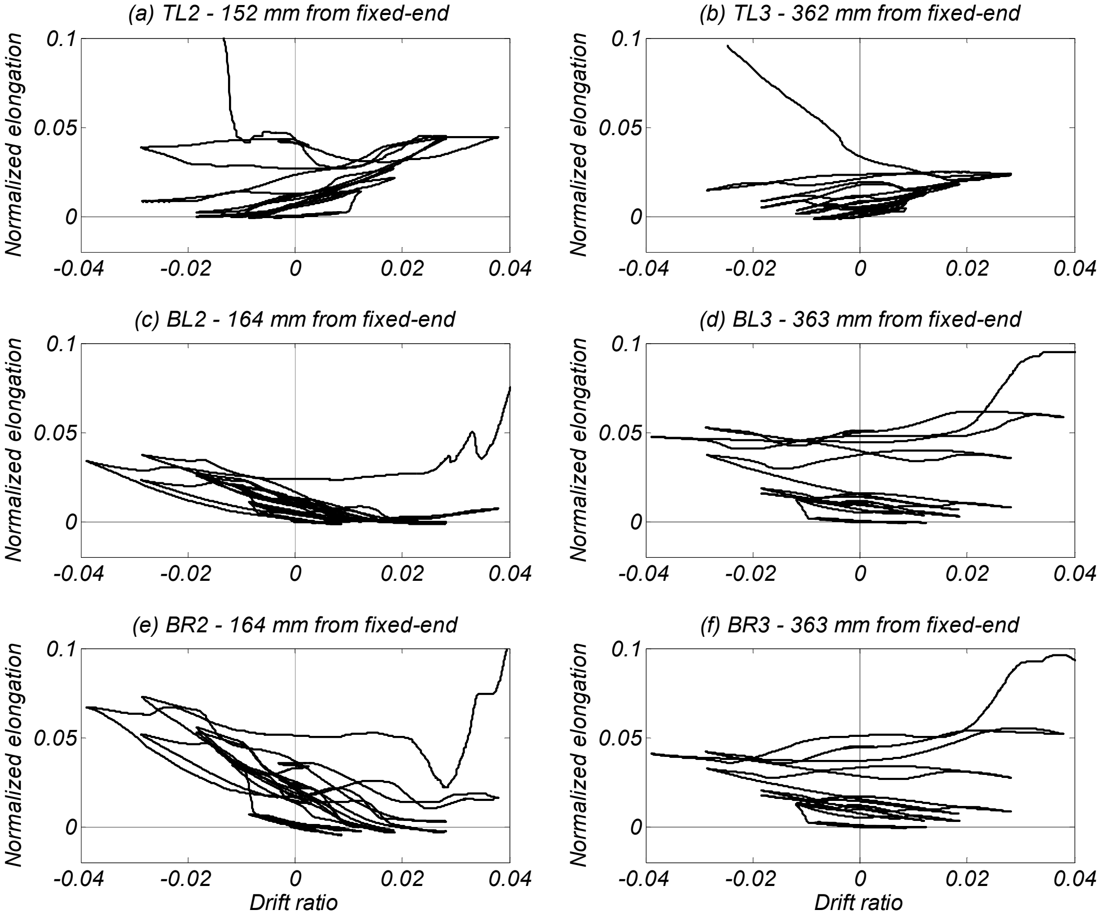

Figure 33 **Beam 2: histories of elongation measured between steel instrumentation rods normalized to gauge length.**

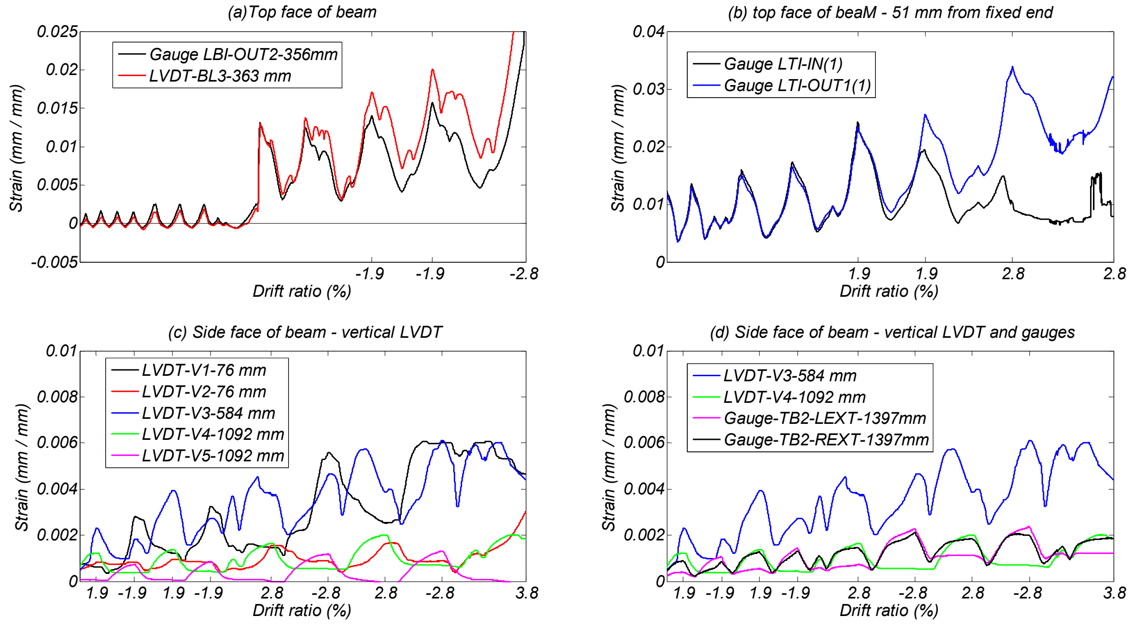

Figure 34 Beam 2: strain histories measured with strain gauges or displacement transducers at different locations of the beam.

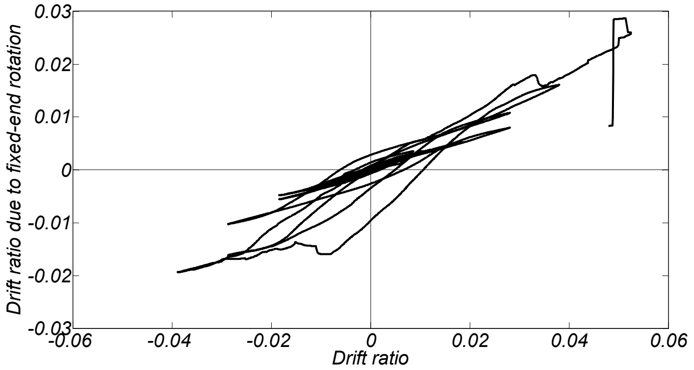

Figure 35 Beam 2: drift due to fixed-end rotation versus total drift ratio.

1.10 COMPARISON OF MOMENT-DEFORMATION RELATIONS

Figure 36 plots the measured relations between resisting moments and drift ratios for the two beams. The moment-drift ratio response of the two beams is similar until the cycle to peak drift ratio of 1.8%. During the cycle with a peak drift ratio of 2.7%, longitudinal bar buckling resulted in rapid and significant loss of strength in Beam 1. In contrast, Beam 2 did not sustain strength loss until larger drift ratio (3.9%), and strength degradation was more gradual.

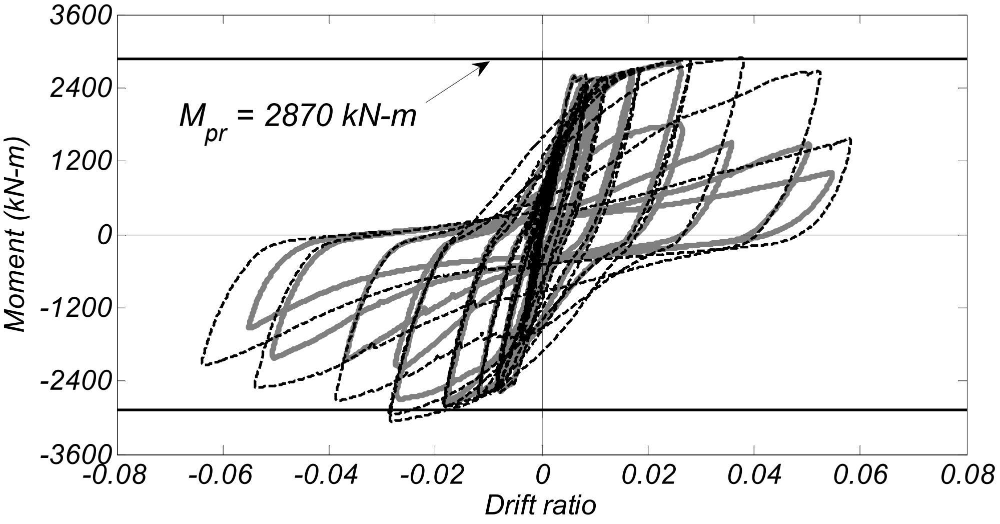

Figure 36 Relation between beam moment and beam drift ratio for Beams 1 and 2.

1.11 ESTIMATED SHEAR DEFORMATIONS

Instrumentation attached along the beam length near the anchor block enabled calculation of beam shear deformations. Figure 37 shows the relations between the beam shear and the estimated shear deformations within 1092 mm (43 in.) from the anchor block for the two beams. This relationship is plotted only for the cycles prior to the onset of longitudinal bar buckling; after this point, the LVDT measurements were distorted. For Beam 1, this includes cycles with drift ratio amplitude lower than and equal to 1.8%, while for Beam 2, the cycles with drift ratio amplitude less than and equal to 2.9% are included.

Although the peak applied force did not exceed 70% and 40% of the computed nominal shear strength provided by the hoops in Beams 1 and 2, respectively, shear degradation is noted through the progression of cycles for both specimens. Shear stiffness deterioration is also evident in the increased pinching of the moment-drift ratio curves at larger drift amplitudes (Figure 36). Overall, Beam 2 exhibited smaller shear deformations compared with Beam 1. During the last cycle with 1.8% drift ratio, approximate shear deformation of Beam 2 was roughly 50% of that measured in Beam 1 for the same amplitude cycle.

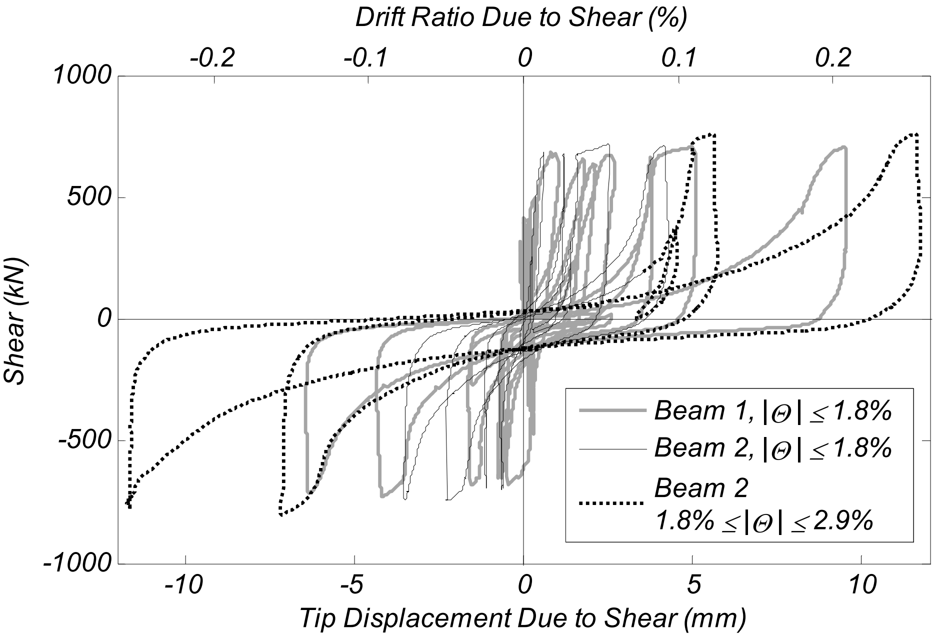

Figure 37 **Relation between measured force and estimated shear deformations for Beams 1 and 2 and cycles preceding the bar buckling.**

1.12 BUCKLING BEHAVIOR OF LONGITUDINAL REINFORCEMENT

In this laboratory study, inelastic cyclic buckling of the longitudinal reinforcement determined the progress of damage and strength deterioration. Previous experimental studies of cyclic inelastic behavior of reinforcing bars [Monti and Nuti 1992; Rodriguez et al. 1999] have demonstrated that the ratio of the unsupported length L_b to the bar diameter d_b is the primary factor that determines the buckling behavior of bars, while the steel material properties and loading history are secondary factors. In reinforced concrete specimens where the transverse reinforcement (spaced at s_h) provides the lateral support of the longitudinal bars, the ratio s_h / d_b can be considered as the primary factor affecting the buckling behavior.

In a reinforced concrete beam without prestressing, the longitudinal reinforcement strain history is characterized by increasing peak tensile strain as drift increases, with relatively little, if any, compressive strain. This behavior was observed for longitudinal bars in the present study (see Figure 17 and Figure 34). Rodriguez et al. [1999] hypothesized that buckling under this type of strain history would depend on the strain range ϵ_p, defined as the strain for which the bar is subjected to compressive stress after unloading from maximum tensile strain ϵ_s^+, as illustrated in Figure 38. Rodriguez et al. [1999] shows that, if the strain range is represented in terms of ϵ_p, then data from tests with strain histories representative of both beams and columns can be combined. The results are shown in Figure 39. Also shown are the s_h / d_b ratios for Beams 1 and 2. Taking the average curve as representative, estimated strains at buckling are approximately 0.02 for Beam 1 and 0.06 for Beam 2.

For various reasons, the strain estimates from the preceding paragraph should be interpreted as very approximate representations of values expected in Beams 1 and 2. First, the basic material properties are inherently variable. Even in the tests reported by Rodriguez et al [1999], using a single source of reinforcement, a wide variation of buckling behavior was observed. Second, it is difficult in a test to identify the exact instant in which buckling initiates. Third, in a reinforced concrete beam, the concrete cover, if intact as it was in the case of these beams, acts to restrain buckling. Finally, stirrup yielding, which was apparent in the beam tests, results in reduced lateral support for the restrained bars. For these (and possibly other reasons), the buckling strain estimates should be considered only as rough approximations.

For Beam 1 the peak tensile strain of the longitudinal reinforcement measured during the cycle with 1.8% peak drift ratio (where buckling initiated) was about 2.0% (see Figure 17). This is in good agreement with the estimate using the curve of Figure 39. For Beam 2 the corresponding strain measured during the cycle with peak drift ratio equal to 2.9% (where buckling initiated) was about 2.5% (see Figure 34). This level of strain is significantly smaller than the strain estimate using the curve of Figure 39; however, during this cycle the stirrups experienced yielding (see Figure 34), resulting in increase of the effective s_h / d_b.

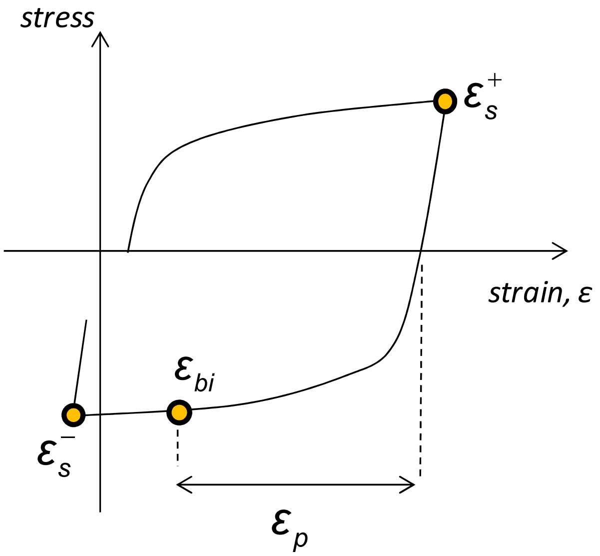

Figure 38 **Cyclic stress strain of steel and definition of characteristics strains.**

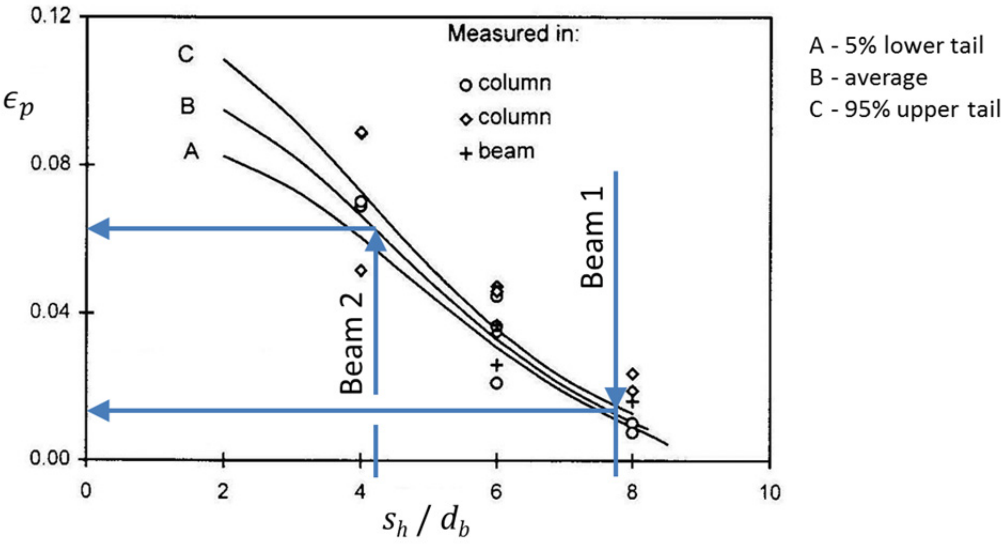

Figure 39 Strain range ϵ_p as function of L_b / d_b (taken as being equivalent to s_h / d_b) [after Rodriguez et al. (1999)].

1.13 COMPARISON OF MEASURED AND CALCULATED FLEXURAL RESPONSE

Conventional procedures for flexural response analysis were carried out for Beams 1 and 2. These include moment-curvature analyses, integration of flexural curvatures along the beam span to determine displacements, and analyses to estimate the onset of longitudinal reinforcement buckling. The procedures are summarized in the following paragraphs, followed by comparison between measured and calculated responses. See Appendix B for complete details,.

Moment-curvature analyses were carried out using the usual assumption that strains vary linearly across the depth of the section. Longitudinal reinforcement was modeled based on the measured material properties including strain-hardening. Unconfined concrete (the cover) was modeled based on stress-strain relations obtained from cylinder tests. Effects of confinement on core concrete behavior were considered using a confined concrete model. Only monotonic loading was considered. Moment-curvature calculations were carried out using the software XTRACT [2009].

Displacement corresponding to onset of longitudinal reinforcement yielding, δ_y, was calculated using the approximation that the concrete was fully cracked along the entire beam length, with effective flexural rigidity EI taken equal to $0.3E_cI_g$, in which E_c = Young's modulus of concrete, and I_g is the second moment of inertia of the gross section. The multiplier 0.3 is in accordance with the multiplier for beam stiffness in ASCE 41 (2006). Displacement corresponding to ultimate curvature, δ_u, was calculated using a plastic-hinge model, and is taken as the sum of δ_y and the displacement due to rotation of a plastic hinge. Two plastic hinge rotations were considered. In one of the models, the rotation was taken equal to product of the calculated inelastic curvature capacity ($\phi_u - \phi_y$) and a plastic hinge length approximated as l_p =

$h/2$. In the other model, the rotation was taken equal to the Collapse Prevention rotation capacity for a conforming beam with low shear acting as a primary member, that is $\theta_p = 0.025$. If the member was redefined as a secondary member, then the same model could be extended to Collapse Prevention for secondary members, in which case the maximum displacement at residual capacity could be calculated using $\theta_p = 0.05$ in accordance with ASCE 41.

To estimate the curvature at buckling of longitudinal reinforcement, the relation between longitudinal bar strain and curvature was obtained from the moment-curvature analyses for both negative and positive curvature. Assuming that these relations were adequate representations of the relations for reversed cyclic loading, the positive and negative curvatures were gradually increased (analytically) until the longitudinal reinforcement strain difference (for the positive versus the negative curvatures) was equal to the strain range at buckling, ϵ_p, as identified in Figure 39. Corresponding displacement was then calculated using the plastic-hinge model, with ultimate curvature defined as the curvature corresponding to buckling.

Figure 40 and Figure 41 compare the measured responses of Beams 1 and 2 versus calculated responses. Calculated flexural stiffness to yield (based on $EI_{\text{eff}} = 0.3E_cI_g$) is higher than the measured stiffness. According to Elwood et al. [2007], actual stiffness of members with zero axial force tends on average to be lower than $0.3E_cI_g$, which is consistent with the results shown here. The measured flexural stiffness of Beam 1 at yield point was $0.13E_cI_g$, while that of Beam 2 was $0.16E_cI_g$.

The ASCE 41 moment-drift envelope follows the response of Beam 1 remarkably well, but underestimates drift capacity of Beam 2. Moment-drift response calculated using a bilinear approximation of the moment-curvature response (based on detailed moment-curvature analysis and a plastic-hinge length equal to $h/2$) grossly overestimates drift ratio capacity if longitudinal reinforcement buckling is ignored. Drift ratio capacity estimates are improved if longitudinal reinforcement buckling is taken into consideration.

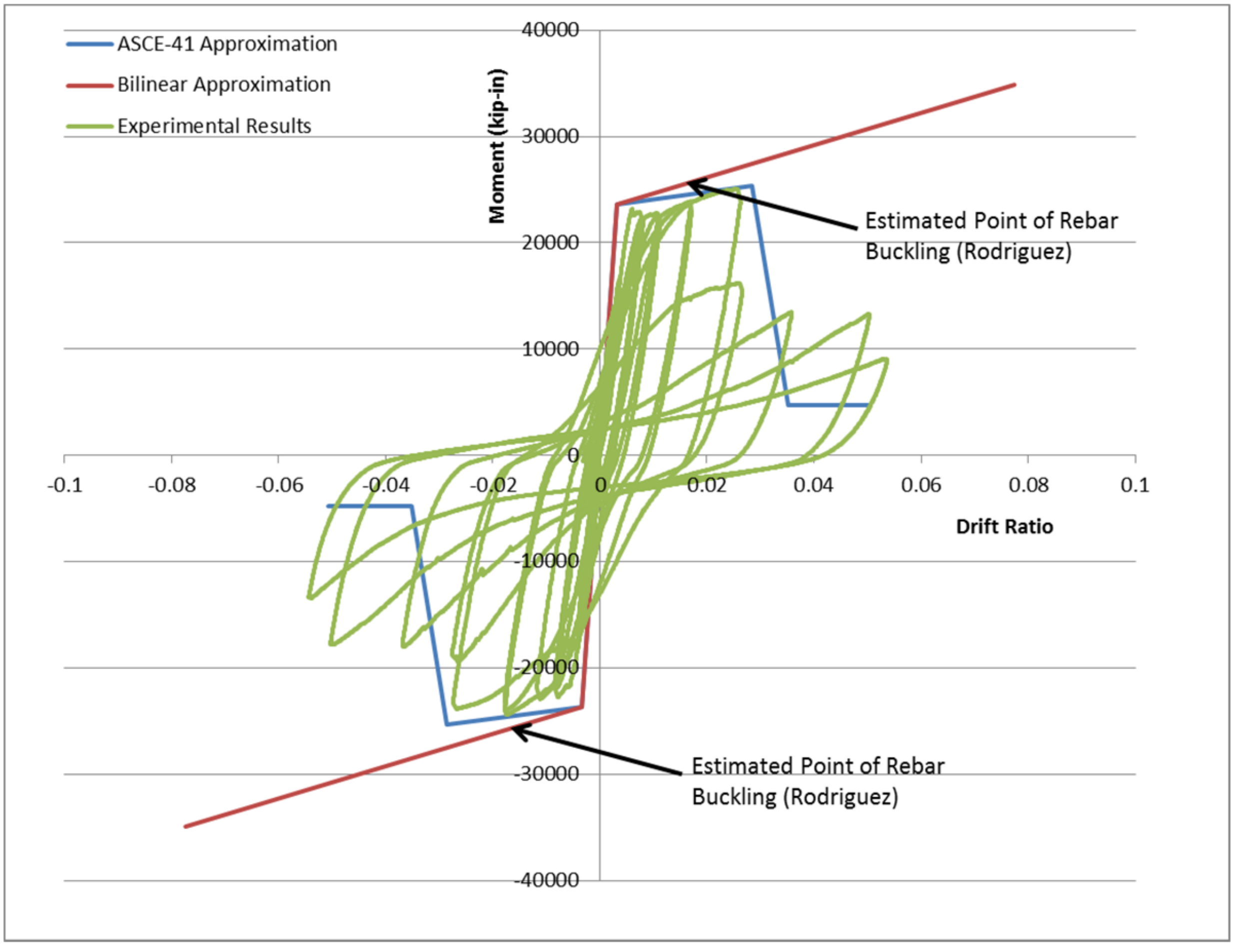

Figure 40 Comparison of calculated response envelopes and the measured response of Beam 1.

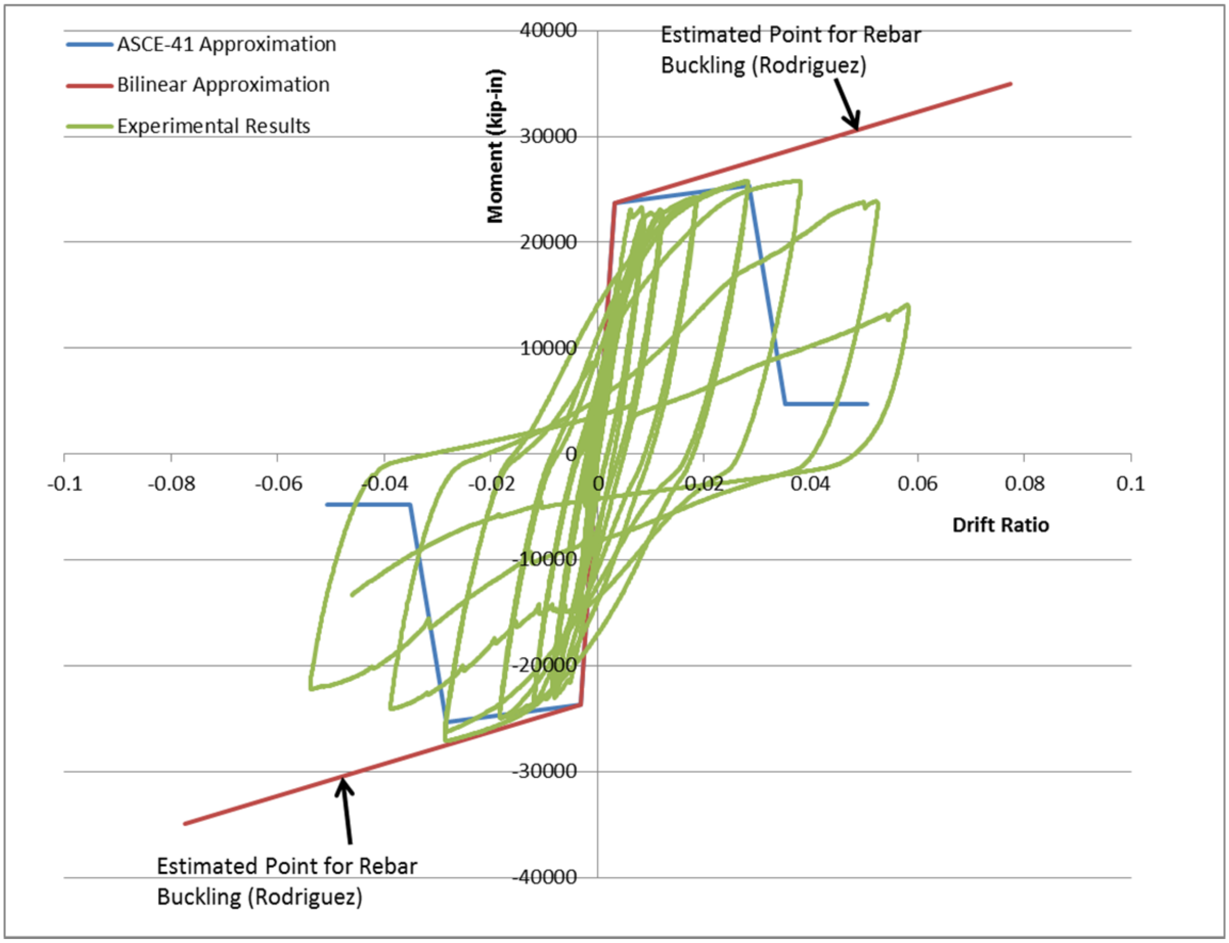

Figure 41 Comparison of calculated response envelopes and the measured response of Beam 2.

1.14 RESIDUAL CRACK WIDTHS

Residual crack width provides a measure of serviceability and repair actions required following an earthquake. Appendix C contains crack width data for the tests. Although the data for Beam 1 were not consistently recorded, nonetheless they provide a useful record of the evolution of cracks throughout the test. The data for Beam 2 were more consistently recorded; they include crack widths for vertical (flexural) and inclined (shear) cracks recorded at displacement peaks and after the beam had completed a series of displacement cycles and was brought back to zero displacement. Figure 42 presents residual crack width (recorded at zero displacement) of the vertical cracks as function of prior peak drift ratio. Residual cracks widths increase at an increasing rate beyond the yield displacement, which corresponds to drift ratio around 0.5%.

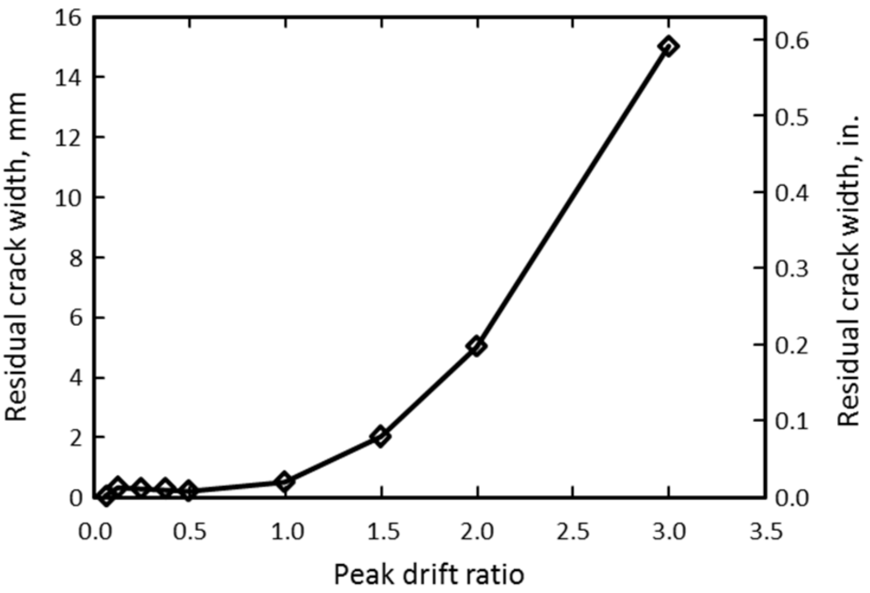

Figure 42 **Beam 2: residual crack width as function of peak drift ratio.**

1.15 DESIGN RECOMMENDATION

Beam 1 was designed and detailed in accordance with ACI 318-08. Specifically, the hoop spacing within the intended plastic hinge zone was 270 mm (11 in.) based on the requirement of Section 21.5.3.2 that spacing not exceed the least of $d/4$, $8d_b$ of the smallest longitudinal bars, $24d_b$ of the hoop bars; and 12 in (305 mm). The beam was able to resist inelastic cyclic deformations up to an equivalent beam rotation of 0.027, at which point buckling of longitudinal reinforcement caused major loss of lateral force-resisting capacity. This performance is deemed, in general, to be unsatisfactory for a beam of a special moment frame, because rotations exceeding this rotation capacity generally can be anticipated for shaking at the MCE level. By decreasing the hoop spacing to 152 mm (6 in.), as was done for Beam 2, longitudinal reinforcement buckling resulting in strength decay was delayed until equivalent beam rotation of 0.039. This performance would generally be considered acceptable for a beam of a special moment frame.

Based on these observations, we recommend a Code Change Proposal to ACI 318-08, which replaces Section 21.5.3.2, Section 21.5.3.3, and associated commentary with the following:

CODE

21.5.3.2 — The first hoop shall be located not more than 50 mm (2 in.) from the face of a supporting member. Spacing of the hoops shall not exceed the smallest of (a), (b), and (c):

(a) $d/4$;

(b) Six times the diameter of the smallest primary flexural reinforcing bars excluding longitudinal skin reinforcement required by 10.6.7; and

(c) 6 in.

21.5.3.3 — Where hoops are required, primary flexural reinforcing bars closest to the tension and compression faces shall have lateral support conforming to 7.10.5.3 or 7.10.5.4. The spacing of laterally supported flexural reinforcing bars shall not exceed 14 in. Skin reinforcement required by 10.6.7 need not be laterally supported.

COMMENTARY

<<Replace Figure R21.5.3 and add new paragraph as follows:>>

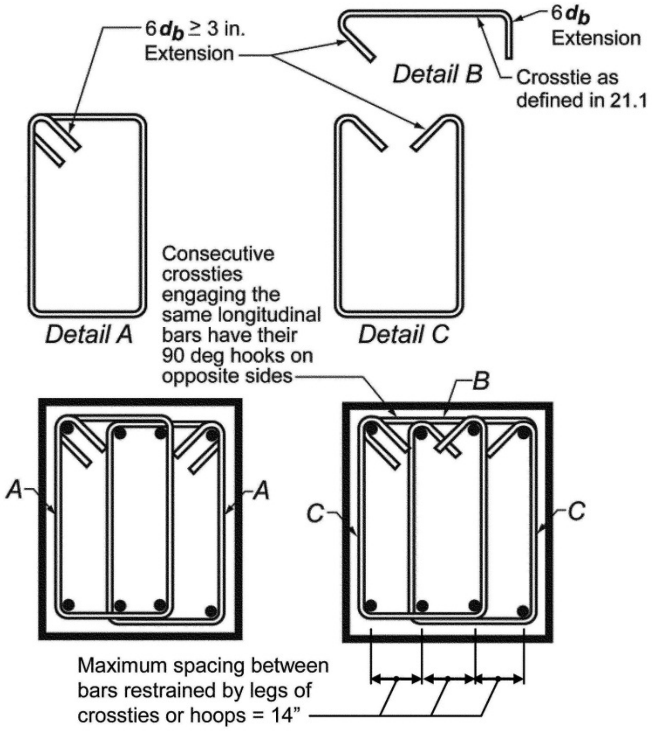

Fig. R21.5.3—Examples of overlapping hoops and illustration of limit on maximum horizontal spacing of supported longitudinal bars.

For many years, the upper limit on hoop spacing was the smallest of $d/4$, 8 longitudinal bar diameters, 24 tie bar diameters, and 12 in. The upper limits were changed because of concerns about adequacy of longitudinal bar buckling restraint and confinement of large beams.

1.16 SUMMARY AND CONCLUSIONS

Two beams were designed, constructed, and tested under reversed cyclic displacements in a laboratory. The beams had depth of 1219 mm (48 in.) and width of 762 mm (30 in.). Both beams had five No. 36 (11) A706 Grade 60 longitudinal bars at top and bottom faces, resulting in longitudinal steel ratio equal to 0.58%. The beams satisfied ACI 318-08 code provisions for special moment frame beams. Transverse reinforcement comprised No. 16 (5) hoops made up of a stirrup closed by a crosstie, with an additional vertically oriented crosstie in each hoop set. In Beam 1 the hoop sets had longitudinal spacing of 279 mm (11 in.), while in Beam 2 the hoop sets had longitudinal spacing of 152 mm (6 in.). The ratios of hoop spacing to longitudinal bar diameter correspond to $s_h / d_b = 7.8$ and 4.25 in Beams 1 and 2, respectively. Both beams used normal-weight concrete with nominal compressive strength of 34 MPa (5000 psi). The beams were subjected to displacement reversals of increasing amplitude, simulating the effects of deformations due to strong earthquake shaking.

The following conclusions are drawn:

1. Beam 2 with reduced hoop spacing was capable of more displacement cycles and larger displacement amplitude than Beam 1 with wider hoop spacing. Beam 1 lost 38% of its peak resistance during a second cycle to peak drift ratio of 0.027. Beam 2 did not sustain strength loss until during the cycles to peak drift ratio of 0.039, and strength loss was more gradual. Beam 2 was capable of resisting one cycle at peak drift ratio of 0.053 while still resisting 80% of its peak strength.

2. Damage initiation and damage progress in both beams was dominated by buckling of the longitudinal reinforcement. For Beam 1, buckling initiated during a cycle with a peak drift ratio of 1.8%. Buckling became more extensive during the cycles with 2.7% peak drift ratio, when significant strength loss occurred. For Beam 2 with reduced hoop spacing, buckling was delayed until the first cycle with a peak drift ratio of 2.9% and became more extensive during the cycle with 3.9% peak drift ratio.

3. Tendency for reinforcing bar buckling depends on the ratio of hoop spacing to bar diameter (s_h / d_b) and on the strain history. Based on tests of bars in air, Rodriguez et al. [1999] hypothesized a relation between the strain range (defined as the strain for which the bar is subjected to compressive stress after unloading from maximum tensile strain) and s_h / d_b. According to that hypothesis, buckling in a beam is primarily a function of s_h / d_b and maximum tensile strain in the longitudinal reinforcement. For Beams 1 and 2, the Rodriguez et al. model suggests maximum longitudinal reinforcement strain capacity of 0.02 and 0.06, respectively. Measured tensile strains in the beams varied significantly, depending on the measurement device (LVDT or strain gauge) and measurement location. Overall, the strains were in the range suggested by the Rodriguez et al. model.

4. Longitudinal bar buckling in both beams initiated at the top of the beam where local concrete strength would be expected to be lowest. It seems more likely, however, that the tendency for earlier buckling at the top of the beam was influenced mainly by the

presence of the cap ties that closed the hoops at the top of the beam. Cap ties are likely to be most effective in closing a hoop where a slab is cast at the top of the beam. Where there is no slab, or where the beam is upturned with the slab at the bottom of the beam, the presence of cap ties creates a weakness at the top of the beam that should be considered when detailing the transverse reinforcement.

5. Beam 1 developed peak moment strength equal to $0.99M_{pr}$, where M_{pr} is probable moment strength calculated in accordance with ACI 318. Beam 2 developed peak moment strength equal to $1.10M_{pr}$.
6. Maximum nominal shear stresses for both beams were on the order of $0.14\sqrt{f_c'}$ MPa ($1.7\sqrt{f_c'}$ psi) using measured concrete compressive strength. For Beams 1 and 2, respectively, maximum shear forces were on the order of 70% and 40% of V_s, or 95% and 57% of ϕV_s, where $\phi = 0.75$ and V_s is calculated in accordance with ACI 318. Even though shear forces were less than provided shear strengths, some yielding of beam transverse reinforcement was recorded. Lateral support of longitudinal bars may have been reduced because of yielding of transverse reinforcement. This may have contributed to buckling of the longitudinal bars.
7. Rigid body displacements associated with slip of reinforcement from the anchorages constituted approximately 30% to 45% of the total beam displacement.
8. Initial stiffness was calculated using flexural rigidity equal to $0.3E_cI_g$, as recommended in ASCE 41. The coefficient 0.3 is intended to take into consideration the combined effects of concrete cracking and slip of reinforcement from the anchorages. Actual beam secant stiffness to yielding was less than this calculated value.
9. A plastic-hinge model based on ASCE 41 parameters was successful in representing the load-displacement behavior of Beam 1 but was overly conservative for Beam 2. Plastic-hinge models based on theoretical moment-curvature relations grossly overestimated displacement capacity of both beams if buckling was not taken into consideration. Results were improved if longitudinal reinforcement buckling according to the Rodriguez et al. [1999] model was taken into account. In all cases, the plastic-hinge length was taken equal to $h/2$ in accordance with ASCE 41.
10. Residual crack widths increased at an increasing rate beyond the yield displacement. At drift ratio of 0.02, residual crack width was 5 mm (0.2 in.).
11. In a large reinforced concrete beam similar to those tested in this study, with equal areas of top and bottom longitudinal reinforcement, flexural tension cracks formed during loading in one direction tend to remain open for loading in the reversed direction. Therefore, flexural compression is resisted mainly by the longitudinal reinforcement near the flexural compression face and not by the concrete. Thus, requirements for hoop reinforcement need not be based on considerations of concrete confinement, but instead these requirements should be based on considerations of beam shear and longitudinal reinforcement buckling restraint.

12. On the basis of the tests and supporting analyses, it is recommended that hoop spacing within the plastic-hinge region of special moment frame beams not exceed the least of $d/4$, $6d_b$ of the smallest longitudinal bars excluding skin reinforcement, and 150 mm (6 in.). A code change proposal for ACI 318-08, consistent with this recommendation, is presented in the main body of the report.

REFERENCES

ACI (2008). *Building Code Requirements for Structural Concrete*, *ACI 318-08*, American Concrete Institute, Farmington Hills, MI.

ACI (2011). *Building Code Requirements for Structural Concrete*, *ACI 318-11*, American Concrete Institute, Farmington Hills, MI.

ASCE (2006). *Seismic Rehabilitation of Existing Buildings*, *ASCE/SEI Standard 41-06 including Supplement 1*, American Society of Civil Engineers, Reston, VA.

Beckingsale C.W. (1980). Post-elastic behaviour of reinforced concrete beam-column joints, *Research Report No. 80-20*, Department of Civil Engineering, University of Canterbury, Christchurch, New Zealand, 398 pgs.

Blakeley R.W.G., Megget L.M., Priestley M.J.N. (1975). Seismic performance of two full size reinforced concrete beam-column joint units, *Bull. New Zealand Soc. Earthq. Eng.*, 8(1): 38–69.

Chang B.J., Hutchinson T.C., Englekirk R.E (2008) Experimental seismic performance evaluation of innovative beam-column subassemblies, *Report SSRP-08/01*, University of California, San Diego, CA.

Elwood K.J., Matamoros A.B., Wallace J.W., Lehman D.E., Heintz J.A., Mitchell A.D., Moore M.A., Valley M.T., Lowes L.N., Comartin C.D., Moehle J.P. (2007). Update to ASCE/SEI 41 concrete provisions, *Earthq. Spectra*, 23(3): 493–523.

Haselton C.B., Liel A.B., Deierlein G.G., Dean B.S., Chou, J.H. (2011). Seismic collapse safety of reinforced concrete buildings: I. assessment of ductile moment frames, ASCE, *J. Struct. Eng.,* 137: 481–491.

Monti G., Nuti C. (1992). Nonlinear cyclic behavior of reinforcing bars including buckling, ASCE, *J. Struct. Eng*., 118(12): 3268–3284.

Popov E.P., Bertero V.V., Krawinkler H. (1972). Cyclic behavior of three reinforced concrete flexural members with high shear, *Report No. EERC 72-5*, Earthquake Engineering Research Center, University of California, Berkeley, CA.

Restrepo J.I., Park R., Buchanan A. (1990) Seismic behaviour of connections between precast concrete elements, *Research Report 93-3*, Department of Civil Engineering, University of Canterbury, Christchurch, New Zealand.

Rodriguez M., Botero J., Villa J. (1999). Cyclic stress-strain behavior of reinforcing steel including effect of buckling, *J. Struct. Eng.,* 125 (6): 605–612.

Visnjic T., Panagiotou M., Moehle J.P. (2012). Seismic response of 20-story reinforced concrete special moment resisting frames designed with current code provisions, *Report No. UCB/SEMM-2012/02*, Department of Civil and Environmental Engineering, University of California, Berkeley, CA.

Warcholik G., Priestley, M.J.N. (1997). Structural systems research project: High strength concrete joints tests, *Report No.TR-97/10*, University of California, San Diego, CA.

XTRACT (2009). XTRACT, version 3.0.8. TRC/Imbsen Software Systems, http://www.imbsen.com/xtract.htm.

APPENDIX A: RECORDED INSTRUMENTATION DATA HISTORIES

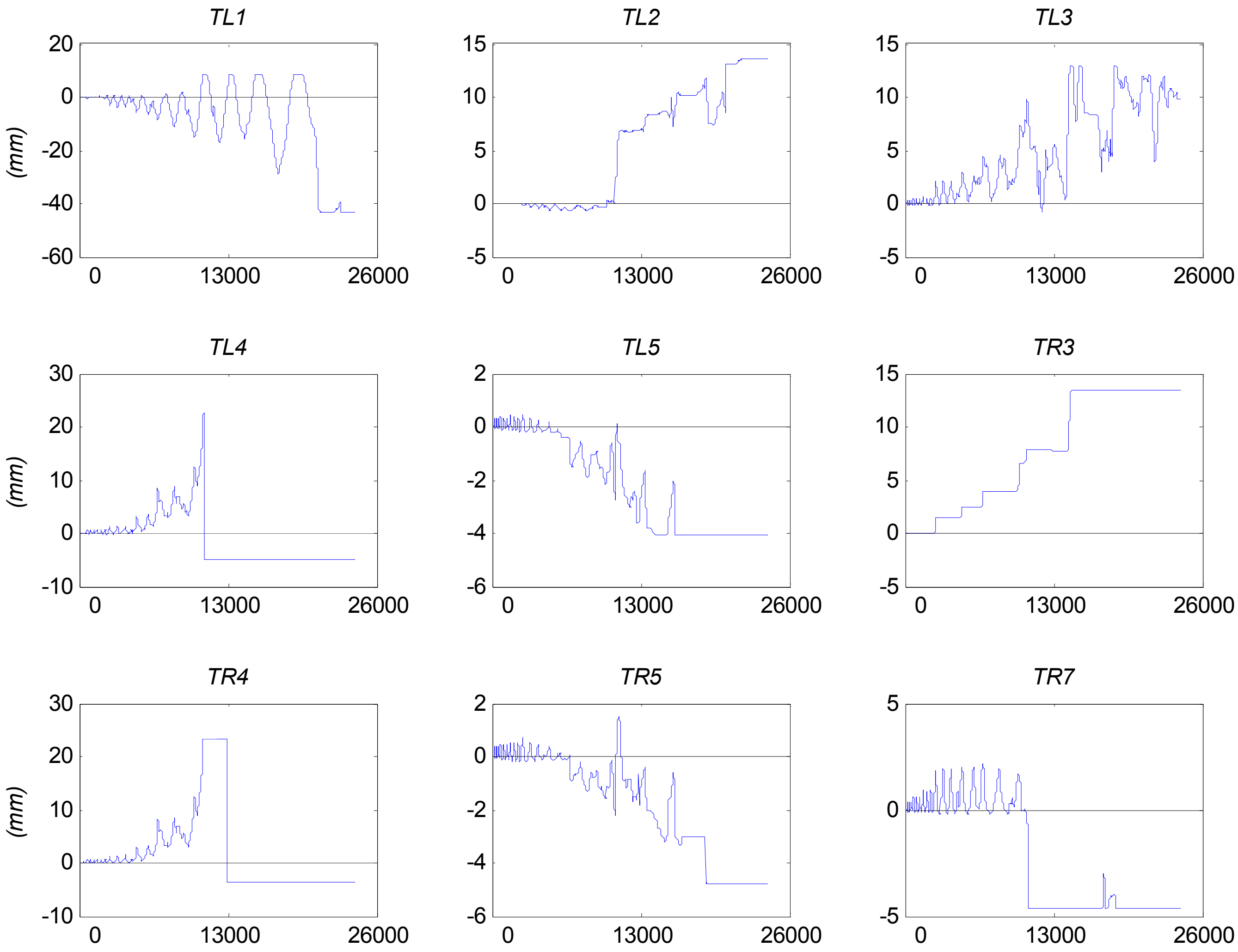

Figure A.1 **Beam 1: histories of displacement transducers.**

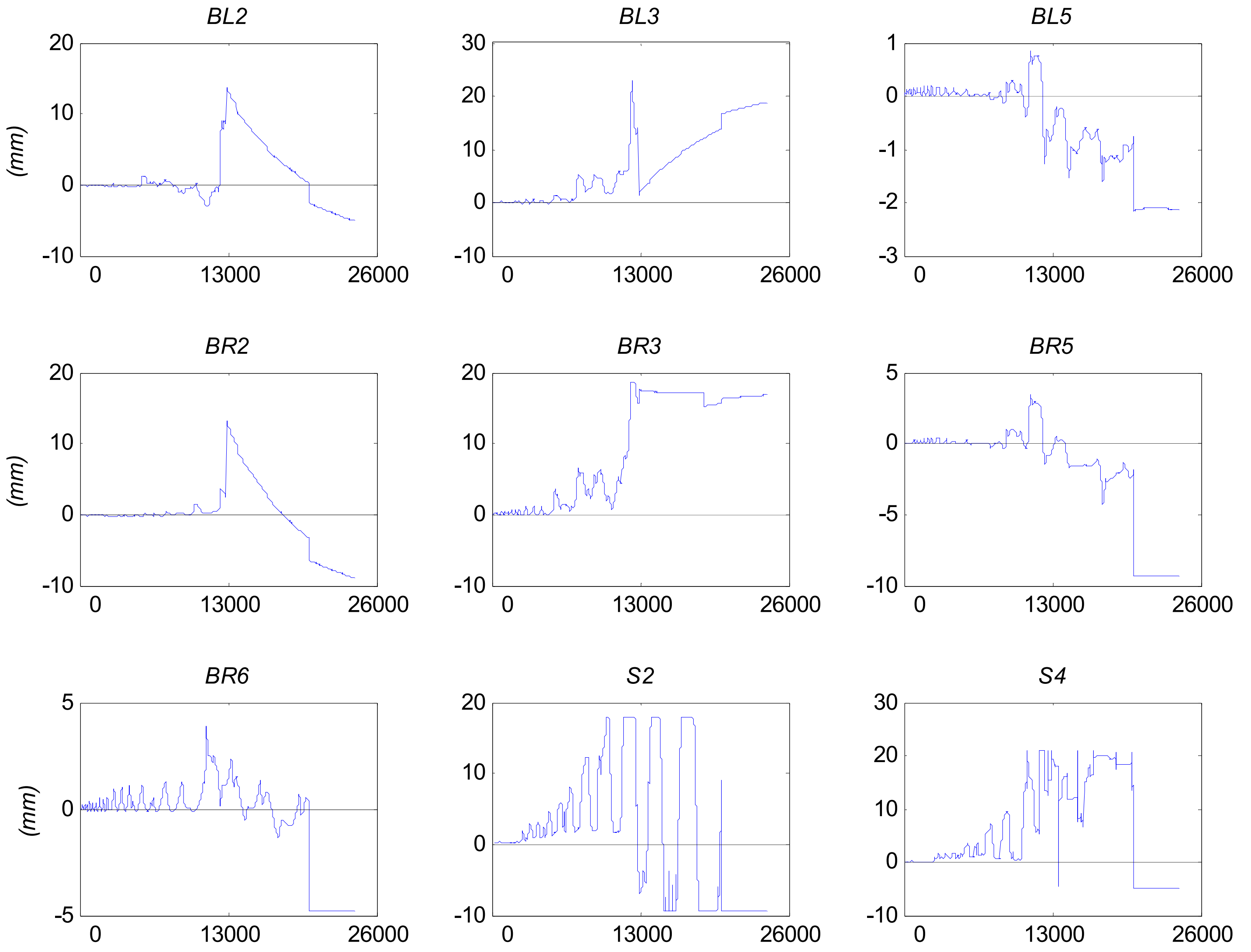

Figure A.2 Beam 1: histories of displacement transducers.

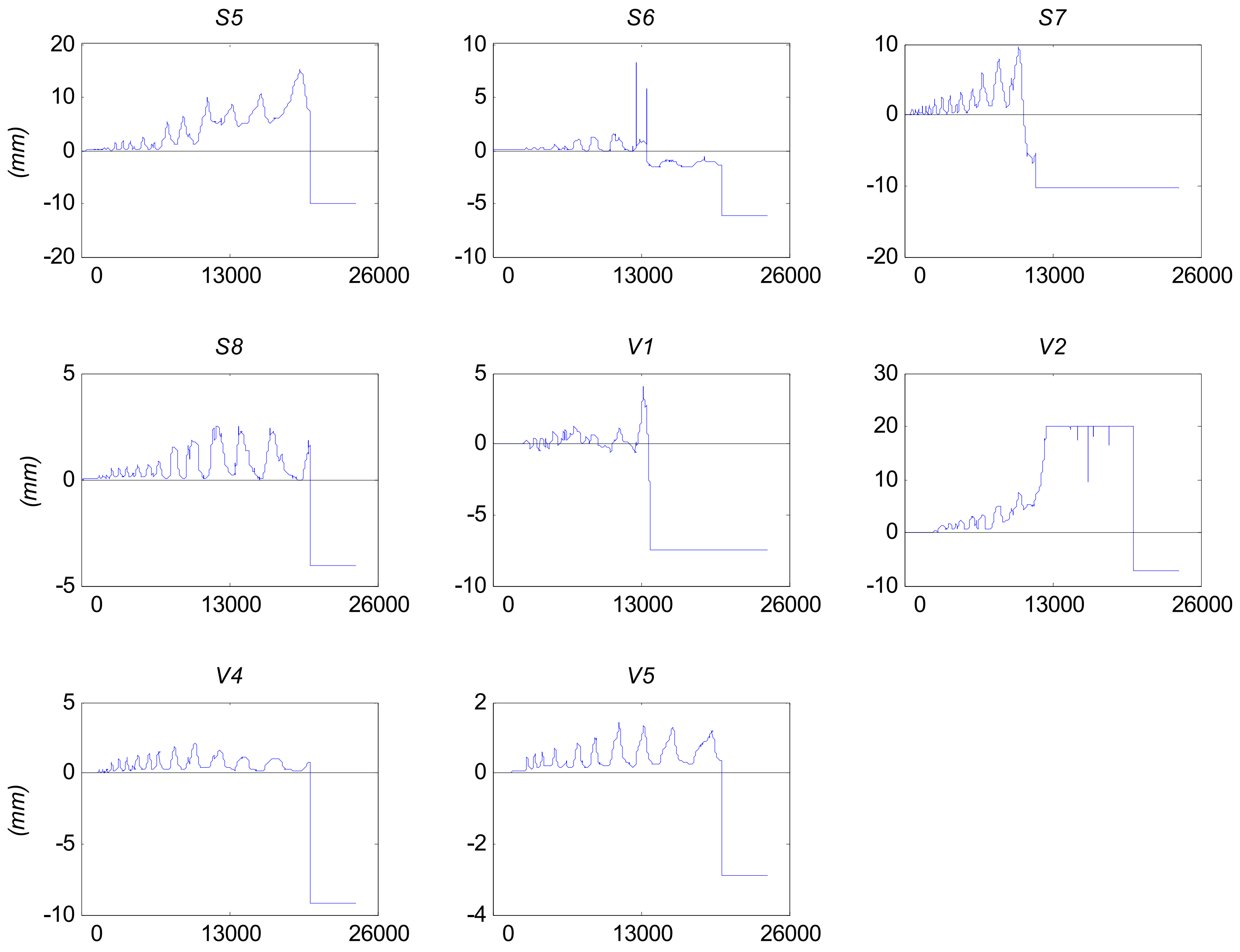

Figure A.3 **Beam 1: histories of displacement transducers.**

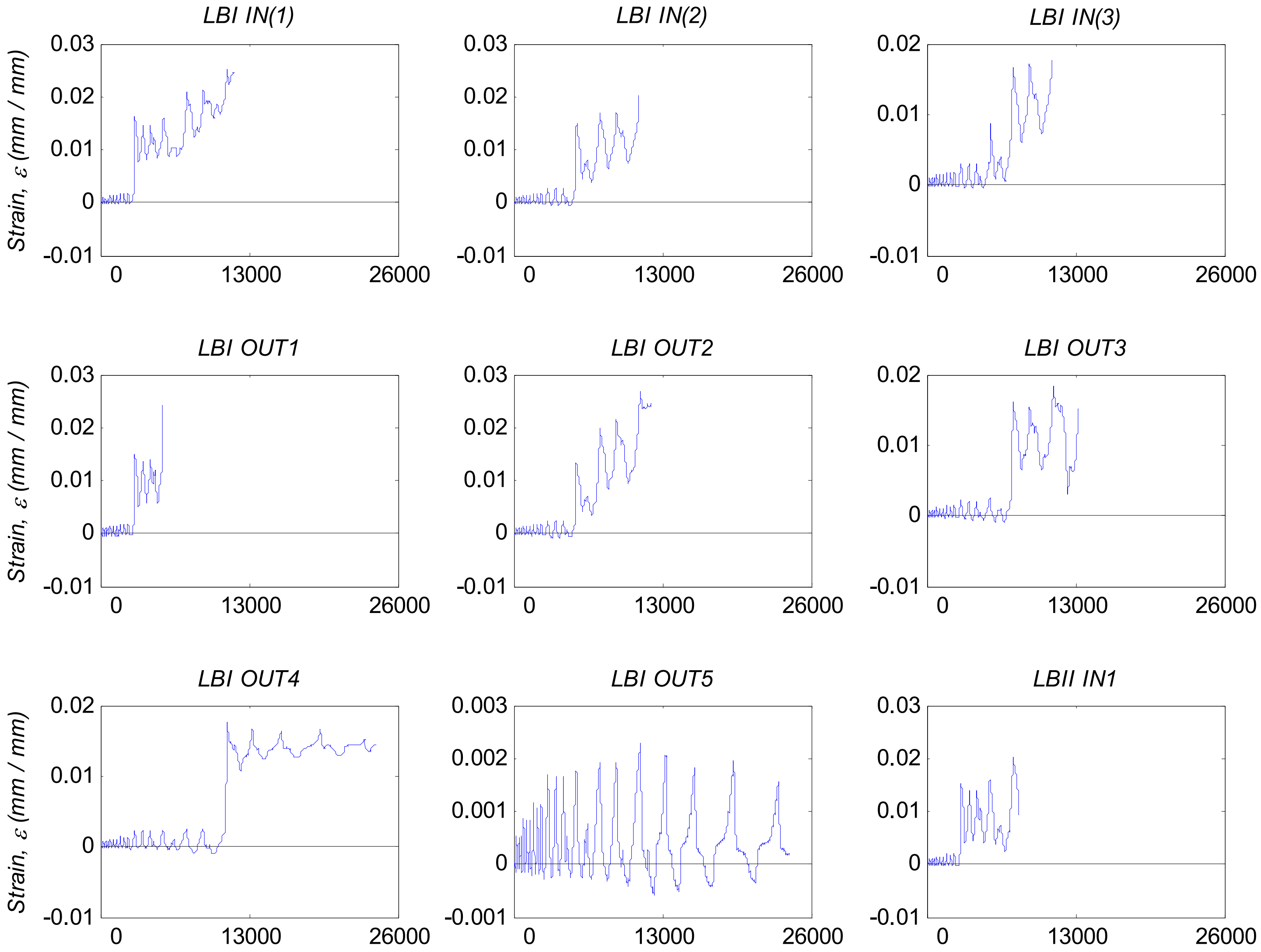

Figure A.4 **Beam 1: histories of strain gauges.**

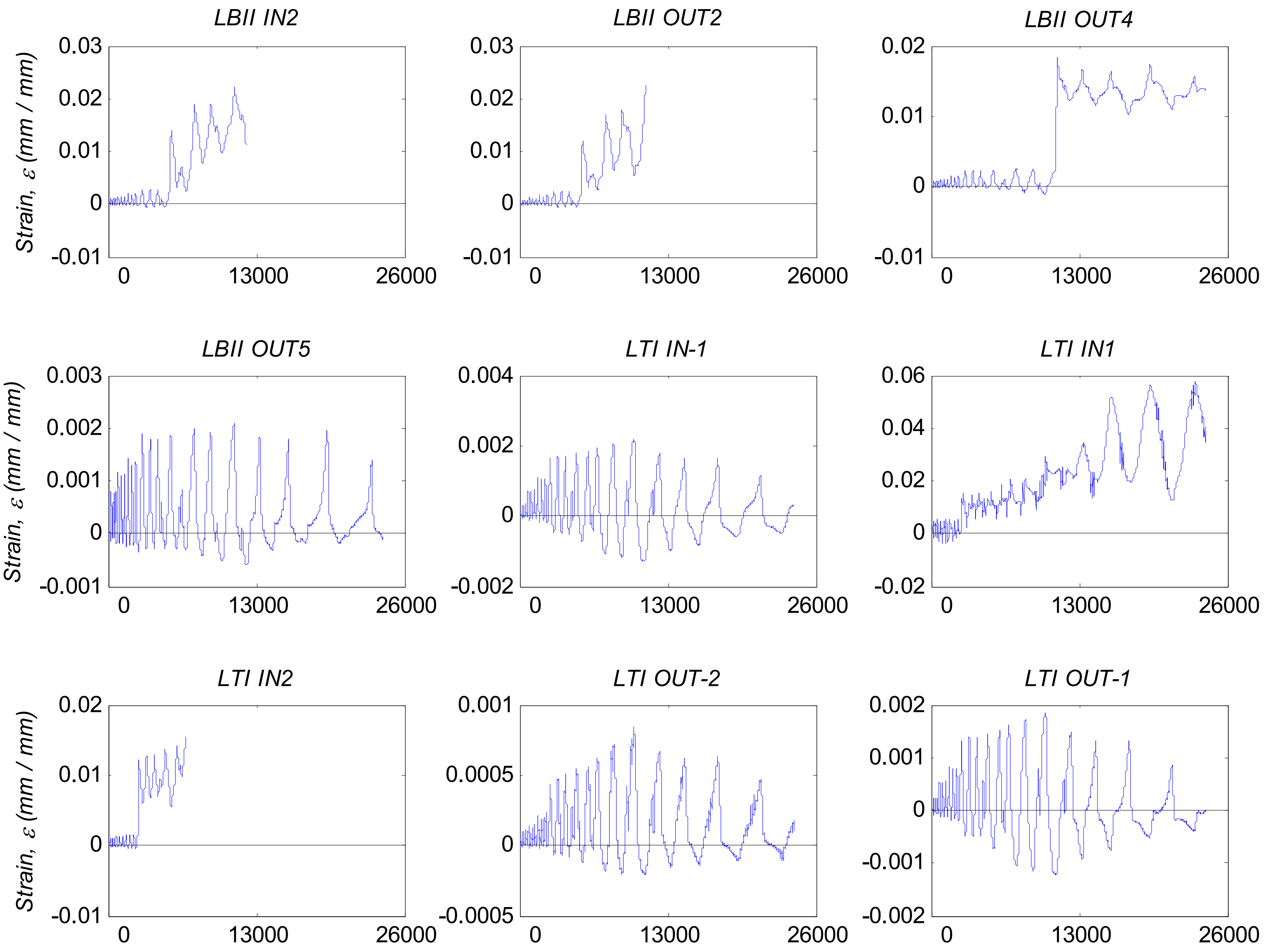

Figure A.5 Beam 1: histories of strain gauges.

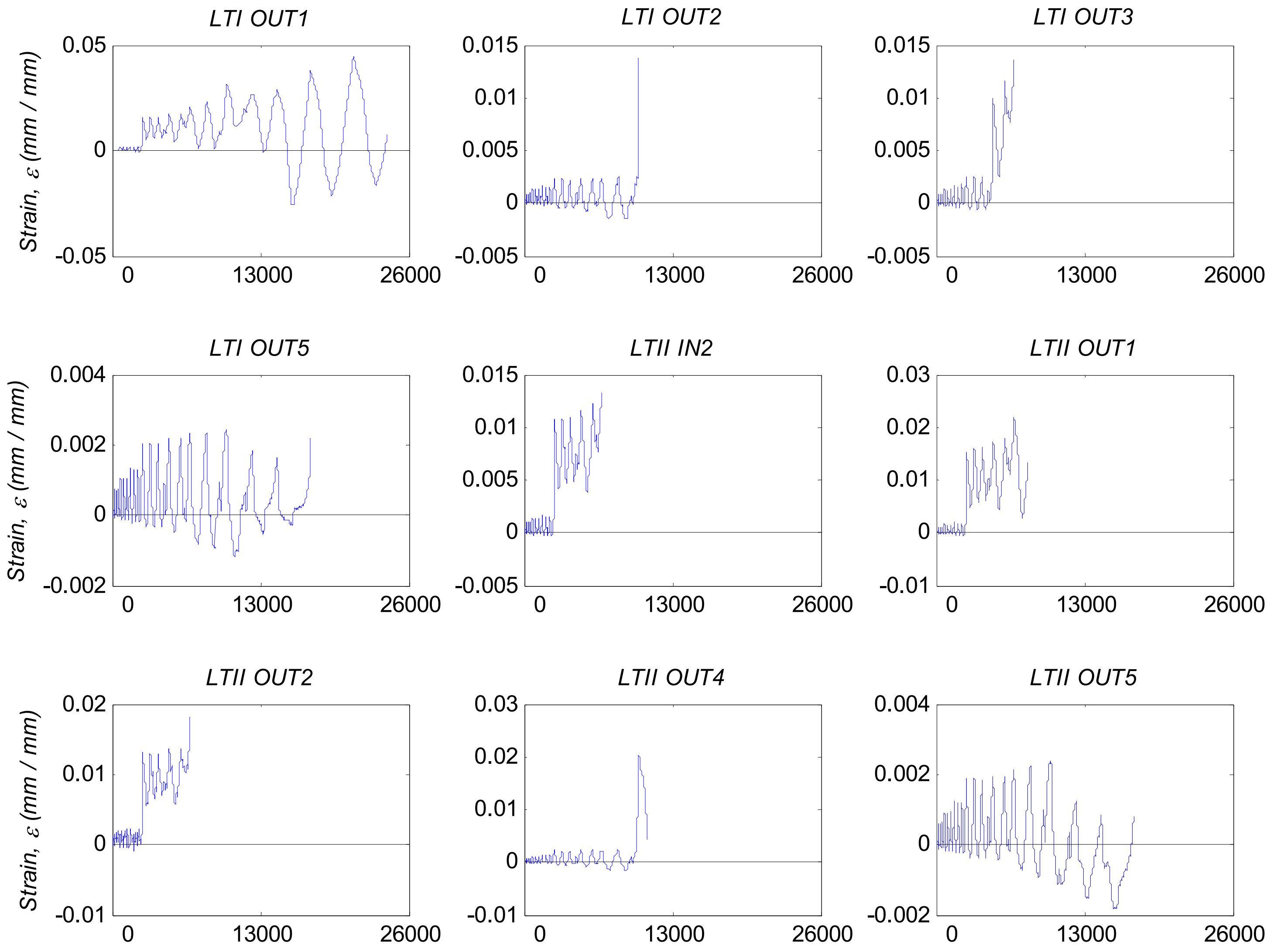

Figure A.6 **Beam 1: histories of strain gauges.**

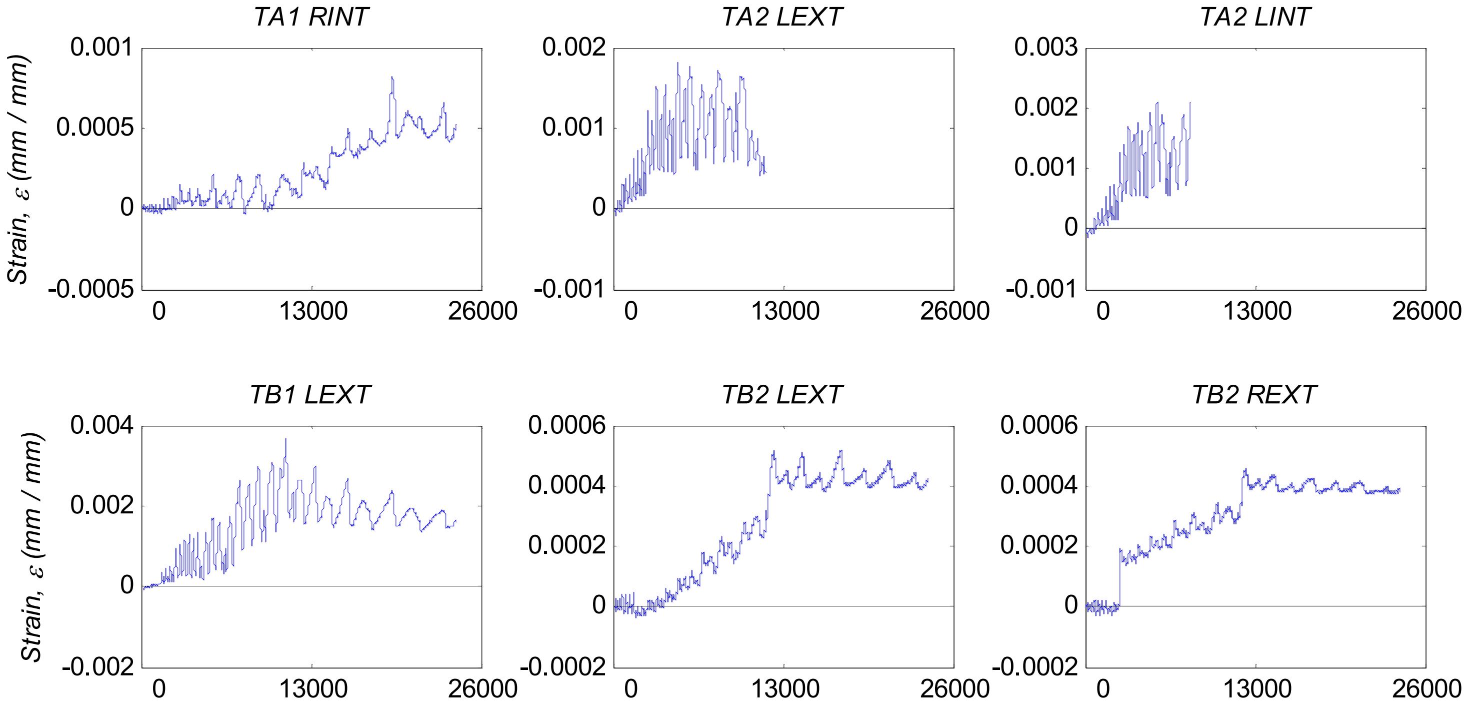

Figure A.7 **Beam 1: histories of strain gauges.**

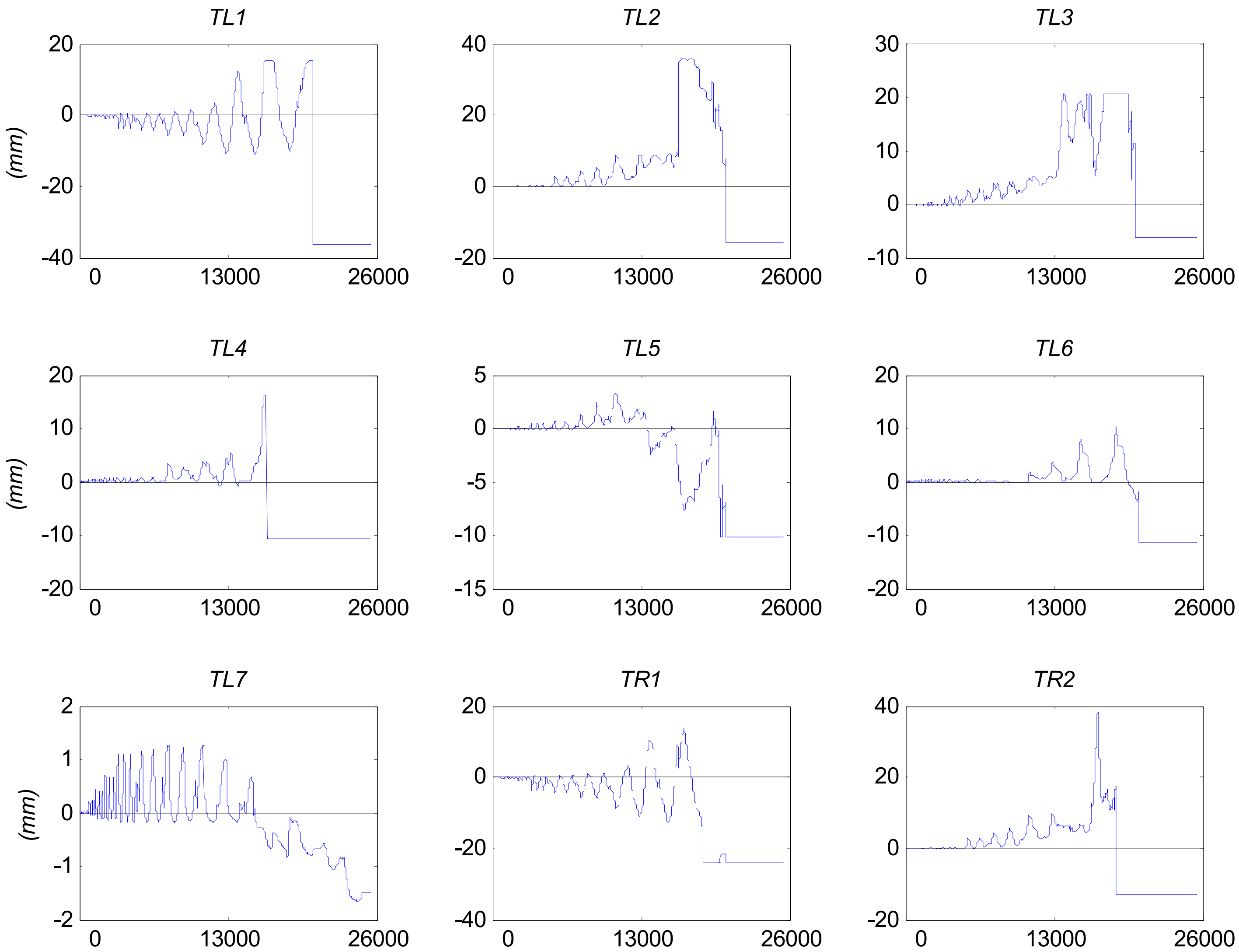

Figure A.8 **Beam 1: histories of displacement transducers.**

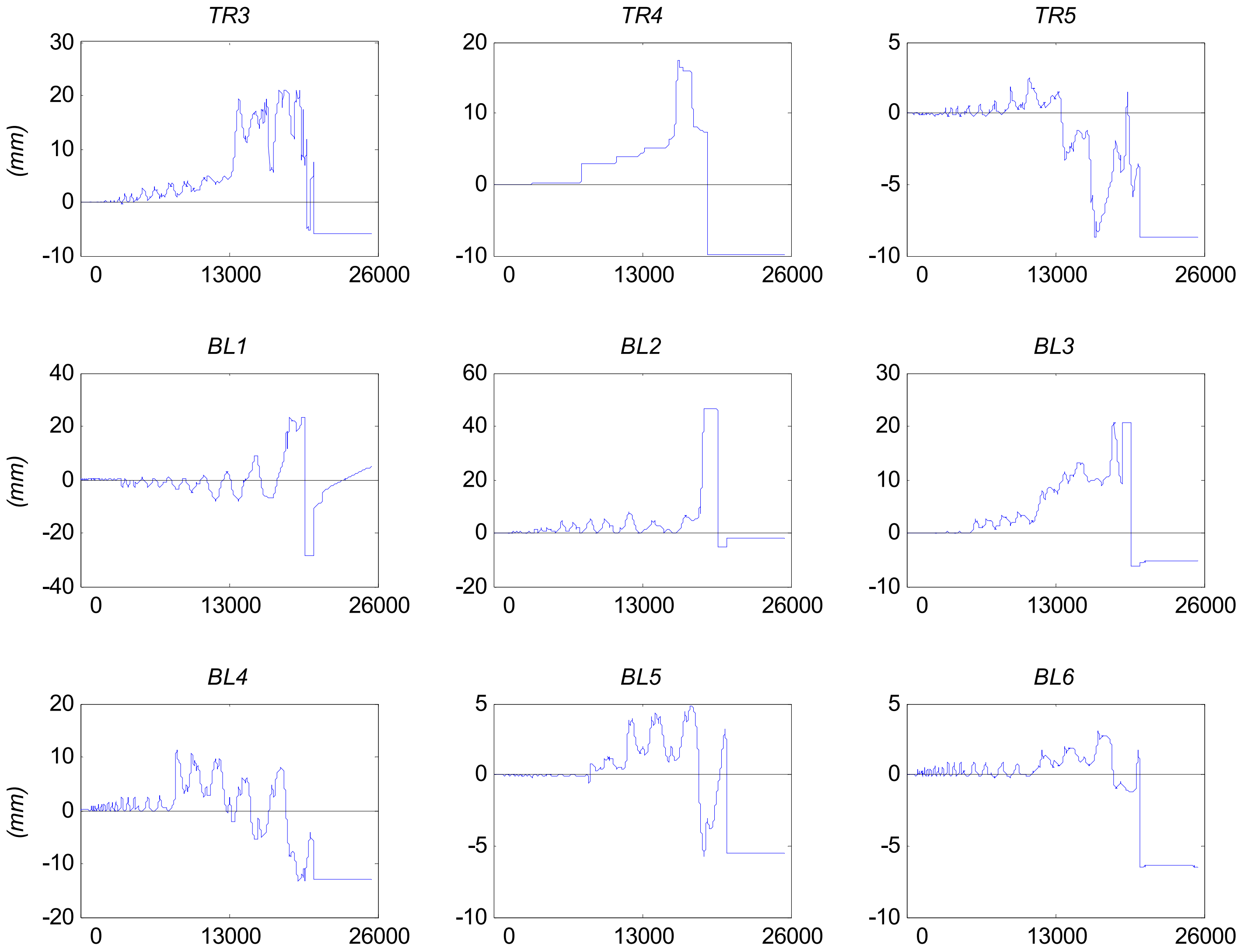

Figure A.9 **Beam 2: histories of displacement transducers.**

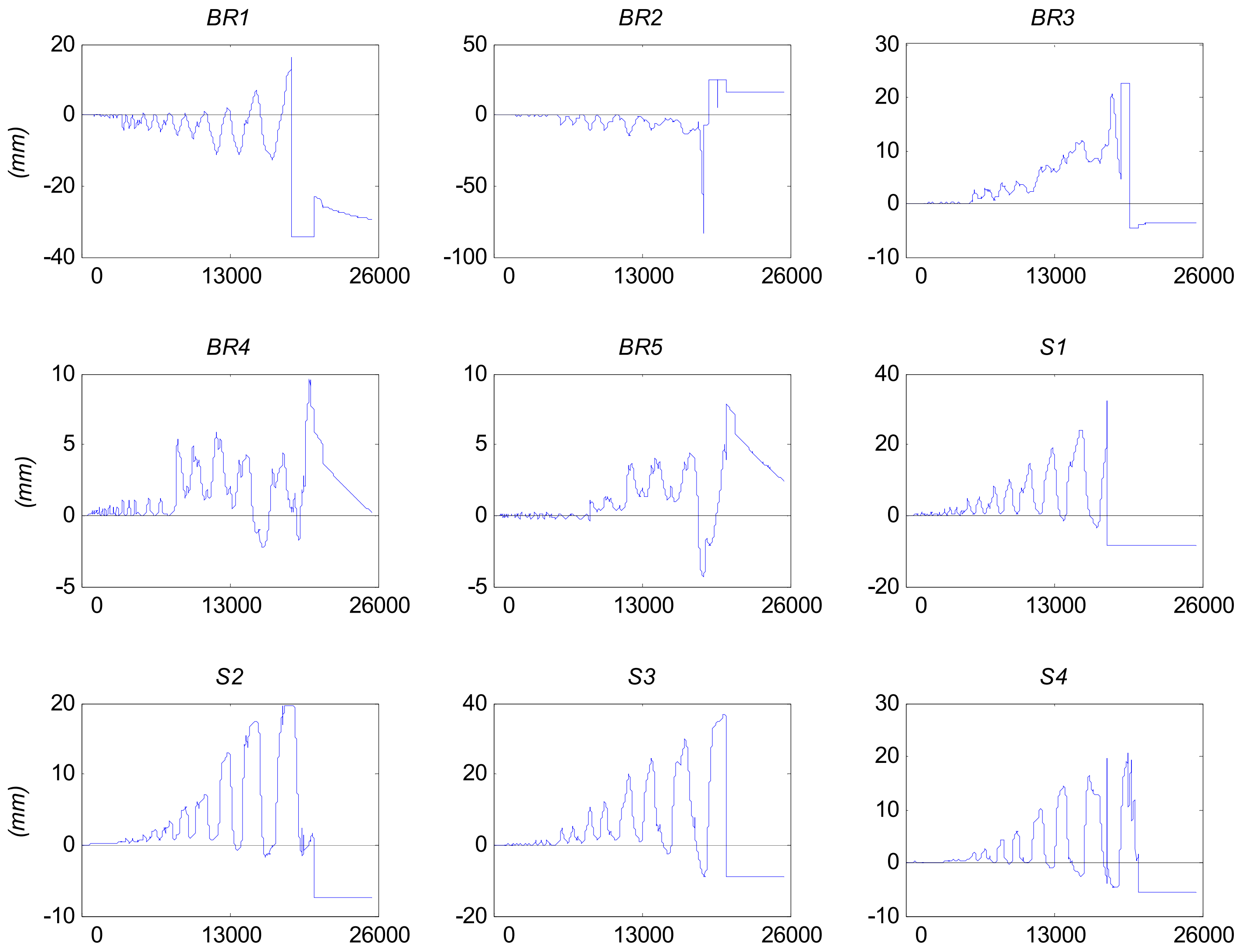

Figure A.10 **Beam 2: histories of displacement transducers.**

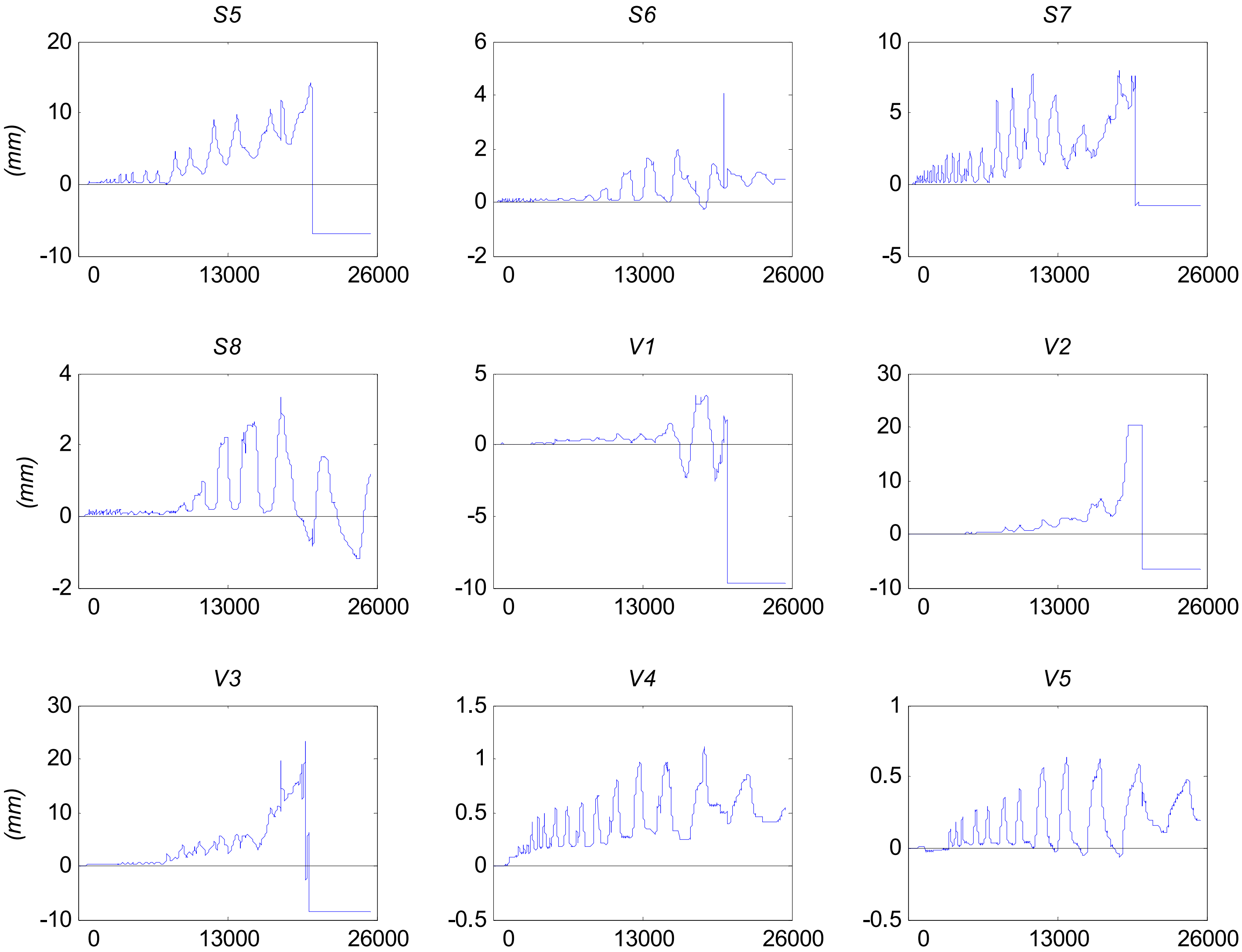

Figure A.11 Beam 2: histories of strain gauges.

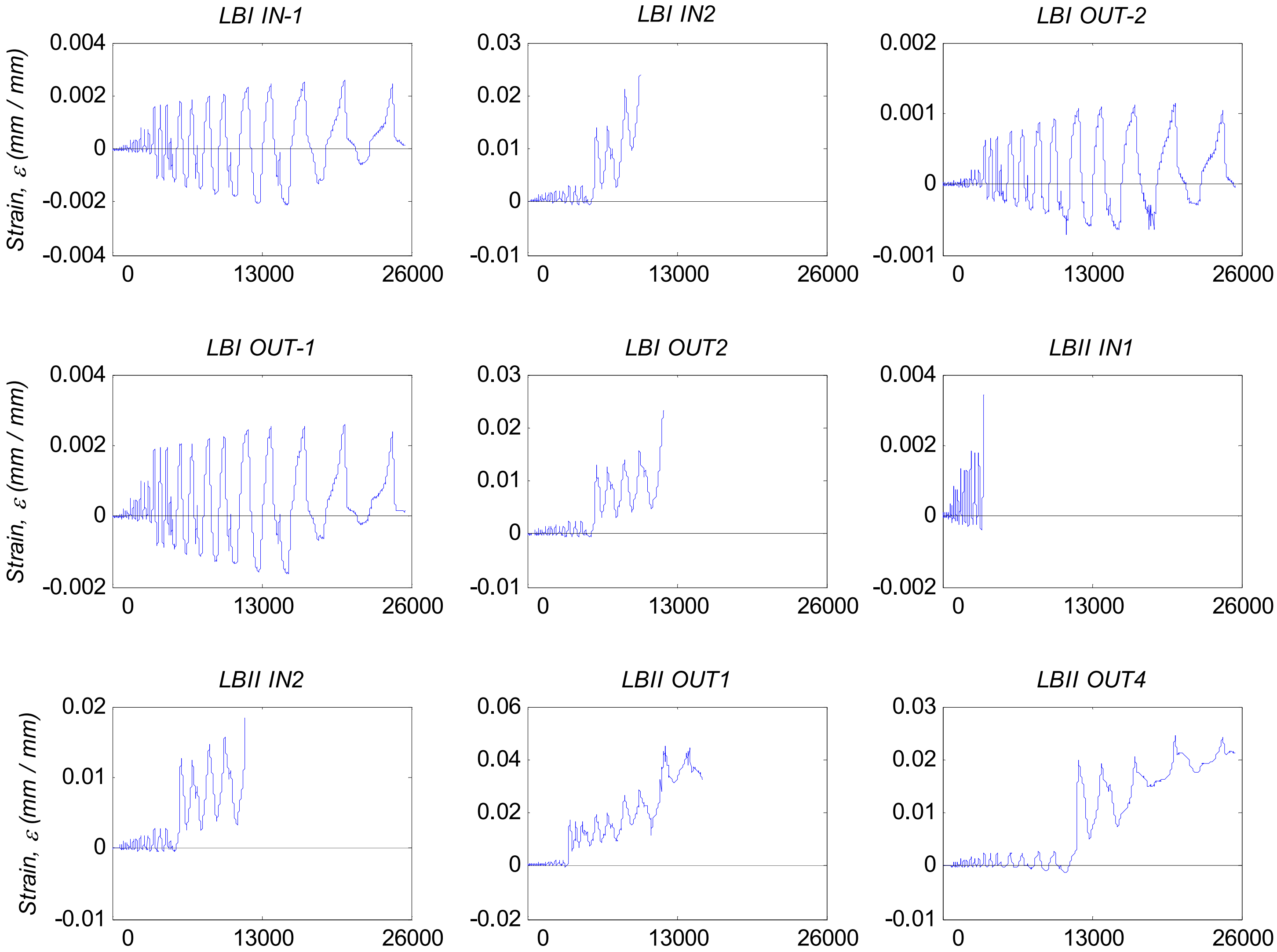

Figure A.12 Beam 2: histories of strain gauges.

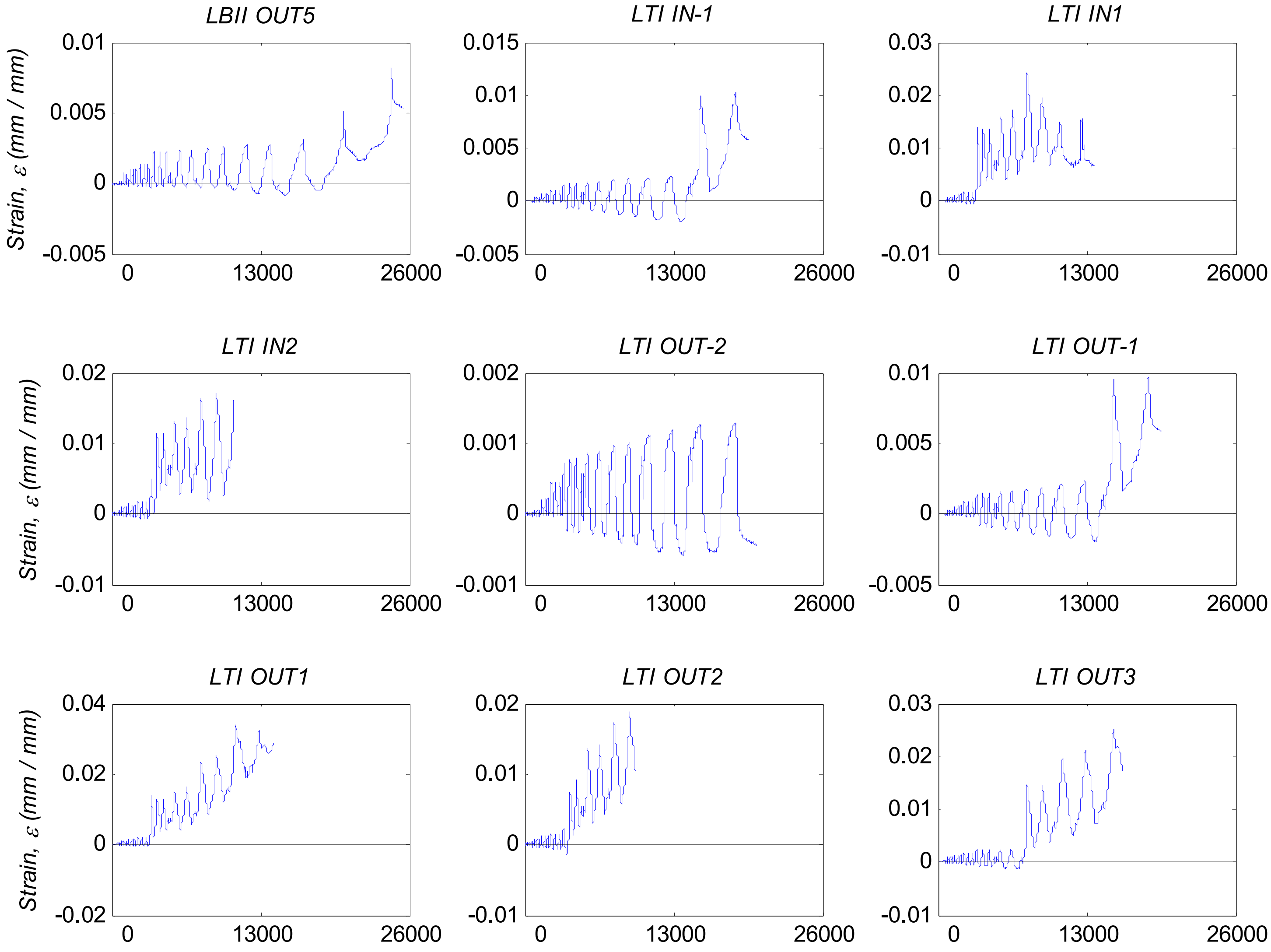
LBII OUT5

LTI IN-1

LTI IN1

LTI IN2

LTI OUT-2

LTI OUT-1

LTI OUT1

LTI OUT2

LTI OUT3

Figure A.13 **Beam 2: histories of strain gauges.**

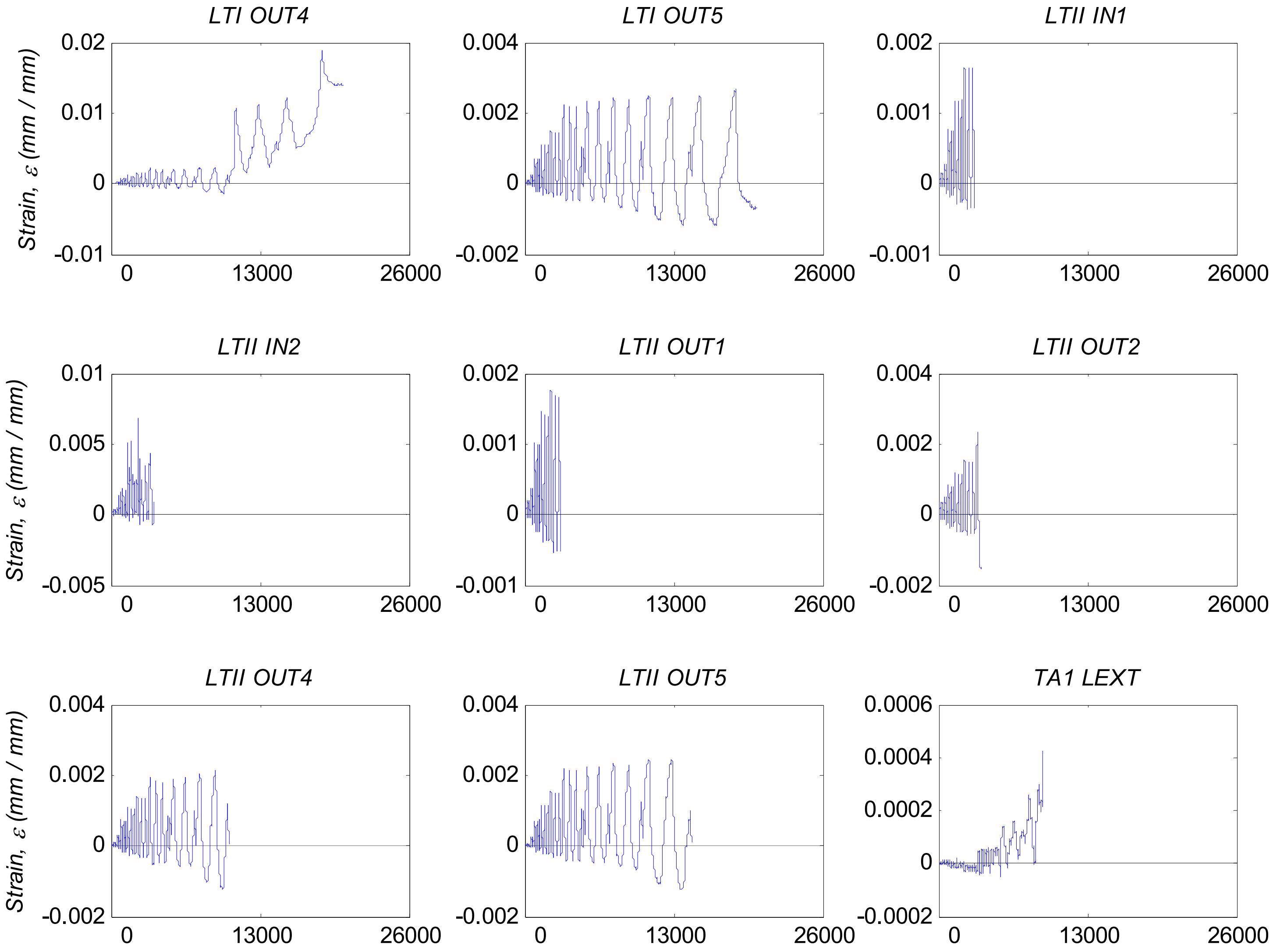

Figure A.14 **Beams 2: histories of strain gauges.**

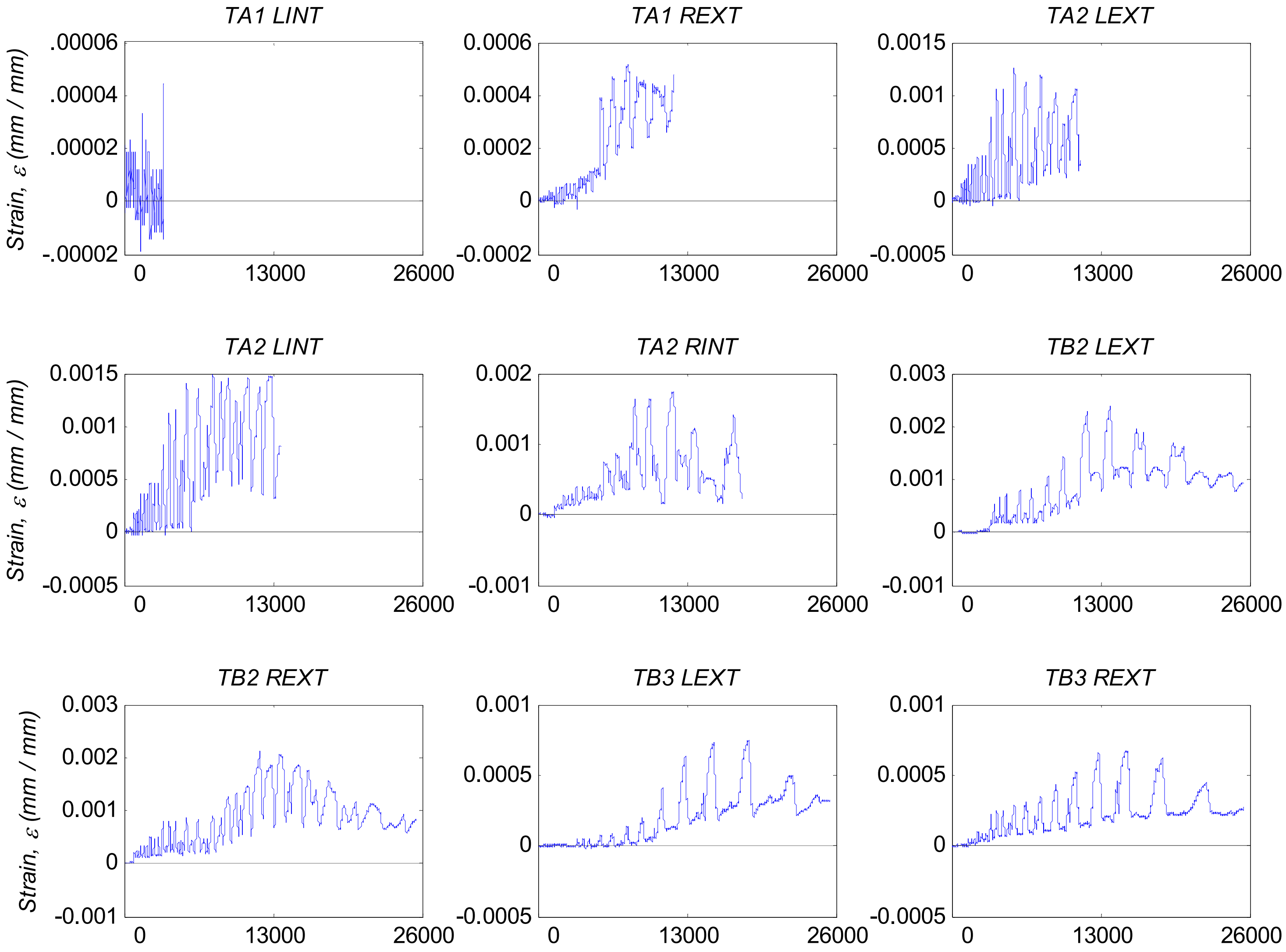

Figure A.15 **Beam 2: histories of strain gauges..**

APPENDIX B: FLEXURAL RESPONSE CALCULATIONS

Beam 1

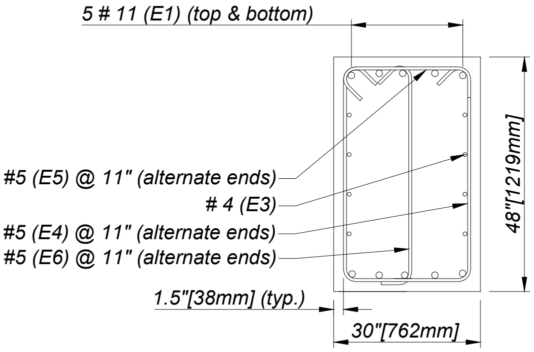

a) SECTION A-A
BEAM 1 CROSS SECTION

Core Dimensions:

Core beam width: b_c = 30-3 = 27 in.

Core beam depth: h_c = 48-3 = 45 in.

Transverse Reinforcement: 3-legged #5 bars

Transverse reinforcement area: $A_v = 3 * 0.31 = 0.93$ in.^{2}

Volumetric transverse reinforcement ratio: $\rho_s = 0.93 / (27 * 11) = 0.313\%$

Calculation of Concrete Confinement:

The confinement stress equals: $f_1 = f_s * A_v / (b_c * s) = 66 * 0.93 / (27 * 11) = 0.2067$, where $f_s = f_y = 66$ ksi is the transverse reinforcement yield strength, A_v is the transverse reinforcement ratio, b_c is the core beam width, and s is the transverse reinforcement spacing.

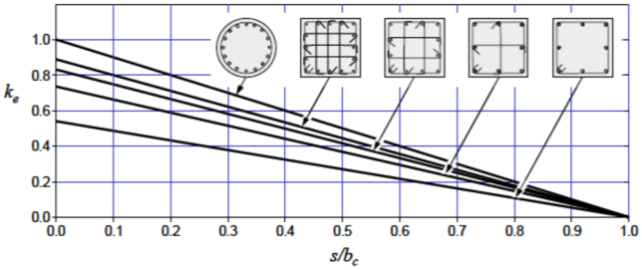

Figure a: Confinement effectiveness for various confinement configurations and hoop spacing

Using the s/b_c ratio, the effectiveness coefficient is calculated for a rectangular beam with a cross-tie. For $s/b_c = 11/27 = 0.4074$ – $k_e = 0.43$. The effective confinement stress equals: $f_{1e} = k_e * f_1 = 0.43 * 0.2067 = 0.0889$ ksi.

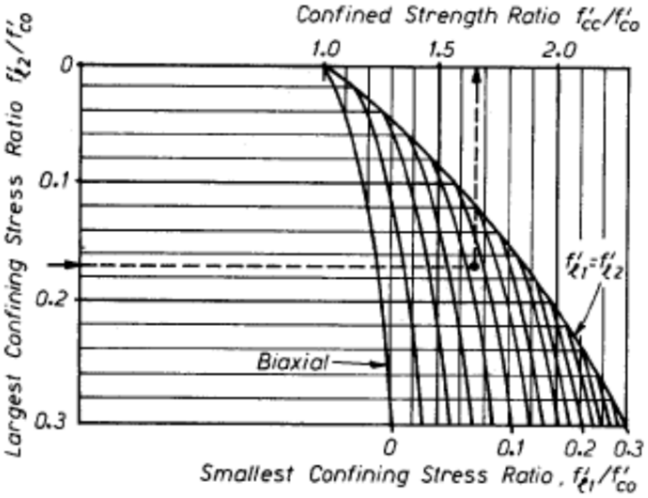

Figure b: Confined concrete strength as function of effective confinement stresses

For $f_{1e} / f'_c = 0.0889 / 5.82 = 0.0153$ - $f'_{cc} / f'_c = 1.09$, where f'_{cc} is the confined concrete compressive strength, and f'_c is the unconfined concrete strength.

The ultimate confined concrete compressive strain capacity: $\varepsilon_{cu} = 0.004 + 0.17 * f_{1e} / f'_c = 0.004 + 0.25 * 0.00889 / 5.82 = 0.00782$.

The confined concrete compressive strain at peak stress is: $\varepsilon_{cc} = \varepsilon_0 *[1 + 5*(f'_{cc} / f'_c - 1)] = 0.003 * [1 + 5*(1.09 - 1.00] = 0.00435$, where ε_0 corresponds to the unconfined concrete strain at peak stress.

Moment Curvature Calculation:

Moment curvature calculation was performed using XTract analysis software. The geometry of the analyzed cross section is shown below:

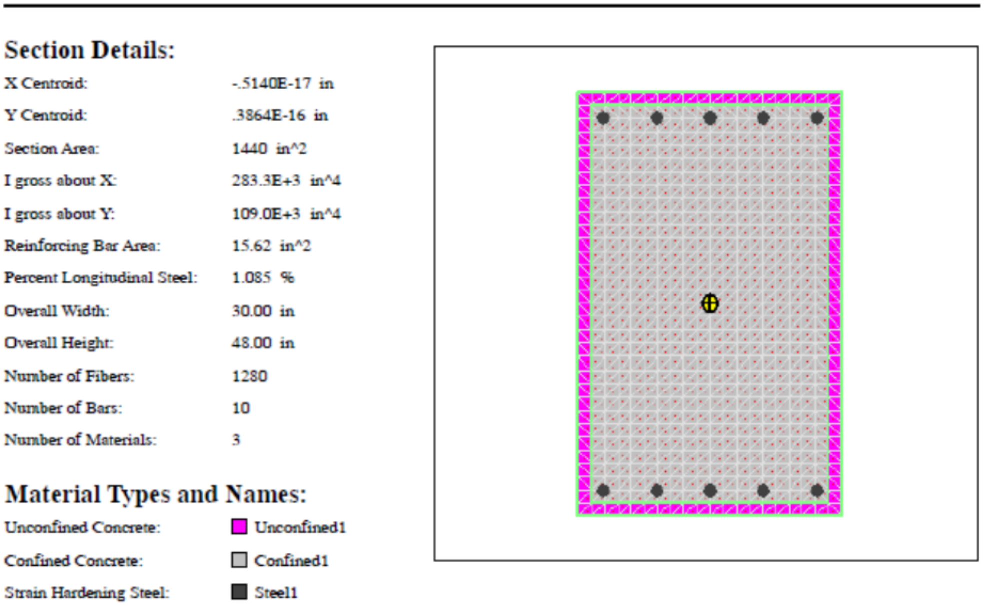

Section Details:

X Centroid:	-.5140E-17 in
Y Centroid:	.3864E-16 in
Section Area:	1440 in^2
I gross about X:	283.3E+3 in^4
I gross about Y:	109.0E+3 in^4
Reinforcing Bar Area:	15.62 in^2
Percent Longitudinal Steel:	1.085 %
Overall Width:	30.00 in
Overall Height:	48.00 in
Number of Fibers:	1280
Number of Bars:	10
Number of Materials:	3

Material Types and Names:

Unconfined Concrete:	🟪 Unconfined1
Confined Concrete:	⬜ Confined1
Strain Hardening Steel:	⬛ Steel1

Figure c: Geometric properties of beam cross section

It should be noted that for the analysis of the beam cross section the 8 No. 4 longitudinal bars that act as skin reinforcement were not included in the moment curvature analysis due to the lack of full development in the anchorage block.

Cited below are the material properties utilized for the moment curvature calculation of Beam 1.

Steel 1[1]

Input Parameters:

Yield Stress:	73.00 ksi
Fracture Stress:	105.0 ksi
Yield Strain:	2.517E-3
Strain at Strain Hardening:	12.00E-3
Failure Strain:	.1500
Elastic Modulus:	29.00E+3 ksi
Additional Information:	Symetric Tension and Comp.

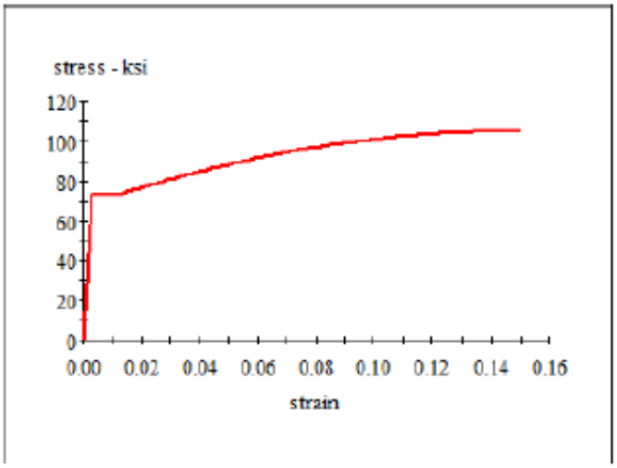

Model Details:

For Strain - $\varepsilon < \varepsilon_y$ $\quad fs = E \cdot \varepsilon$

For Strain - $\varepsilon < \varepsilon_{sh}$ $\quad fs = f_y$

For Strain - $\varepsilon < \varepsilon_{su}$ $\quad fs = f_u - (f_u - f_y) \cdot \left(\frac{\varepsilon_{su} - \varepsilon}{\varepsilon_{su} - \varepsilon_{sh}} \right)^2$

ε = Steel Strain

fs = Steel Stress

f_y = Yield Stress

f_u = Fracture Stress

ε_y = Yield Strain

ε_{sh} = Strain at Strain Hardening

ε_{su} = Failure Strain

E = Elastic Modulus

Figure d: Steel uniaxial material behavior

---

[1] The moment curvature analysis does not take into account the effect of buckling of longitudinal steel reinforcement that was observed during the experiment.

Confined Concrete[2]

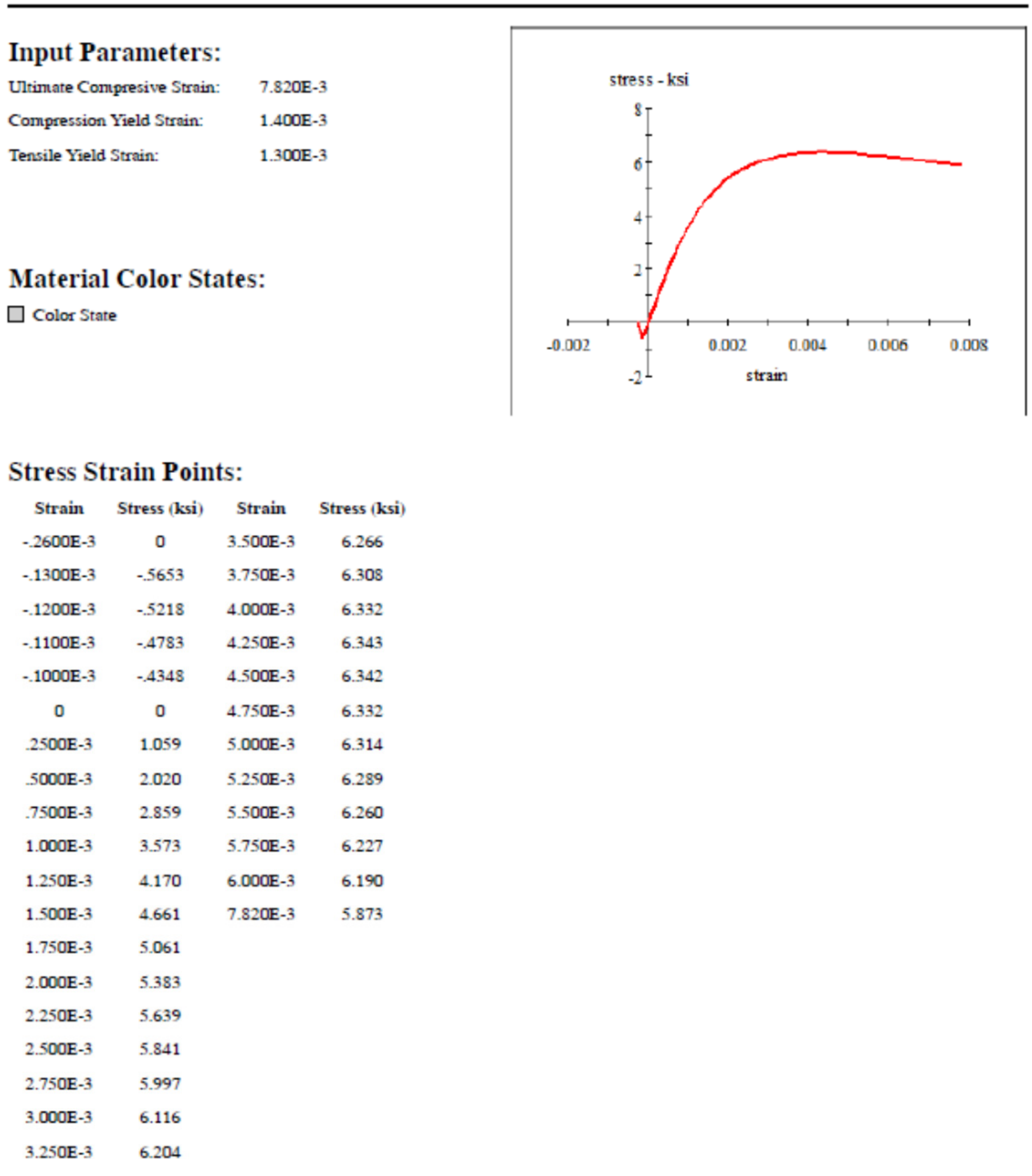

Input Parameters:

Ultimate Compresive Strain:	7.820E-3
Compression Yield Strain:	1.400E-3
Tensile Yield Strain:	1.300E-3

Material Color States:

☐ Color State

Stress Strain Points:

Strain	Stress (ksi)	Strain	Stress (ksi)
-.2600E-3	0	3.500E-3	6.266
-.1300E-3	-.5653	3.750E-3	6.308
-.1200E-3	-.5218	4.000E-3	6.332
-.1100E-3	-.4783	4.250E-3	6.343
-.1000E-3	-.4348	4.500E-3	6.342
0	0	4.750E-3	6.332
.2500E-3	1.059	5.000E-3	6.314
.5000E-3	2.020	5.250E-3	6.289
.7500E-3	2.859	5.500E-3	6.260
1.000E-3	3.573	5.750E-3	6.227
1.250E-3	4.170	6.000E-3	6.190
1.500E-3	4.661	7.820E-3	5.873
1.750E-3	5.061		
2.000E-3	5.383		
2.250E-3	5.639		
2.500E-3	5.841		
2.750E-3	5.997		
3.000E-3	6.116		
3.250E-3	6.204		

Figure e: Confined concrete material behavior

---

[2] The confined concrete material behavior was modeled according to the relationship suggested by Mander et al. (1988).

Unconfined Concrete[3]

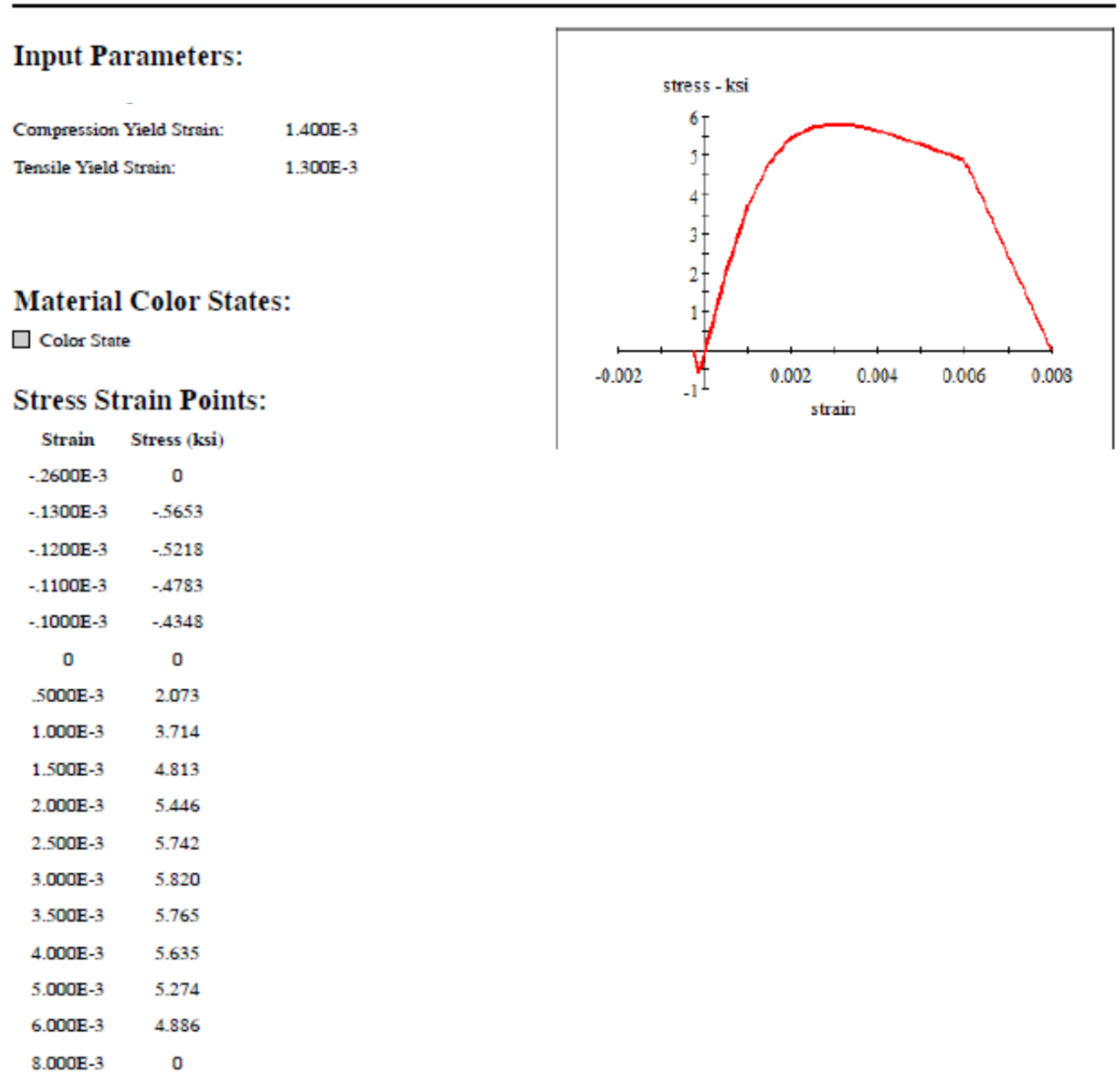

Input Parameters:

Compression Yield Strain: 1.400E-3
Tensile Yield Strain: 1.300E-3

Material Color States:

☐ Color State

Stress Strain Points:

Strain	Stress (ksi)
-.2600E-3	0
-.1300E-3	-.5653
-.1200E-3	-.5218
-.1100E-3	-.4783
-.1000E-3	-.4348
0	0
.5000E-3	2.073
1.000E-3	3.714
1.500E-3	4.813
2.000E-3	5.446
2.500E-3	5.742
3.000E-3	5.820
3.500E-3	5.765
4.000E-3	5.635
5.000E-3	5.274
6.000E-3	4.886
8.000E-3	0

Figure f: Unconfined concrete material behavior

---

[3] The unconfined concrete material behavior was modeled according to the relationship suggested by Mander et al. (1988).

The analytical results of moment curvature analysis are presented below:

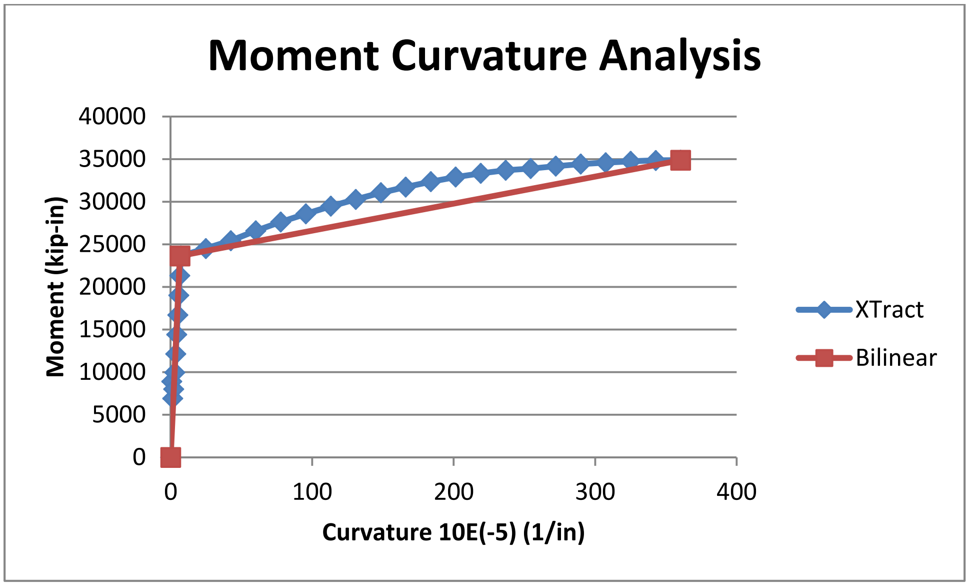

Figure g: Moment curvature analysis

As illustrated in the figure above:

The estimated ultimate moment strength: M_{ult} = 34,880 kip-in.

The estimated ultimate moment curvature: $\varphi_{\text{ult}} = 3.60 * 10^{-3}$ in.$^{-1}$

An equivalent bilinear moment curvature curve was also used to approximate the cross-section behavior. The following values were used for the bi-linearization of the moment curvature curve:

Effective curvature stiffness = $0.3 * E_{\text{concrete}} * I_g = 0.30 * 4348.47 * 276480 = 360.679 * 10^6$ kip-in.^{2}, where E_{concrete} is the concrete Young's Modulus, calculated as 57,000 sqrt (f'_c) according to ACI 318-08, I_g is the second moment of inertia of the beam gross cross section, and 0.30 is the modification cracking factor according to ASCE 41 (Supplement 1).

Approximate yielding moment strength: M_{yield} = 23650 kip –in.

Approximate yielding moment curvature: $\varphi_{\text{yield}} = 6.557 * 10^{-5}$

Approximate ultimate moment strength: M_{ult} = 34,880 kip-in.

Approximate ultimate moment curvature: $\varphi_{\text{ult}} = 3.60 * 10^{-3}$ in.$^{-1}$

Calculation of Beam Tip Displacement

To evaluate the analytical results with the beam tip displacement was calculated analytically and compared to the observed experimental results. For the analytical calculation of beam tip displacement, two approaches were employed:

a. use the bilinear approximation of moment curvature analysis assuming that the material nonlinear behavior was concentrated in a plastic hinge zone l_p=0.5 * h, where h is the beam depth

b. use the moment rotation values as suggested by ASCE-41 for modeling of beam members

Bilinear Approximation

	Moment (kip-in)	Displacement (in.)	Drift Ratio[4]
Undeformed State	0.0	0.00000	0.0000
Reinforcement Yielding[5]	23,650.0	0.49178	0.0033
Ultimate Strength[5]	34,880.0	11.6163	0.0774

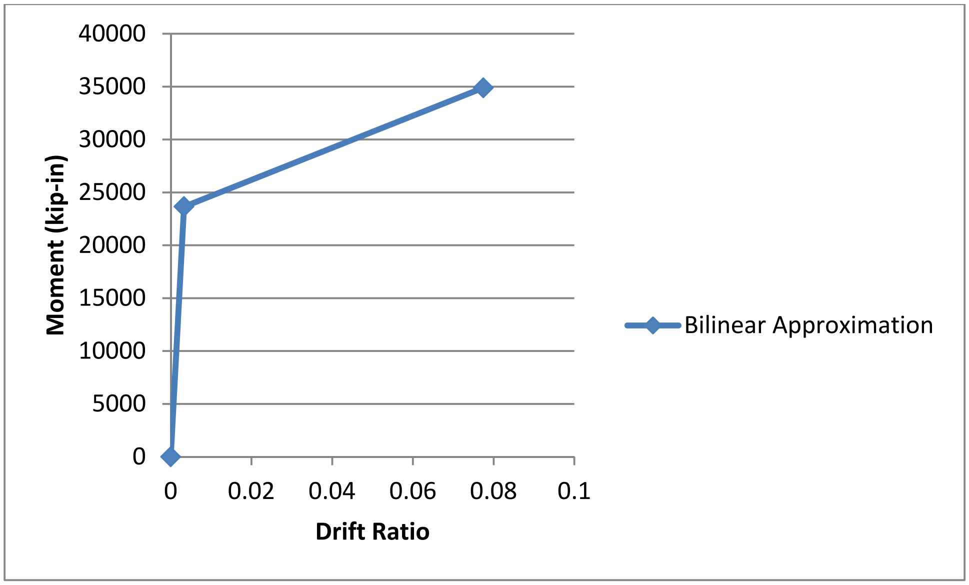

Figure h: Moment – drift ratio curve

---

[4] The drift ratio was calculated as (displacement) / (beam length) (=150 in.).

[5] The calculation of the tip displacement for the states where yielding and ultimate moment strength occurs was performed using integration of the calculated curvature as follows: $\Delta_y = \varphi'_y * l^2/3$ and $\Delta_{\text{ult}} = \varphi_y * l^2 / 3 + (\varphi_{\text{ult}} - \varphi_y) * l_p * (l - l_p/2)$, where φ'_y corresponds to the curvature where reinforcement yielding is observed, $\varphi_y = \varphi'_y * M_{\text{ult}} / M_y = 6.557 * 10^{-5} * 34{,}880 / 23{,}650 = 9.67 * 10^{-5}$ in.$^{-1}$.

ASCE -41 Approximation

The probable moment M_{pr} according to ASCE-41 is calculated using nominal material properties ($f'_c = 5$ ksi and $1.25 * f_y = 1.25 * 60 = 75.0$ ksi), $M_{pr} = 25{,}340$ kip-in.

For the beam section, the following properties apply:

> $(\rho - \rho') / \rho_{\text{bal}} = 0.0$
>
> transverse reinforcement has code conforming details with 135° hooks
>
> $V / [bw * d * \text{sqrt}\,(f'_c)] = 168{,}933.33 / (27*45.17*76.30) = 1.815 < 3.00$, assuming $V = V_{pr} = 25{,}340 / 150 = 168.93$ kips
>
> Stirrup spacing 11 in < $d/2$

According to ASCE 41 (Supplement 1), the beam is suggested to be simulated using lumped plasticity model with the following backbone curve:

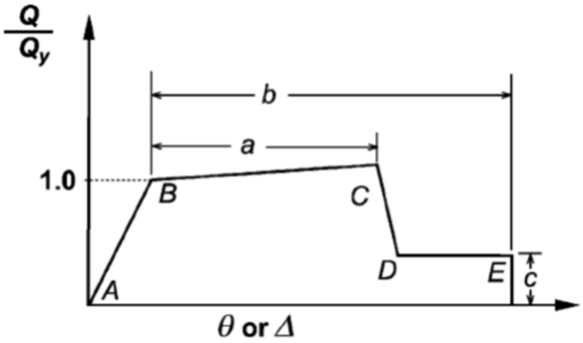

Figure i: Backbone curve (ASCE-41)

The beam is controlled by flexure, therefore the deformation quantities according to Table 6-7 of ASCE-41 are as follows: $a = 0.025$, $b = 0.05$, and $c = 0.20$

Substituting the above values and using the results of moment curvature analysis, we have:

	Moment (kip-in.)	Displacement (in.)	Drift Ratio[6]
Undeformed State	0.0	0.00000	0.0000
Reinforcement Yielding[7]	23,650.0	0.49178	0.0033
Ultimate Strength[7]	25,340.0	4.27692	0.0285
Residual Strength[7]	4730.0	7.59836	0.0507

---

[6] The drift ratio was calculated as (displacement) / (beam length) (=150 in.).

[7] The calculation of the tip displacement for the states where yielding, ultimate, and residual moment strength occurs was performed using integration of the calculated curvature as follows: Δ_y (calculated using effective stiffness), $\Delta_{\text{ult}} = (M_y / EI_{\text{eff}})*l^2/3 + 0.025 * l$ and $\Delta_{\text{res}} = (M_{\text{res}} / EI_{\text{eff}}) * l^2/ 3 + 0.050 * l$.

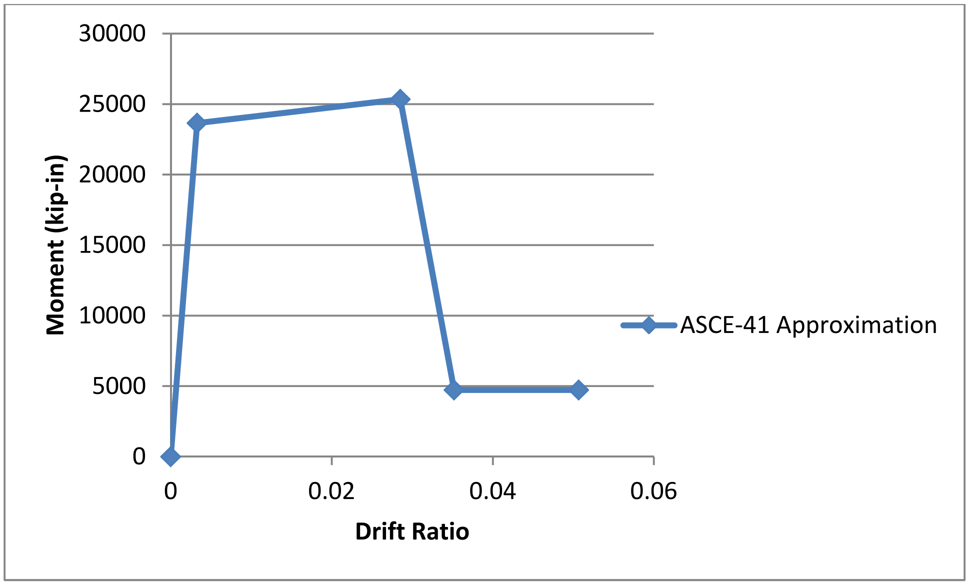

Figure j: Moment – drift ratio curve (according to ASCE-41)

Comparison of Analytical Approximations with Experimental Results

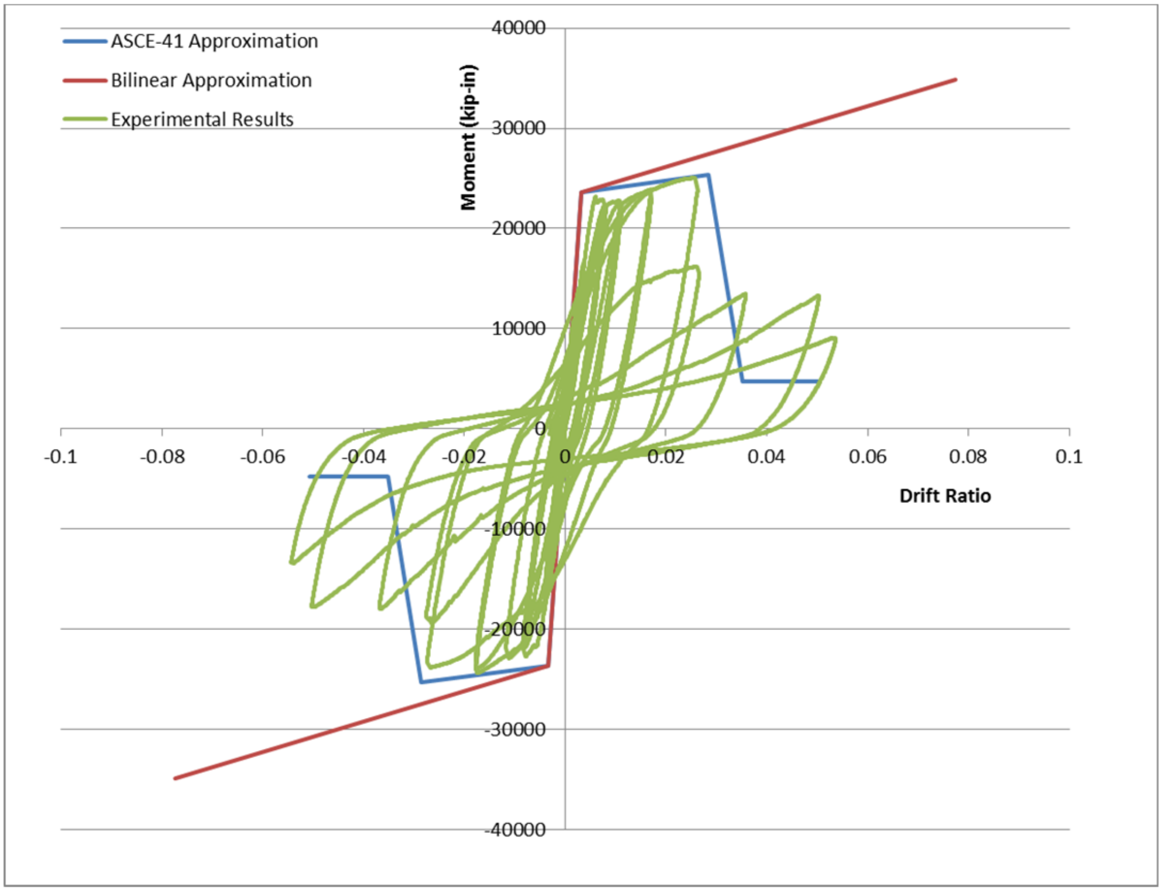

Figure k: Comparison of analytical and experimental results

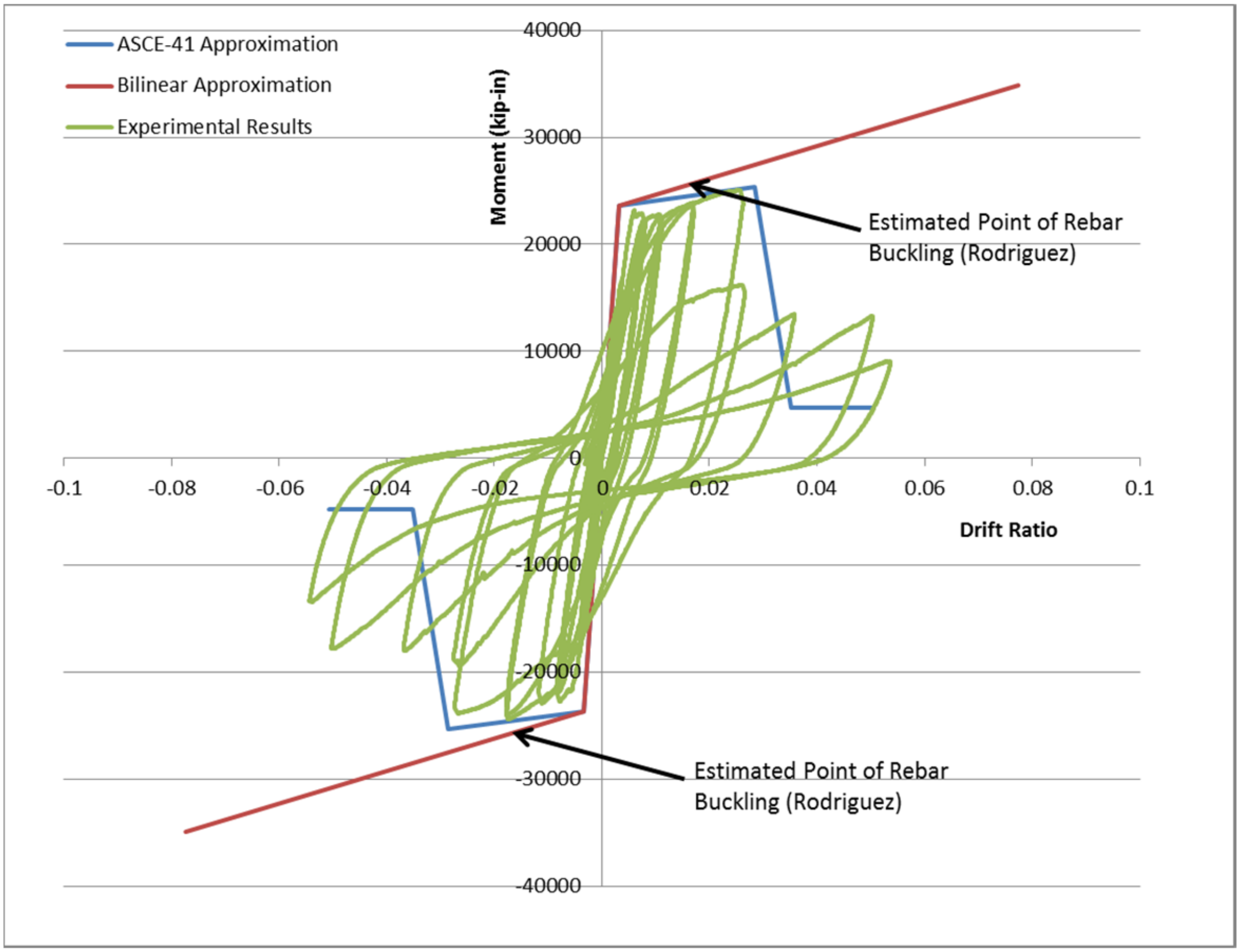

Figure l: Comparison of analytical and experimental results (includes estimated point where buckling occurs according to Rodriguez)

Beam 2

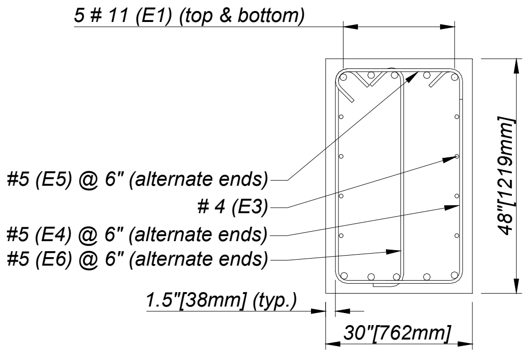

b) SECTION B-B
BEAM 2 CROSS SECTION

Core Dimensions:

Core beam width: $b_c = 30\text{-}3 = 27$ in.

Core beam depth: $h_c = 48\text{-}3 = 45$ in.

Transverse Reinforcement: 3-legged #5 bars

Transverse Reinforcement Area: $A_v = 3 * 0.31 = 0.93$ in.^{2}

Volumetric Transverse Reinforcement Ratio: $\rho_s = 0.93 / (27*6) = 0.574\%$

Calculation of Concrete Confinement:

The confinement stress equals: $f_l = f_s * A_v / (b_c * s) = 66 * 0.93 / (27*6) = 0.3789$, where $f_s = f_y = 66$ ksi is the transverse reinforcement yield strength, A_v is the transverse reinforcement ratio, and b_c is the core beam width and s is the transverse reinforcement spacing.

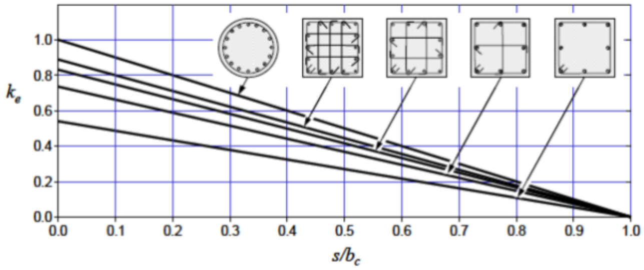

Figure a: Confinement effectiveness for various confinement configurations and hoop spacing

Using the s/b_c ratio the effectiveness coefficient is calculated for a rectangular beam with a cross-tie. For $s/b_c = 6/27 = 0.222$ – $k_e = 0.57$.

The effective confinement stress equals: $f_{le} = k_e * f_l$ = 0.57 * 0.3789= 0.2160 ksi.

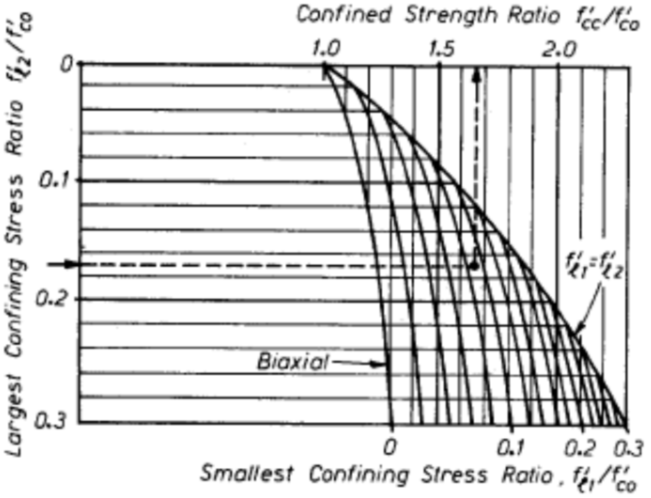

Figure b: Confined concrete strength as function of effective confinement stresses

For f_{le} / f'_c = 0.2160 / 6.13 = 0.0352 - f'_{cc} / f'_c = 1.22, where f'_{cc} is the confined concrete compressive strength, f'_c is the unconfined concrete strength.

The ultimate confined concrete compressive strain capacity: ε_{cu} = 0.004 +0.17 * f_{le} / f'_c = 0.004 + 0.25 * 0.2160 / 6.13 = 0.0128.

The confined concrete compressive strain at peak stress is: $\varepsilon_{cc} = \varepsilon_0$ *[1+ 5*(f'_{cc} / f'_c -1)] = 0.003 * [1+5*(1.09-1.00)] = 0.0063, where ε_0 corresponds to the unconfined concrete strain at peak stress.

Moment Curvature Calculation:

Moment curvature calculation was performed using XTract analysis software. The geometry of the analyzed cross section is shown below:

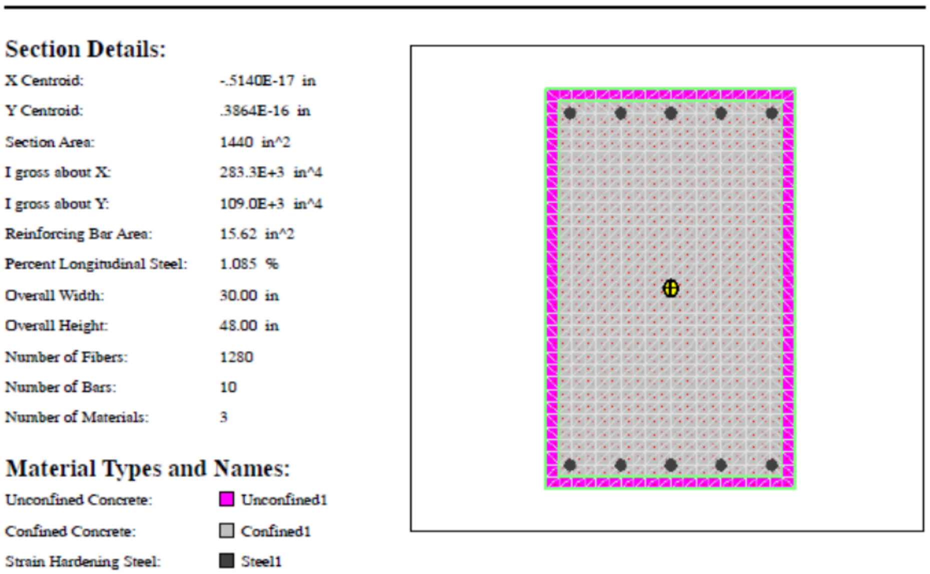

Section Details:

X Centroid:	-.5140E-17 in
Y Centroid:	.3864E-16 in
Section Area:	1440 in^2
I gross about X:	283.3E+3 in^4
I gross about Y:	109.0E+3 in^4
Reinforcing Bar Area:	15.62 in^2
Percent Longitudinal Steel:	1.085 %
Overall Width:	30.00 in
Overall Height:	48.00 in
Number of Fibers:	1280
Number of Bars:	10
Number of Materials:	3

Material Types and Names:

Unconfined Concrete:	🟪 Unconfined1
Confined Concrete:	◻ Confined1
Strain Hardening Steel:	■ Steel1

Figure c: Geometric properties of beam cross section

It should be noted that for the analysis of the beam cross section the 8 No. 4 longitudinal bars that act as skin reinforcement were not included in the moment curvature analysis due to the lack of full development in the anchorage block.

Cited below the material properties utilized for the moment curvature calculation of beam 1.

Steel 1[8]

Input Parameters:

Yield Stress:	73.00 ksi
Fracture Stress:	105.0 ksi
Yield Strain:	2.517E-3
Strain at Strain Hardening:	12.00E-3
Failure Strain:	.1500
Elastic Modulus:	29.00E+3 ksi
Additional Information:	Symetric Tension and Comp.

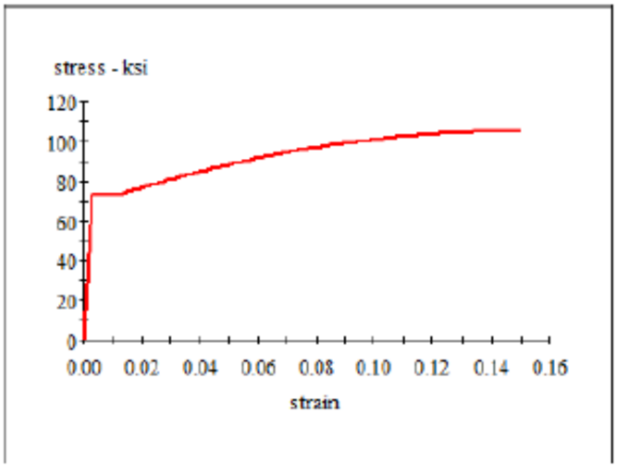

Model Details:

For Strain - $\varepsilon < \varepsilon_y$ $\quad fs = E \cdot \varepsilon$

For Strain - $\varepsilon < \varepsilon_{sh}$ $\quad fs = f_y$

For Strain - $\varepsilon < \varepsilon_{su}$ $\quad fs = f_u - (f_u - f_y) \cdot \left(\frac{\varepsilon_{su} - \varepsilon}{\varepsilon_{su} - \varepsilon_{sh}} \right)^2$

ε = Steel Strain

fs = Steel Stress

f_y = Yield Stress

f_u = Fracture Stress

ε_y = Yield Strain

ε_{sh} = Strain at Strain Hardening

ε_{su} = Failure Strain

E = Elastic Modulus

Figure d: Steel uniaxial material behavior

---

[8] The moment curvature analysis is not taking into account the effect of buckling of longitudinal steel reinforcement which was observed in the during the experiment

Confined Concrete[9]

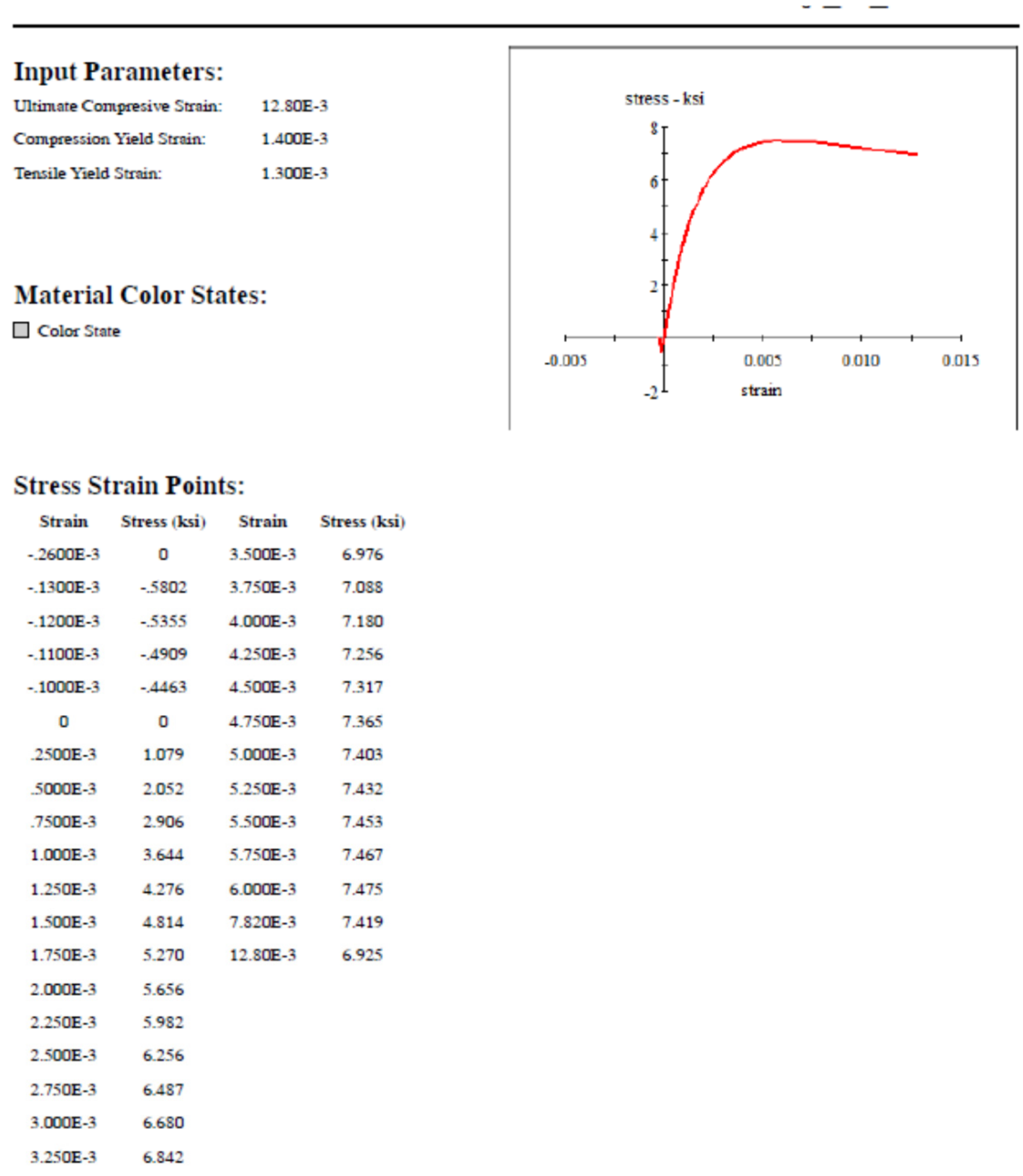

Input Parameters:

Ultimate Compresive Strain:	12.80E-3
Compression Yield Strain:	1.400E-3
Tensile Yield Strain:	1.300E-3

Material Color States:

▨ Color State

Stress Strain Points:

Strain	Stress (ksi)	Strain	Stress (ksi)
-.2600E-3	0	3.500E-3	6.976
-.1300E-3	-.5802	3.750E-3	7.088
-.1200E-3	-.5355	4.000E-3	7.180
-.1100E-3	-.4909	4.250E-3	7.256
-.1000E-3	-.4463	4.500E-3	7.317
0	0	4.750E-3	7.365
.2500E-3	1.079	5.000E-3	7.403
.5000E-3	2.052	5.250E-3	7.432
.7500E-3	2.906	5.500E-3	7.453
1.000E-3	3.644	5.750E-3	7.467
1.250E-3	4.276	6.000E-3	7.475
1.500E-3	4.814	7.820E-3	7.419
1.750E-3	5.270	12.80E-3	6.925
2.000E-3	5.656		
2.250E-3	5.982		
2.500E-3	6.256		
2.750E-3	6.487		
3.000E-3	6.680		
3.250E-3	6.842		

Figure e: Confined concrete material behavior

---

[9] The confined concrete material behavior was modeled according to the relationship as suggested by Mander et al. (1988).

Unconfined Concrete[10]

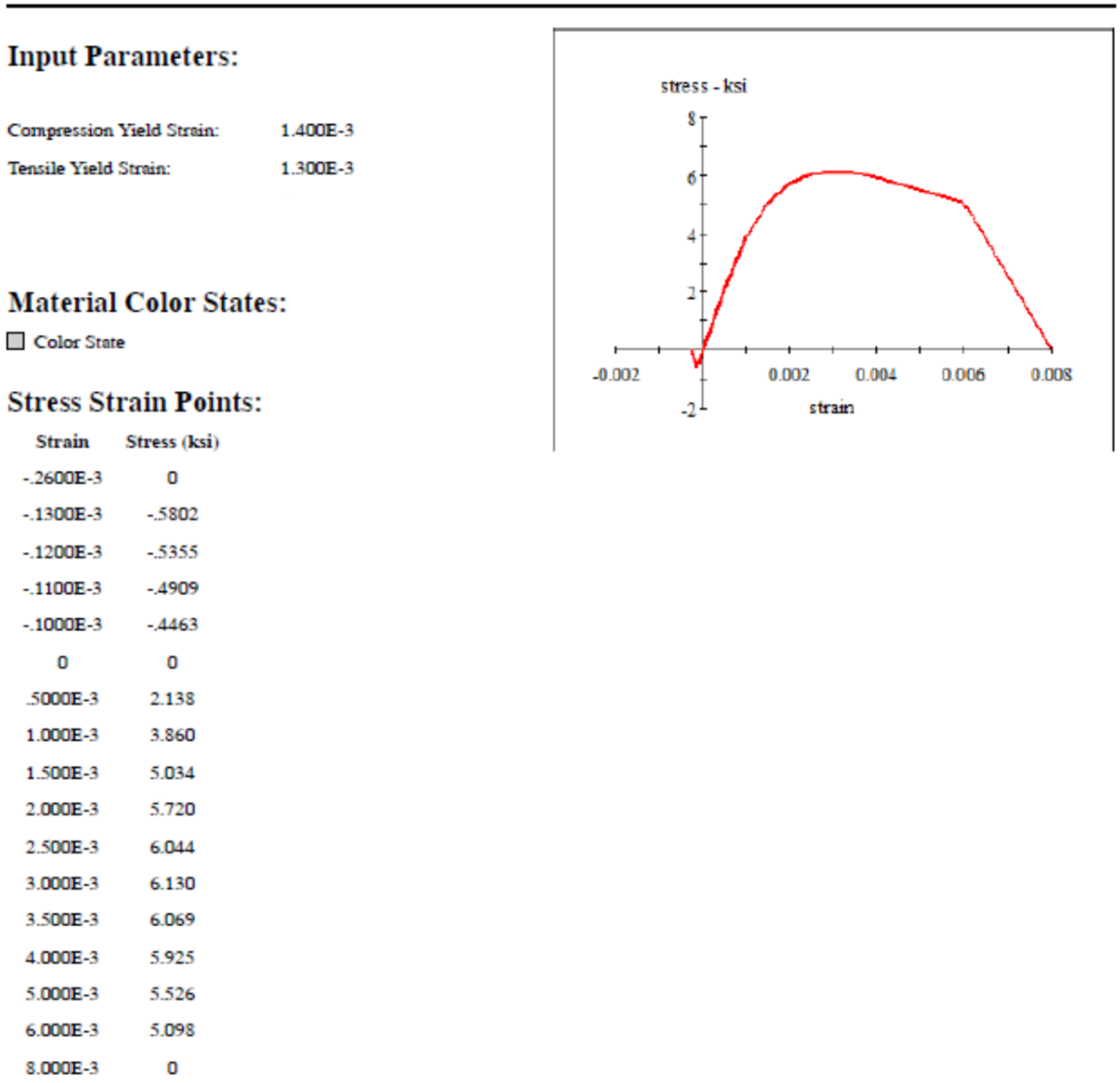

Input Parameters:

Compression Yield Strain:	1.400E-3
Tensile Yield Strain:	1.300E-3

Material Color States:

▨ Color State

Stress Strain Points:

Strain	Stress (ksi)
-.2600E-3	0
-.1300E-3	-.5802
-.1200E-3	-.5355
-.1100E-3	-.4909
-.1000E-3	-.4463
0	0
.5000E-3	2.138
1.000E-3	3.860
1.500E-3	5.034
2.000E-3	5.720
2.500E-3	6.044
3.000E-3	6.130
3.500E-3	6.069
4.000E-3	5.925
5.000E-3	5.526
6.000E-3	5.098
8.000E-3	0

Figure f: Unconfined concrete material behavior

The analytical results of moment curvature analysis are presented below.

---

[10] The unconfined concrete material behavior was modeled according to the relationship as suggested by Mander et al. (1988).

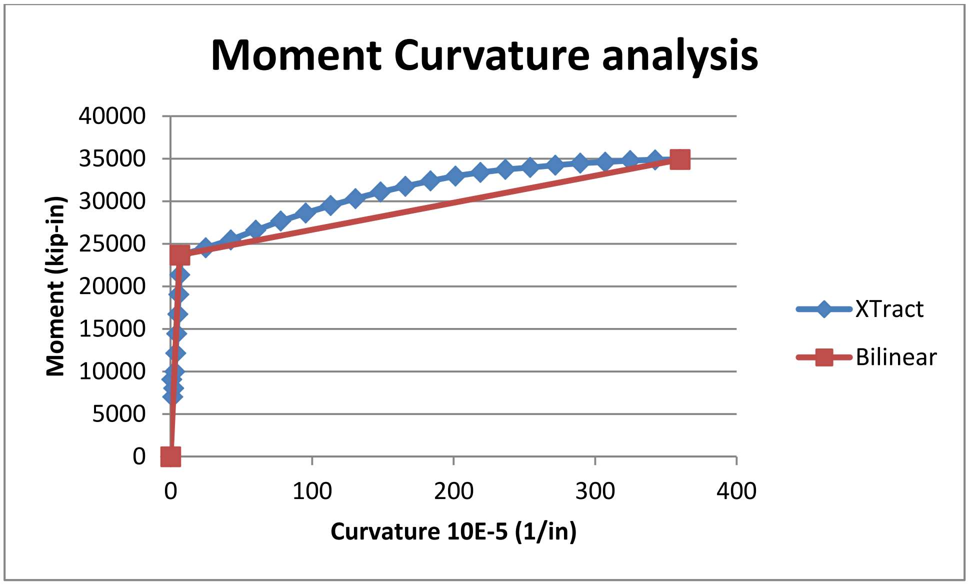

Figure g: Moment curvature analysis

As illustrated in the figure above:

The estimated ultimate moment strength: M_{ult} = 34,920 kip-in.

The estimated ultimate moment curvature: $\varphi_{\text{ult}} = 3.60 * 10^{-3}$ in.$^{-1}$

An equivalent bilinear moment curvature curve was also used to approximate the cross section behavior. The following values were used for the bi-linearization of the moment curvature curve:

Effective Curvature Stiffness = 0.3 * E_{concrete} * I_g = 0.30* 4462.78 * 276,480 = 370.1608 * 10^6 kip-in.^{2}, where E_{concrete} is the concrete Young's modulus, calculated as 57,000 sqrt (f'_c) according to ACI 318-08 , I_g is the second moment of inertia of the beam gross cross section and 0.30 is the modification cracking factor according to ASCE 41 (Supplement 1).

Approximate yielding moment strength: M_{yield} = 23,680 kip –in.

Approximate yielding moment curvature: $\varphi_{\text{yield}} = 6.397 * 10^{-5}$

Approximate ultimate moment strength: M_{ult} = 34920 kip-in.

Approximate ultimate moment curvature: $\varphi_{\text{ult}} = 360 * 10^{-5}$ in.$^{-1}$

Calculation of Beam Tip Displacement

To evaluate the analytical results with the beam tip displacement was calculated analytically and compared to the observed experimental results.

For the analytical calculation of beam tip displacement two approaches were employed:

a. Use the bilinear approximation of moment curvature analysis assuming that the material non-linear behavior was concentrated in a plastic hinge zone $l_p = 0.5 * h$, where h is the beam depth

b. Use the moment rotation values as suggested by ASCE-41 for modeling of beam members

Bilinear Approximation

	Moment (kip-in.)	Displacement (in.)	Drift Ratio[11]
Undeformed State	0.0	0.00000	0.0000
Reinforcement Yielding[12]	23,680.0	0.47979	0.0032
Ultimate Strength[12]	34,920.0	11.6109	0.0774

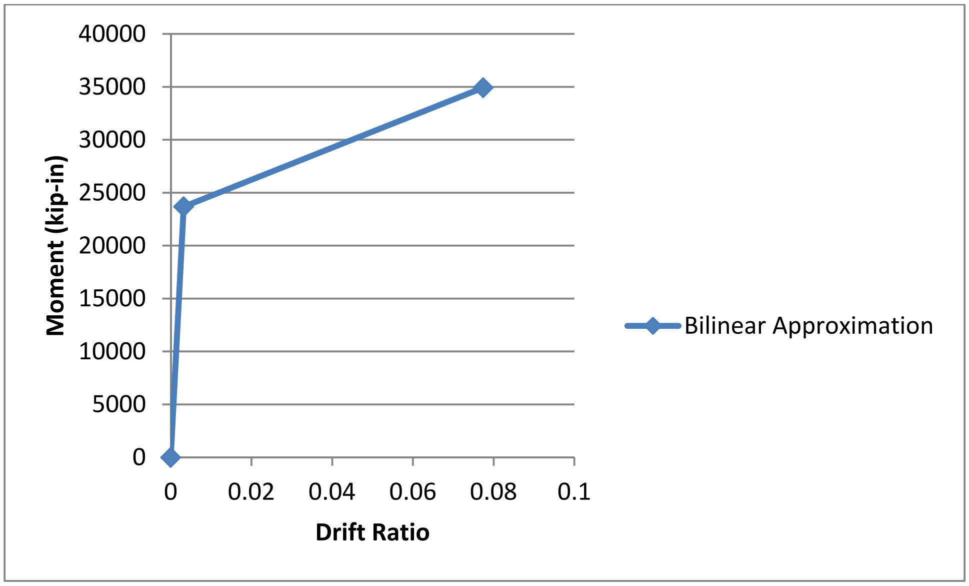

Figure h: Moment – drift ratio curve

---

[11] The drift ratio was calculated as (displacement) / (beam length) (=150 in.).

[12] The calculation of the tip displacement for the states where yielding and ultimate moment strength occurs was performed using integration of the calculated curvature as follows: $\Delta_y = \varphi'_y * l^2/3$ and $\Delta_{\mathrm{ult}} = \varphi_y * 1^2/3 + (\varphi_{\mathrm{ult}} - \varphi_y) * l_p * (l - l_p/2)$, where φ'_y corresponds to the curvature where reinforcement yielding is observed, $\varphi_y = \varphi'_y * M_{\mathrm{ult}} / M_y = 6.397 * 10^{-5} * 34{,}920 / 23{,}680 = 9.43 * 10^{-5}$ in.$^{-1}$.

ASCE-41 Approximation

The probable moment M_{pr} according to ASCE-41 is calculated using nominal material properties (f'_c = 5 ksi and 1.25 * f_y =1.25 * 60 = 75.0 ksi), M_{pr} = 25,340 kip-in. For the beam section the following properties apply:

$(\rho - \rho') / \rho_{\text{bal}} = 0.0$

transverse reinforcement has code conforming details with 135° hooks

$V / [bw * d * \text{sqrt}(f'_c)] = 168{,}933.33 / (27*45.17*78.29) = 1.77 < 3.00$, assuming $V = V_{pr} = 25340 / 150 = 168.93$ kips

Stirrup spacing 6 in < $d/2$

According to ASCE 41 (Supplement 1) the beam is suggested to be simulated using lumped plasticity model with the following backbone curve:

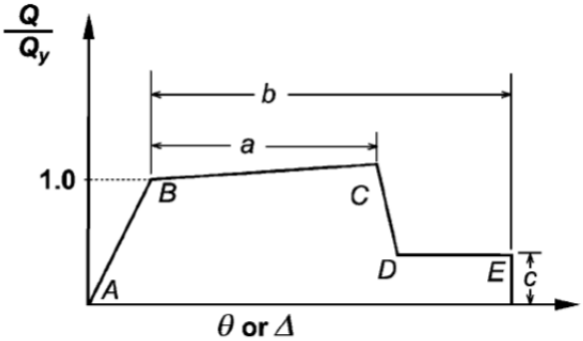

Figure i: Backbone curve (ASCE-41)

The beam is controlled by flexure so the deformation quantities according to Table 6-7 of ASCE-41 are the following: $a = 0.025$, $b = 0.05$, and $c = 0.20$.

Substituting the above values and using the results of moment curvature analysis we have:

	Moment (kip-in.)	Displacement (in.)	Drift Ratio[13]
Undeformed State	0.0	0.00000	0.0000
Reinforcement Yielding[14]	23,680.0	0.47979	0.0032
Ultimate Strength[14]	25,340.0	4.26343	0.0284
Residual Strength[14]	4736.0	7.59596	0.0506

---

[13] The drift ratio was calculated as (displacement) / (beam length) (=150 in.).

[14] The calculation of the tip displacement for the states where yielding and ultimate moment strength occurs was performed using integration of the calculated curvature as follows: Δ_y (calculated using effective stiffness), $\Delta_{\text{ult}} = (M_y / EI_{\text{eff}})*l^2/3 + 0.025 * l$ and $\Delta_{\text{res}} = (M_{\text{res}} / EI_{\text{eff}}) * l^2/3 + 0.050 * l$.

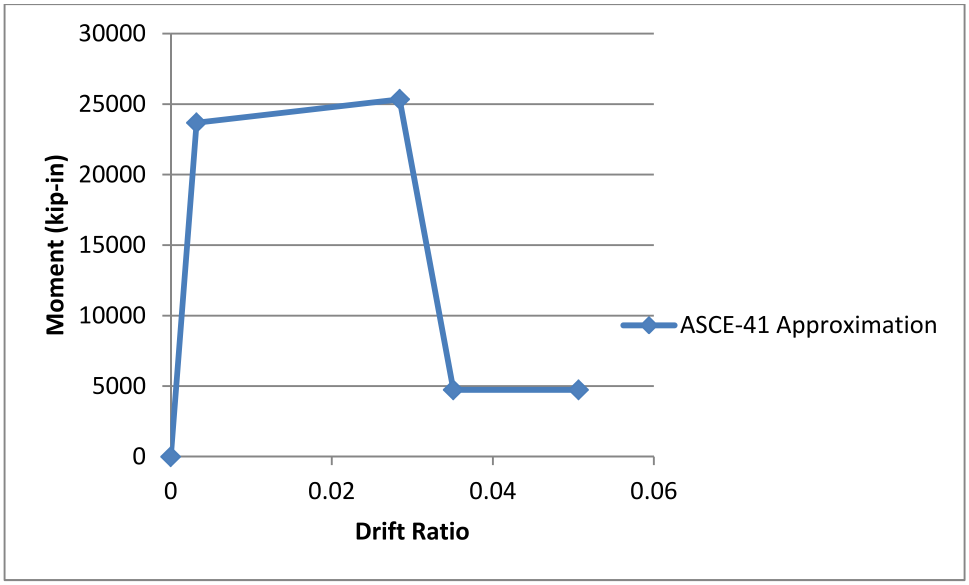

Figure j: Moment–drift ratio curve (according to ASCE-41)

Comparison of Analytical Approximations with Experimental Results

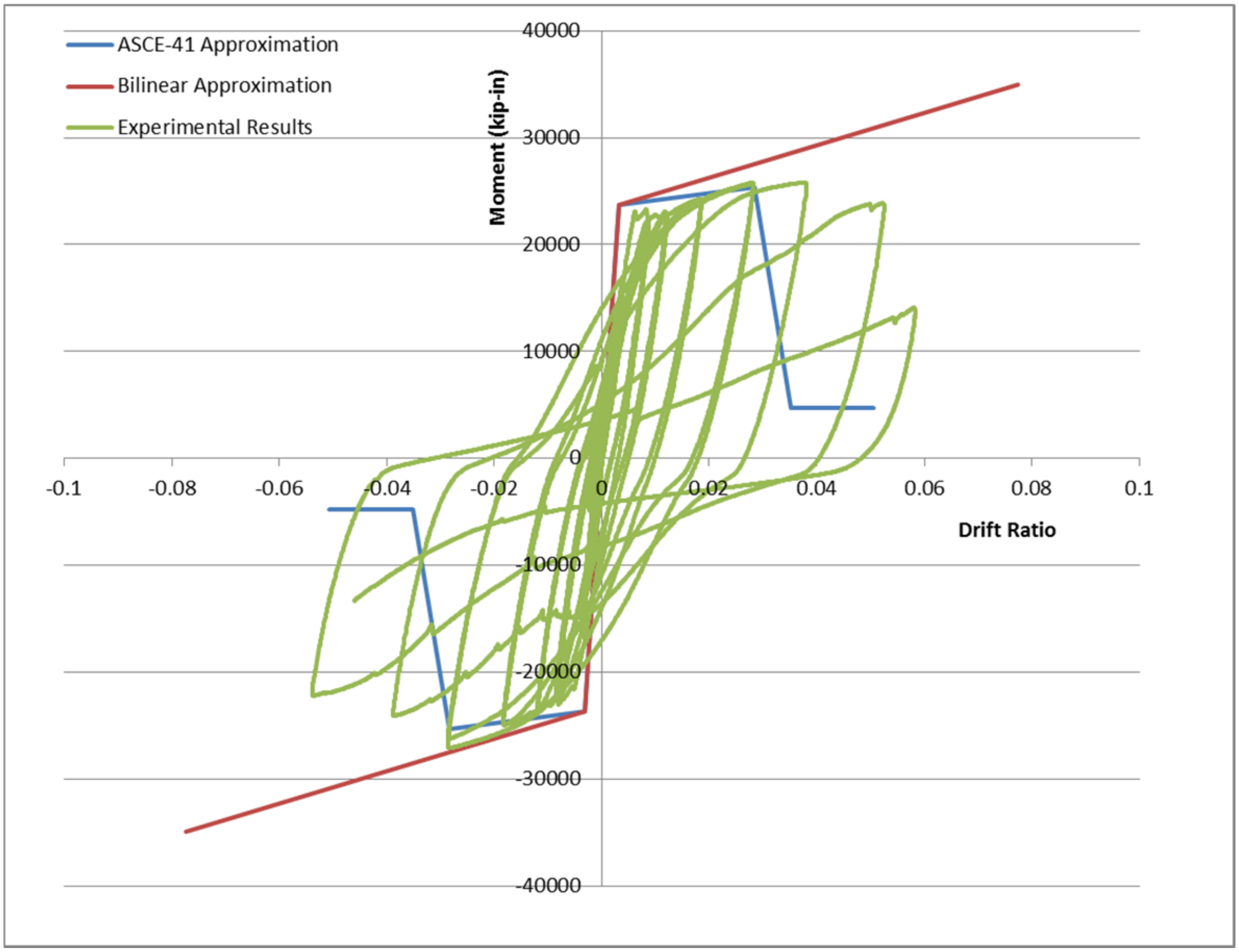

Figure k: Comparison of analytical and experimental results

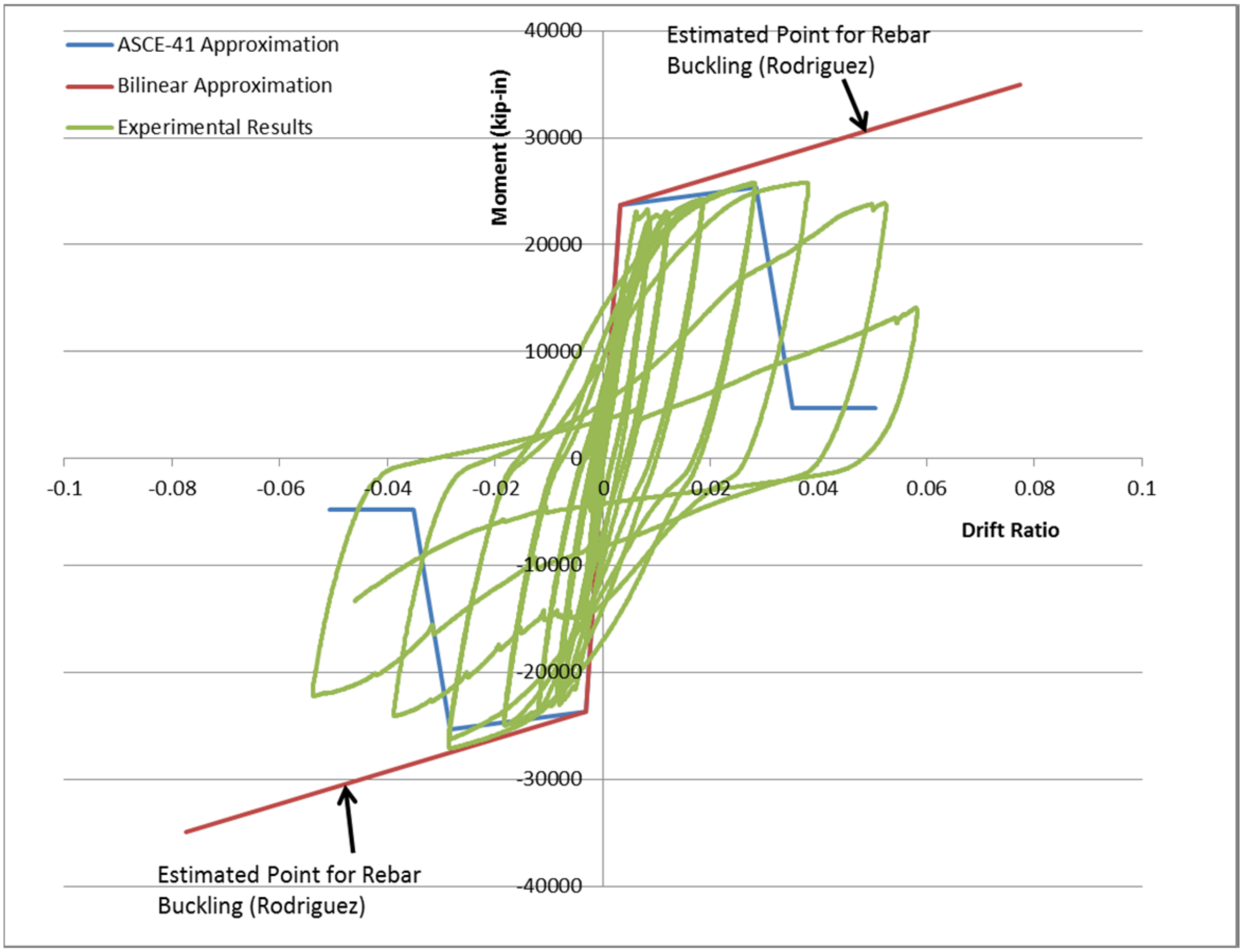

Figure l: Comparison of analytical and experimental results (includes estimated point where buckling occurs according to Rodriguez)

APPENDIX C: RECORDED CRACK WIDTHS

Beam 1

step	# of cycles	tip displ. (mm)	drift ratio	μ_Δ	current cycle #	direction of beam tip displacement	max. diagonal crack width (mm)	max. vertical crack width (mm)	max. interface crack width (mm)
1	3	3	0.07	0.1	1	down			
					1	up			
					1	zero			
2	3	7	0.18	0.3	1	down		0.25	
					2	up		0.2	
					2	zero			
3	3	11	0.28	0.5	1	down		0.33	
					1	up			
					1	zero			
4	3	14	0.38	0.8	1	down		0.6	
					1	up			
					1	zero			
5	3	31	0.81	1.1	1	down		1	0.6
					1	up			
					1	zero			
6	3	46	1.2	2.1	1	down	1.5		3
					1	up			
					1	zero			
7	1	13	0.33	0.7	1	n/a			2
8	2	69	1.8	3.2	1	down	3	2.5	4
					1	up			
					1	zero			
9	1	13	0.33	0.7	1	n/a			
10	2	103	2.7	4.2	1	down	5		5
					1	up	5		
					3	zero		2.5	
11	1	13	0.33	0.7	1	n/a			
12	2	139	3.6	6.4	1	down	25		
					1	up			
					1	zero			
13	1	13	0.33	0.7	1	n/a			
14	1	194	5.1	8.5	1	n/a			
15	1	13	0.33	0.7	1	n/a			
16	1	210	5.5	11.7	1	n/a			

Beam 2

step	# of cycles	tip displ. (mm)	drift ratio	μ_Δ	current cycle #	direction of beam tip displacement	max. diagonal crack width (mm)	max. vertical crack width (mm)	max. interface crack width (mm)
1	3	3	0.07	0.2	1	down		0.08	
						up			
					3	zero			
2	3	6	0.16	0.3	1	down		0.3	
						up			
					3	zero		0.33	
3	3	11	0.28	0.6	1	down	0.2	0.4	
						up	0.2	0.4	
					3	zero	0.1	0.25	
4	3	15	0.4	0.9	1	down	0.3	0.4	
						up	0.2	0.3	
					3	zero	0.15	0.25	
5	3	33	0.87	1.9	1	down	0.5	0.5	
						up	0.3	0.5	
					3	zero	0.15	0.2	
6	3	46	1.2	2.6	1	down	0.6	1	
						up	0.6	1.25	
					3	zero	0.3	0.5	
7	1	13	0.33	0.7	1	n/a	n/a		
8	2	69	1.8	3.9	1	down	1.5	2	
					1	up	0.6	2	
					3	zero	1.5	2	
9	1	13	0.33	0.7	1	n/a	n/a		
10	2	109	2.9	6.2	1	down	3	4	
					1	up	1.5	3	
					3	zero	4	5	
11	1	13	0.33	0.7	1	n/a	n/a		
12	2	147	3.9	8.3	1	down	5	6	11
					1	up	6	8	20
					2	zero	7	15	20
13	1	13	0.33	0.7	1	cycle omitted			
14	1	203	5.3	11.4	1	down	7	9	
15	1	13	0.33	0.7	1	n/a			
16	1	222 (-244)	5.8 (-6.4)	12.5 (-13.7)	1	n/a			